SHIP DYNAMICS

KHIONE

AALTO UNIVERSITY

SCHOOL OF ENGINEERING

Juhan Voutilainen

Juho Elias Suortti

Stephan van Reen

Zongyu Jiang

Contents

1 Operational Profile, ship dynamics requirements, maneuvering devices, and hull form features 5

1.1 Environmental condition and operational profile 5

1.2 The requirement of ship dynamics 7

1.3 Maneuvering devices 7

1.4 Hull features 10

1.5 Literature Review 11

1.5.1 “Experimental Studies on Seakeeping and Maneuverability of Ships in Adverse Weather Conditions” (Cura-Hochbaum et al., 2017) 11

1.5.2 Article 2: "Open Water Resistance and Seakeeping Characteristics of Ships with Icebreaking Bows" (Moton, 1991) 12

2 Environment 16

2.1 Water depth in the route 16

2.2 3Wind 19

2.3 Sea Ice 22

2.4 Shallow and Deep Water Waves 26

2.5 Wave spectra 29

2.6 Literature Review 31

2.6.1. Book Chapter: Ochi (2005) – Ocean waves: stochastic approach, Chapter 5: Sea severity 31

2.6.2. Book Chapter: Ochi (1993): Marine environment and its impact on design of ships and marine structures 36

2.6.3. Cherneva, Guedos Soarez (2014): Time–frequency analysis of the sea state with the Andrea freak wave 40

3 Wave Induced Motions in Regular and Irregular Waves 42

3.1 Equations of Motion 42

3.2 Khione’s parameters affecting the equations of motion 42

3.2.1 Hull form 42

3.2.2 Operation profile 43

3.2.3 General arrangement 44
3.2.4 Mission 45
3.3 Seakeeping analysis 46
3.4 Motions of Khione in regular waves 46
3.4.1 RAO from AQWA and Hydrostar 48
3.4.2 RAO from NAPA 60
3.5 Motion response in irregular waves 67
3.6 Literature review 70
3.6.1 Book chapter, Jerzy Matusiak, Dynamics of a Rigid Ship: Chapter 4, General form of equations of motions 70
3.6.2 Comparative study on the time-domain analysis of non-linear ship motions and loads 71
3.6.3 Quick Strip Theory Calculations in Ship Design 72
4. Global Loads in Irregular Waves 74
4.1 Calculation of global loads 74
4.2 Discussion 81
4.3 Literature review 82
4.3.1 Static Loads 82
4.3.2 Quasi-Static Loads 83
4.3.3 Dynamic loads 84
5. Seakeeping Criteria, Maneuvering Tests, and Resistance 87
5.1 Seakeeping criteria 87
5.2 Maneuvering tests 94
5.3 Added Resistance 98
5.4 Literature review 101
5.4.1 Bertram, Practical ship hydrodynamics: 6.2.8 CFD for maneuvering 101
5.4.2 Journée, Massie, Huijsmans; Offshore hydromechanics: 8.8 Added resistance in waves 103
References 104

1 Operational Profile, ship dynamics requirements, maneuvering devices, and hull form features

Khione is an Arctic research and re-supply vessel operating in the Arctic waters. She shall be able to independently operate in the extreme conditions of the Arctic waters. Figure 1.1 shows some of the predicted operating routes. Consequently, Khione shall be designed to resist such extreme conditions: 1) low temperature; 2) sea ice; 3) the Arctic storm; 4) long time of darkness; 5) large distance from supporting ports and infrastructures; 6) polar navigation. The condition 2 and 3 are relevant to the ship dynamics.

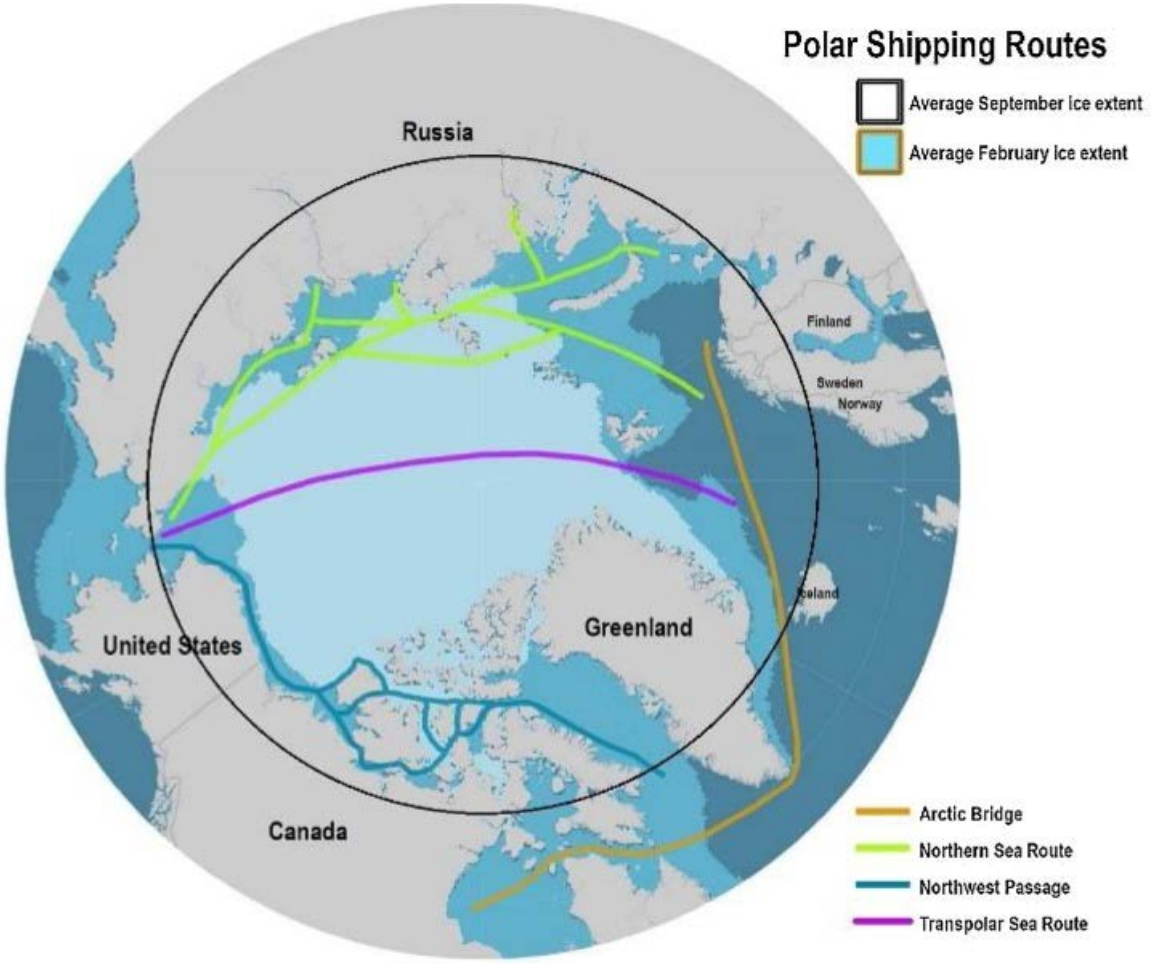

Figure 1.1 Arctic shipping routes (Rodriguez, 2010)

1.1 Environmental condition and operational profile

The Arctic waters is a kind of ice-infested waters, where the vessel highly possibly encounter the first-year ice and multi-year ice. So far, there is no detailed ice chart for the whole Arctic waters so it is not possible to specify the ice breaking capability of Khione based on the ice condition.

Nevertheless, the ice breaking capability can be designed according to the relevant regulations of International Maritime Organization and class rules. As a Polar re-supply and research vessel, Khione shall be capable to break 1.65 m thick first-year ice at a speed of 3 knots. According to the *International code for ships operating in polar waters* (Polar Code), PC4 ships must be able to operate in thick first-year ice which may include old ice inclusions (IMO, 2015). The thick first-year ice is defined as 1.2-2 m thick ice (Headland, 2020). Therefore, PC4 is a suitable ice class for the polar re-supply and research vessel.

As mentioned above, Khione normally operates in the Arctic waters. However, she should not be restricted in this region. For example, she may navigate through the Atlantic Ocean to the Antarctic waters. Thus, it is reasonable to consider the wave condition globally. In addition, the wave condition is more severe in the North Atlantic region so wave condition of the North Atlantic is used for the wave loads calculation. Table 1 shows the scatter diagram of significant wave height and zero crossing period for the North Atlantic (DNV, 2010). Table 2 shows the parameters of the joint model for the scatter diagrams (DNV, 2010).

Table 1.1 Scatter diagram for the North Atlantic

Table C-2 Scatter diagram for the North Atlantic

T_Z (s) / H_S (m)	3.5	4.5	5.5	6.5	7.5	8.5	9.5	10.5	11.5	12.5	13.5	14.5	15.5	16.5	17.5	18.5	Sum
0.5	1.3	133.7	865.6	1186.0	634.2	186.3	36.9	5.6	0.7	0.1	0.0	0.0	0.0	0.0	0.0	0.0	3050
1.5	0.0	29.3	986.0	4976.0	7738.0	5569.7	2375.7	703.5	160.7	30.5	5.1	0.8	0.1	0.0	0.0	0.0	22575
2.5	0.0	2.2	197.5	2158.8	6230.0	7449.5	4860.4	2066.0	644.5	160.2	33.7	6.3	1.1	0.2	0.0	0.0	23810
3.5	0.0	0.0	34.9	695.5	3226.5	5675.0	5099.1	2838.0	1114.1	337.7	84.3	18.2	3.5	0.6	0.1	0.0	19128
4.5	0.0	0.0	6.0	196.1	1354.3	3288.5	3857.5	2685.5	1275.2	455.1	130.9	31.9	6.9	1.3	0.2	0.0	13289
5.5	0.0	0.0	1.0	51.0	498.4	1602.9	2372.7	2008.3	1126.0	463.6	150.9	41.0	9.7	2.1	0.4	0.1	8328
6.5	0.0	0.0	0.2	12.6	167.0	690.3	1257.9	1268.6	825.9	386.8	140.8	42.2	10.9	2.5	0.5	0.1	4806
7.5	0.0	0.0	0.0	3.0	52.1	270.1	594.4	703.2	524.9	276.7	111.7	36.7	10.2	2.5	0.6	0.1	2586
8.5	0.0	0.0	0.0	0.7	15.4	97.9	255.9	350.6	296.9	174.6	77.6	27.7	8.4	2.2	0.5	0.1	1309
9.5	0.0	0.0	0.0	0.2	4.3	33.2	101.9	159.9	152.2	99.2	48.3	18.7	6.1	1.7	0.4	0.1	626
10.5	0.0	0.0	0.0	0.0	1.2	10.7	37.9	67.5	71.7	51.5	27.3	11.4	4.0	1.2	0.3	0.1	285
11.5	0.0	0.0	0.0	0.0	0.3	3.3	13.3	26.6	31.4	24.7	14.2	6.4	2.4	0.7	0.2	0.1	124
12.5	0.0	0.0	0.0	0.0	0.1	1.0	4.4	9.9	12.8	11.0	6.8	3.3	1.3	0.4	0.1	0.0	51
13.5	0.0	0.0	0.0	0.0	0.0	0.3	1.4	3.5	5.0	4.6	3.1	1.6	0.7	0.2	0.1	0.0	21
14.5	0.0	0.0	0.0	0.0	0.0	0.1	0.4	1.2	1.8	1.8	1.3	0.7	0.3	0.1	0.0	0.0	8
15.5	0.0	0.0	0.0	0.0	0.0	0.0	0.1	0.4	0.6	0.7	0.5	0.3	0.1	0.1	0.0	0.0	3
16.5	0.0	0.0	0.0	0.0	0.0	0.0	0.0	0.1	0.2	0.2	0.2	0.1	0.1	0.0	0.0	0.0	1
Sum	1	165	2091	9280	19922	24879	20870	12898	6245	2479	837	247	66	16	3	1	100000

The H_s and T_z values are class midpoints.

Table 1.2 parameters of the joint model for the scatter diagrams of North Atlantic

Table C-4 North Atlantic		
α_{Hs}	β_{Hs}	γ_{Hs}
3.041	1.484	0.661
a_0	a_1	a_2
0.70	1.27	0.131
b_0	b_1	b_2
0.1334	0.0264	-0.1906

1.2 The requirement of ship dynamics

Khione is designed to continuously voyage at a speed of 13 knots in open water and 3 knots in sea ice. Therefore, the issue of ship resistance should be considered in two conditions: 1) open water; 2) sea ice. For the open water, the resistance in calm water should be considered firstly. In addition, it is necessary to consider the added resistance due to wave. For the sea ice condition, the ice resistance should be taken into account.

The second issue relevant to the ship dynamics is the hull strength. Firstly, the wave loads could induce the motions of ship in six degrees of freedom. They also cause the global damage of hull so the hull girder strength should be considered. In order to handle the global strength problem, the main dimensions of the hull should be designed carefully. For example, the depth and free board should be large enough and the ratio of length and depth should be limited into a reasonable value. Secondly, the wave loads could also induce the local damage to the hull, such as slamming and green water. Thus, the hull structure should be strong enough to resist the local damage due to waves. Thirdly, the ice loads could result in the local damage, and consequently, the local ice loads should be considered. To deal with the problem of local strength, it is important to optimize the design of stem and stern. There are some conflicts between the designs for minimizing the slamming load and ice load. For example, the stem angle (angle between the stem line and water line) should be small to minimize the level ice load. However, it may increase the slamming load. It is a big challenge for the design.

The ice can also jeopardize the maneuvering capability of the vessel. Therefore, the design of maneuvering system must concern this situation in ice, such as turning at zero speed. Because of this reason, Khione needs stronger maneuvering capability than ships only voyaging in open water. There are two options: 1) POD; 2) shaft propulsion with bow and stern thrust. The POD propulsion is often used for the vessels operating in ice infested waters in order to achieve a good maneuvering capability, even at zero advancing speed.

1.3 Maneuvering devices

Initially, maneuvering devices of our ship consisted of two rudders, two fixed pitch propellers and bow and stern thrusters. The propulsion of the ship is powered by diesel-electric configuration, where diesel generators produce power for the electric motors that runs the propellers. Two propeller arrangement was chosen to achieve smaller diameters of propellers without compromising the thrust. For an icebreaking vessel it is important that maneuverability is good, thus we reconsidered the use of azimuth propulsion system. Azimuth propulsion would remove the need for the rudders and the stern thruster, increasing the maneuverability and efficiency at the same.

Previously made resistance calculations showed, based on Finnish-Swedish ice class rules, that 29150kW is the required propulsive power to fulfill the requirements set for our ice capability, which is 3knots in 1.65 meters thick ice. To achieve that it is decided to use diesel-electric configuration with diesel generators made by Wärtsilä. Generators of choice are 4-stroke diesel generators. More particularly 2 x 12V31 and 2 x 14V31 engines. The rated power for the 12V31 is 7320 kW and for 14V31 8540 kW which all together will provide 31720 kW. Space required by the generators are presented in Table 3.

Table 1.3 Required space of generators (Wärtsilä, 2019).

Engine type	A*	A	B	C	F	Weight
12V31	7900	7840	3137	3500	1496	77.1
14V31	8540	8480	3137	3500	1496	84.6

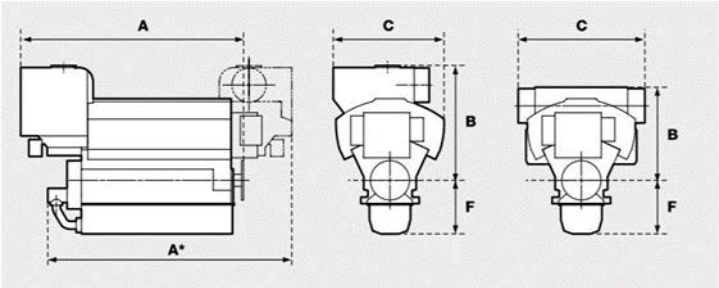

Figure 1.2 Diesel generator dimensions.

Replacing the initial shaft propulsion arrangement of our vessel can be conducted because of the diesel-electric configuration and the flat shape of the stern, which can accommodate the azimuth propulsors. Schematic picture of maneuvering equipment with azimuth propulsion presented in Figure 1.3. Azimuth propulsors are commonly driven by electric motors, which fits our configuration. Two screw arrangement will be replaced with two azimuth propulsors with equal propulsion power. To achieve the required power two ABB Azipod® VI, eah capable of producing 16 MW of power, could be installed (ABB, 2019)

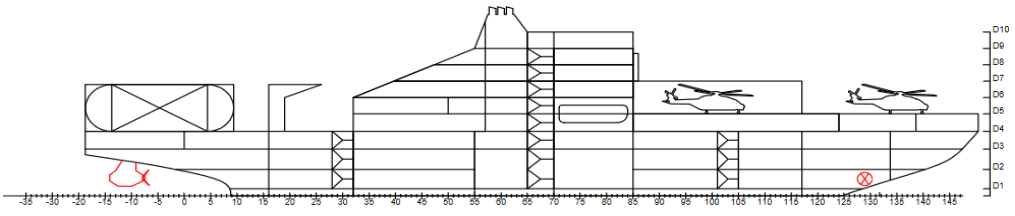

Figure 1.3 Schematic image of maneuvering devices of the vessel.

Figure 1.4 ABB Azipod VI system installed on a ship.

To achieve good maneuverability and possibility for dynamic positioning our vessel is designed to have bow thruster. Thruster can be used for operating in small basins like in ports. With combination of bow thruster and Azipod propulsion our ship can conduct research and resupply in challenging environments. As our vessel has diesel-electric machinery, thrusters can be powered by electric motors, which will get the energy from the main diesel engines. Based on our ship size it is roughly estimated that Wärtsilä's WTT-14 transverse thruster with diameter of 2 m and maximum power of 1440 kW would be sufficient for us.

Space used for the maneuvering devices is roughly presented in Figure 1.5, which is a schematic picture of general arrangement without appendages included. Space reserved for the bow thruster at this point is probably too great but will be defined in more detail during next iterations of the design. Azimuth propulsors saves the space required for the electric motors from inside of the hull, since the electric motors are located inside the Azipods. Maintenance of the Azipods can be done through the propulsion room. Space required for main engines is reserved from lowest two decks at the amidships.

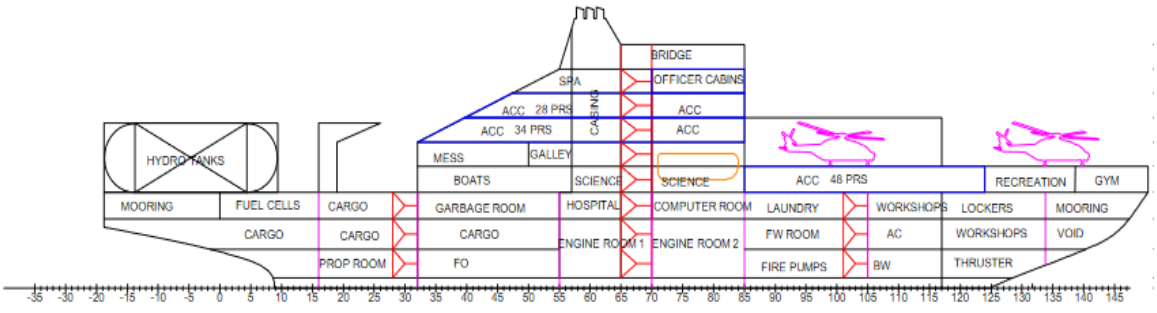

Figure 1.5 Space reserved for different applications.

1.4 Hull features

As an icebreaking vessel, Khione has full, spoon-type bow which enables efficient operation in thick ice. The bow has a stem angle of about 25 degrees, which excerts a maximum amount of vertical force into the ice (Figure 1.6).

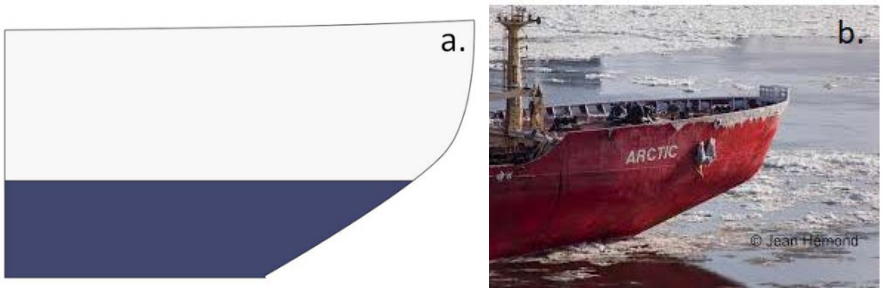

Figure 1.6 a. Basic spoon bow geometry b. Icebreaker with spoon bow

Compared to steeper bows, this arrangement reduces the profile area of the hull and leads to relatively short length between perpendiculars. This leads to lower Reynolds number along the hull and higher wave-making resistance at high speeds. The fullness of the bow shifts the longitudal center of buoyancy forwards of amidships. A wedge at the very stem of the bow helps to divert broken ice to sides, but also increases resistance. Naturally, spoon bow excludes the bulbous bow, which further increases the expected wave-making resistance.

Stern geometry follows that of a typical icebreaker. It is long, streamlined, and the aft section of the stern has gentle rise to accommodate thrusters. The propeller inflow should come from beneath the ship, as very little ice is pushed under the ship. As some ice floes are still expected to reach the propeller, a sufficient clearance between the blades and the hull must be ensured to prevent high local stresses on the hull due to ice. From the hull shape perspective, the stern shoulder area is crucial for good maneuvering characteristics. If the stern shoulders break ice by bending instead of crushing, the ship turns better as the resisting force for turning is this way minimized. (Riska, 2010)

Midbody has no parallel sections, since they are not effective in terms of ice-breaking performance. The ship has a moderate block coefficient of about **0,65** and high freeboard, translating into good open water stability characteristics. At present, no bilge keels or other anti-roll devices are installed, and thus the team must evaluate the risk of parametric roll during the ship's voyage in northern North Atlantic. External appendages are unfavourable due to ice loads, which limits our options into various types of anti-roll tanks.

1.5 Literature Review

1.5.1 "Experimental Studies on Seakeeping and Maneuverability of Ships in Adverse Weather Conditions" (Cura-Hochbaum et al., 2017)

This article concerns an experiment consisting of 1300 model tests with 3 different hull types: a post-Panamax container vessel, a KVLCC2 tanker and a Ropax ferry. The purpose of the experiment is to evaluate the maneuvering and seakeeping performance in waves for these hulls. The results covered in this report are of the turning tests performed as well as the propulsion tests in waves.

The tests performed on turning in different sea states reveal relations between the time a certain turn takes and the direction of the waves. For example, the amount of time required to take a 90 degree turn is greatest in a beam sea state and smallest in a following sea state. The results are summarized in the table below.

Another result of interest is related to the propulsion, in particular to the adjustment to the propulsion properties required to keep the same mean forward speed in different wavelengths. It revealed that when the ship encounters long relative wavelengths, the propeller thrust, torque and revolutions have to be increased in comparison to calm seas to maintain the same speed. However, when the ship encounters short relative wavelengths, the adjustments to the propulsion system required are negligible. (Cura-Hochbaum et al., 2017, p. 149)

Table 1.4 Time and space required to turn in different sea states. (Cura-Hochbaum et al., 2017, p. 150)

	Calm Water	**Beam Seas**	**Head Seas**	**Following Seas**
Amount of time required for 90 degree turn	Second most amount of time	Most amount of time	Second least amount of time	Least amount of time
Amount of time required for 180 degree turn	Same as beam seas, less than following seas	Same as calm water, less than following seas	Less time than following seas	Most amount of time
Time and space required for turning circles	Less space and time required than following seas, more than beam and head seas	Least amount of time and space, tied with head seas.	Least amount of time and space, tied with beams seas.	Most amount of time and space

The turning results provide a way to check future calculations on the turning capability of Khione; if it is found that a 90 degree turn in beam seas takes the least amount of time of all sea states, there is reason to check whether or not the calculations have been done correctly. More importantly though, the article shows that turning in following seas takes the most amount of space, which makes following seas the limiting case for which the ship's maneuvering system should be designed; if the ship can turn within a limited amount of space in following seas, it should be able to make the same turn in all other sea states as well. The propulsion results show that a propulsion system designed for relatively long wavelengths should be capable of maintaining the ship's speed through smaller wavelengths and calm seas as well. The advantage here is that this saves the time that would be required to evaluate the performance in short wavelengths, though some calculations will be necessary to confirm that this assumption is valid. All this being said, one should be note that there is no guarantee that the results from this article are valid for Khione. The results serve as guidelines but they should never be a replacement for sound judgement.

1.5.2 Article 2: "Open Water Resistance and Seakeeping Characteristics of Ships with Icebreaking Bows" (Moton, 1991)

This article covers an open water dynamics experiment on 5 different ice breaking bows, all the same type with slight adjustments to the flare angle (β) and the waterline angle (α), both at 10% LPP aft of the forward perpendicular. These angles were determined to be significant to icebreaking performance; in general increasing these angles improves icebreaking capability, however β should not exceed about 45°. In the table below, the angles of each of the 5 bows are summarized.

Table 1.5: Flare and waterline angles of the 5 different bow shapes. (Moton, 1991, p. 39)

Bow	**Flare angle (β) [°]**	**Waterline angle (α) [°]**
1 (Baseline)	24.5	20.5
2	31.5	22.0
3	18.75	16.5
4	36.25	23.0
5	42.5	26.25

It should be noted that bow 3 represents the smallest angles that still allow for light icebreaking, while bow 5 represents a heavy icebreaker.

The first test was an open water resistance test in calm water. For lower ship speeds up until about 10 kts (341.21 m long ship), there is very little difference in the required power of each bow, while

at a ship speed of 15 kts bow 5 starts to require slightly more power than bow 1 (2.2% more). Interestingly enough, bows 2 and 4 require less power than bow 1, despite being fuller than bow 1. Bow 3 requires the least amount of power. (Moton, 1991, p. 55-56)

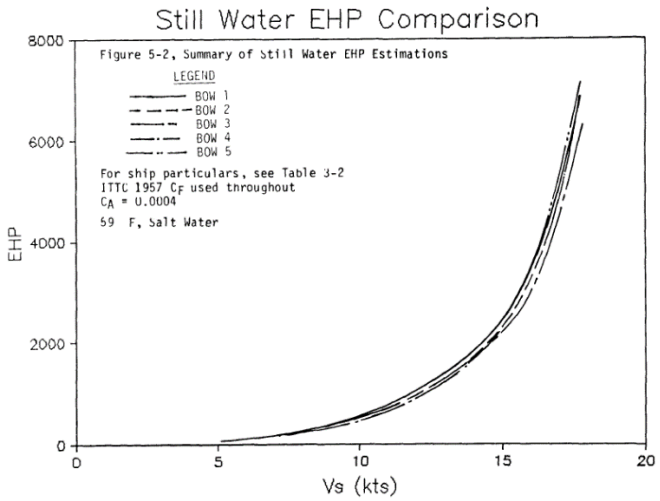

Figure 1.7 Still water power requirements for the 5 different bows. (Moton, 1991, p. 54)

As for seakeeping performance, experiments were done to measure the pitch, heave and relative bow movement response as well as added resistance in waves at two different speeds (4.01 fps and 2.67 fps). The former two are shown in Figure 1.8, with the following results: bow 5 has the smallest response in both pitch and heave, while bow 1 and 2 have the biggest response and bow 3 and 4 are in between. The results for the other speed (2.67 fps) are similar. (Moton, 1991, p. 62-69)

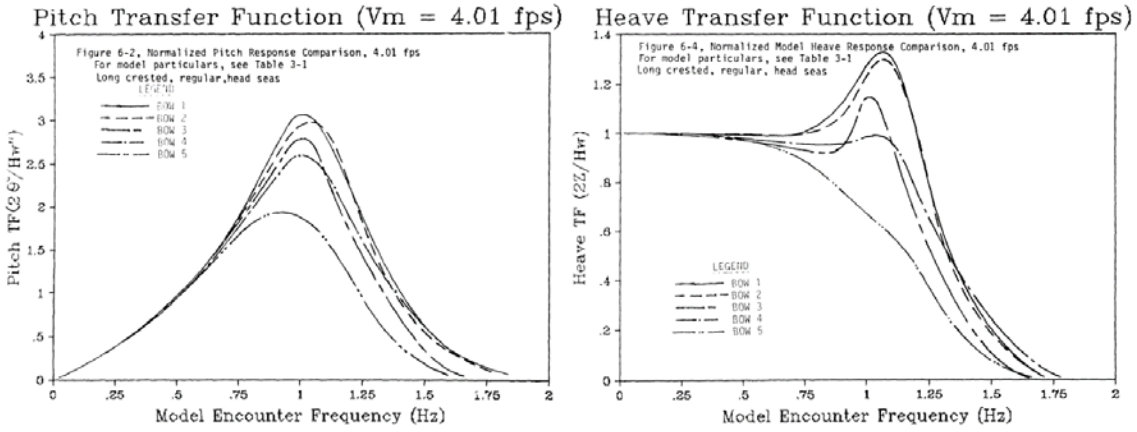

Figure 1.8 Pitch (left) and heave (right) response for different wave encounter frequencies at the highest of the two speeds. (Moton, 1991, p. 64 and p. 68)

The relative bow movement response (Figure 1.9) shows a similar shape to the pitch response, which is to be expected. Once again, bow 5 shows the lowest response while bow 2 shows the highest and bow 3 is in between. It is likely that the response of bow 1 and bow 4 would be close

to bow 2 and bow 3, respectively. The relative bow movement is an important response, as it reveals whether or not the bow of the ship will be submerged in certain wave encounter frequencies. (Moton, 1991, p. 73)

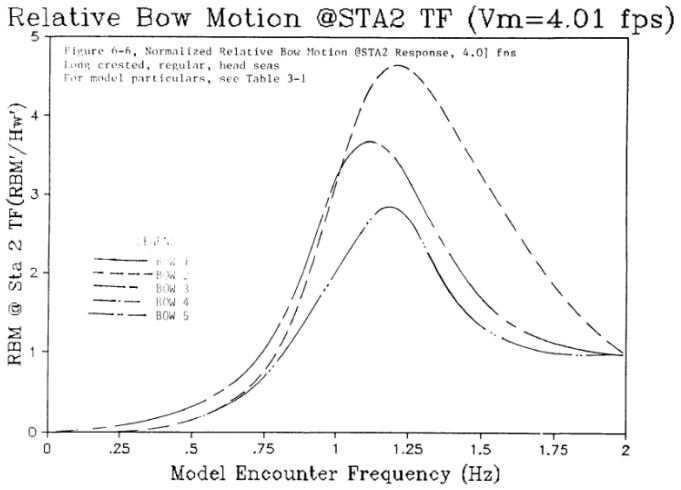

Figure 1.9 Relative bow motion for different wave encounter frequencies at the highest of two speeds. No results available for bow 1 and 4. (Moton, 1991, p. 71)

Finally, the added resistance from waves at different encounter frequencies is shown in Figure 1.10. The resistance is lowest for bow 5, and highest for bow 2 and 1 with bow 3 being in between. The experiment for bow 4 failed so there is no data for that. The curves follow a similar pattern to the pitch and heave response which is to be expected as added resistance is almost exclusively a function of these two responses. (Moton, 1991, p. 77)

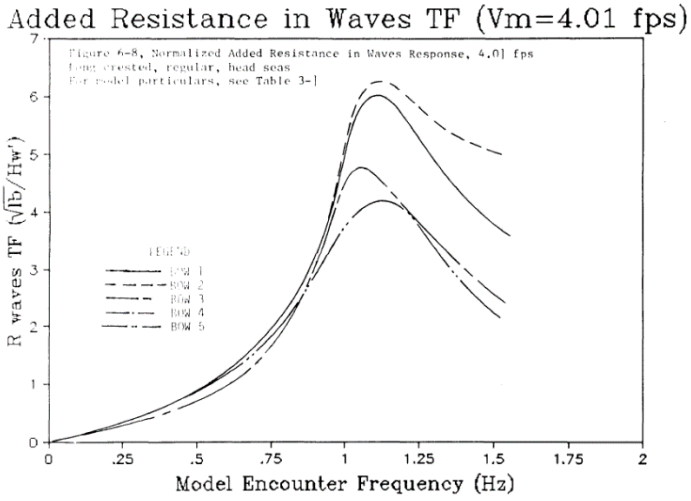

Figure 1.10 Added resistance in waves for different wave encounter frequencies at the highest of two speeds. No results available for bow 4. (Moton, 1991, p. 76)

The results from this paper show that improving a ship's ice breaking capability by increasing the flare and waterline angle leads to a decrease in heave and pitch response, as well as decreasing the added resistance, with only a slight calm water resistance penalty. Since Khione is also an icebreaker that should be able to sail in open water, the icebreaking bow must be changed to work properly in open water as well. But this paper suggests that improving the icebreaking capability of the bow also improves vertical seakeeping ability so no trade-off has to be made between the ice and open water vertical seakeeping performance. This result is unintuitive but because Aalto university has no access to many articles related to this topic, it is difficult to compare these results with other experiments. One should note that this article says nothing about roll, yaw and directional stability. That being said, this article gives insight in what effect improving the bow for horizontal seakeeping performance can have on the vertical seakeeping performance and resistance.

2 Environment

Khione (Holthuijsen, 2007) is an Arctic research and re-supply vessel operating in the Arctic waters. She shall be able to independently operate in the extreme conditions of the Arctic waters. Fig. 7 shows some of the predicted operating routes. Consequently, Khione shall be designed to resist such extreme conditions: 1) low temperature; 2) sea ice; 3) the Arctic storm; 4) long time of darkness; 5) large distance from supporting ports and infrastructures; 6) polar navigation. The condition 2 and 3 are relevant to the ship dynamics.

2.1 Water depth in the route

It is extremely important to be aware of the water depth in the route for the safety of Khione. The draft of the ship shall be designed to less than the smallest water depth with a reasonable margin. It is easy to understand that the draft should be less the water depth otherwise the ship would ground. The margin is a kind of distance between the water depth and ship bottom. When the ship voyages in the shallow water, the water velocity in between the bottom and seabed will be accelerated and the water pressure will be accordingly decreased in this region, which can be analyzed with the Bernoulli's principle. Consequently, the hull will sink with a specific magnitude. This phenomenon is called squat, which can be calculated by using the designed speed and hull form coefficients. The shallow water depth can also increase the resistance. In addition, the water depth also influences the wave pattern. As a result, different wave theories should be utilized according to the water depth to achieve precise structure-wave interaction, as shown in Fig. 2.1.

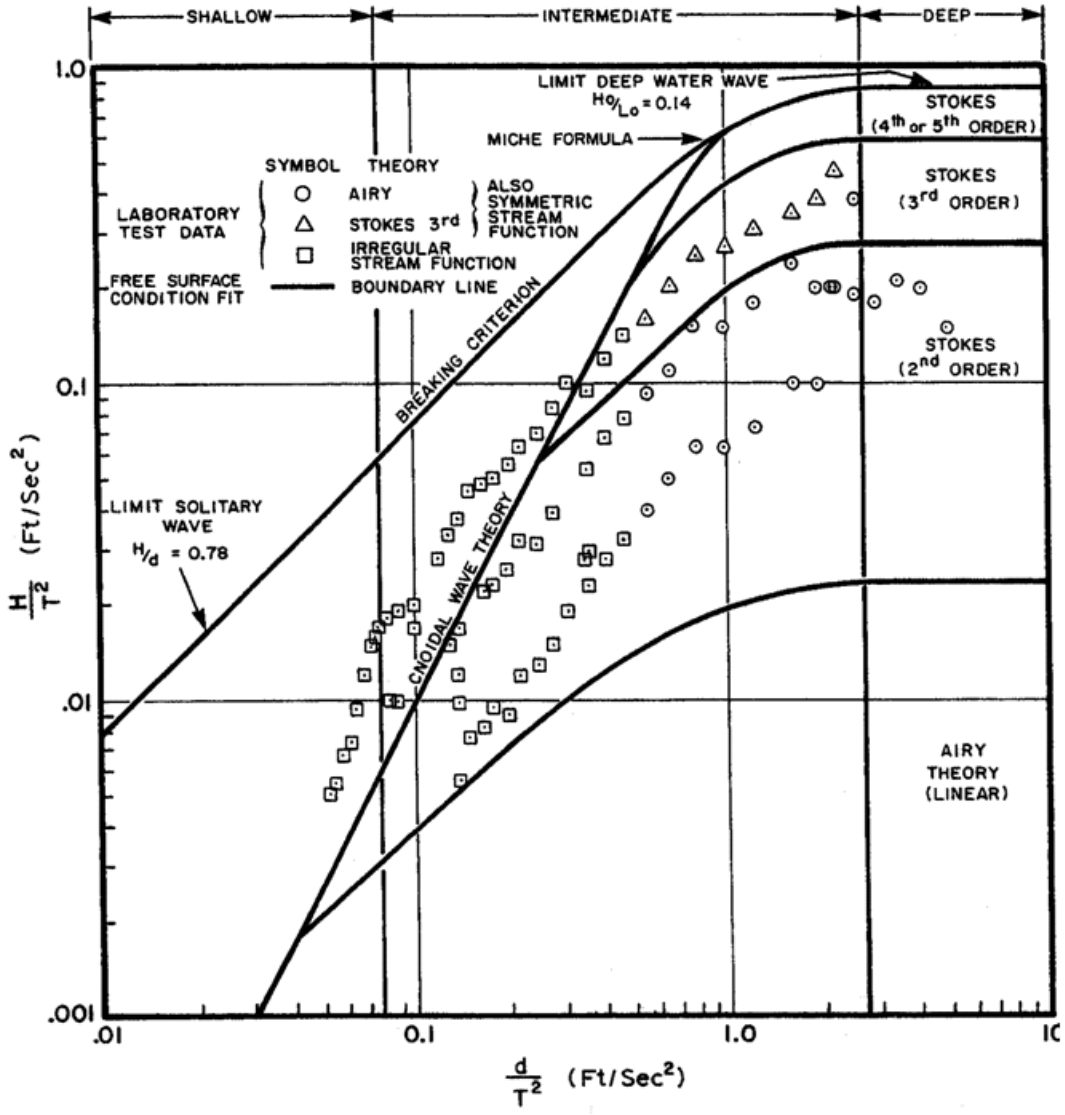

Figure 2.1 Ranges of validity for various wave theories. The horizontal axis is a measure of shallowness while the vertical axis is a measure of steepness (Chakrabarti, 1987)

The water depth in the open sea is usually larger than 1000 m so its influence can be ignored on the wave pattern. Fig. 2.2 shows the water depth in the North Atlantic between Iceland and Greenland. Thus, this section focuses on the water depth around three locations: Reykjavik, Aasiaat, and Resolute. Table 2.1 and Fig. 2.3 shows the water depth at berth of each port. There is no berth at Resolute so no depth information is shown in Table 2.1.

Table 2.1: Water depth at berth (http://ports.com/)

Port	Reykjavik	Aasiaat	Resolute
Water depth /m	7.1	7.1	NA

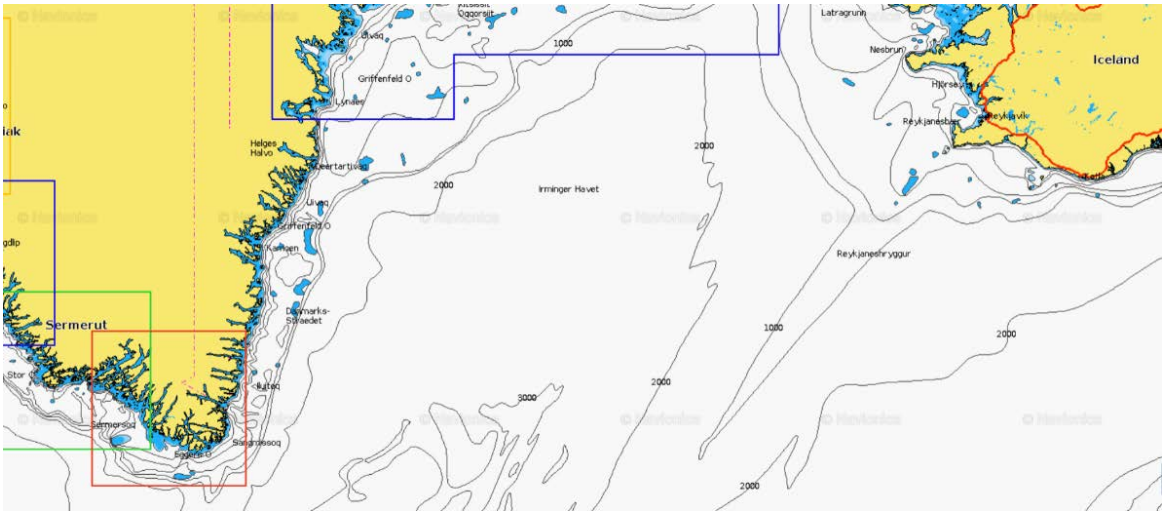

Figure 2.2 Water depth in the open sea between Iceland and Greenland. (www.navionics.com)

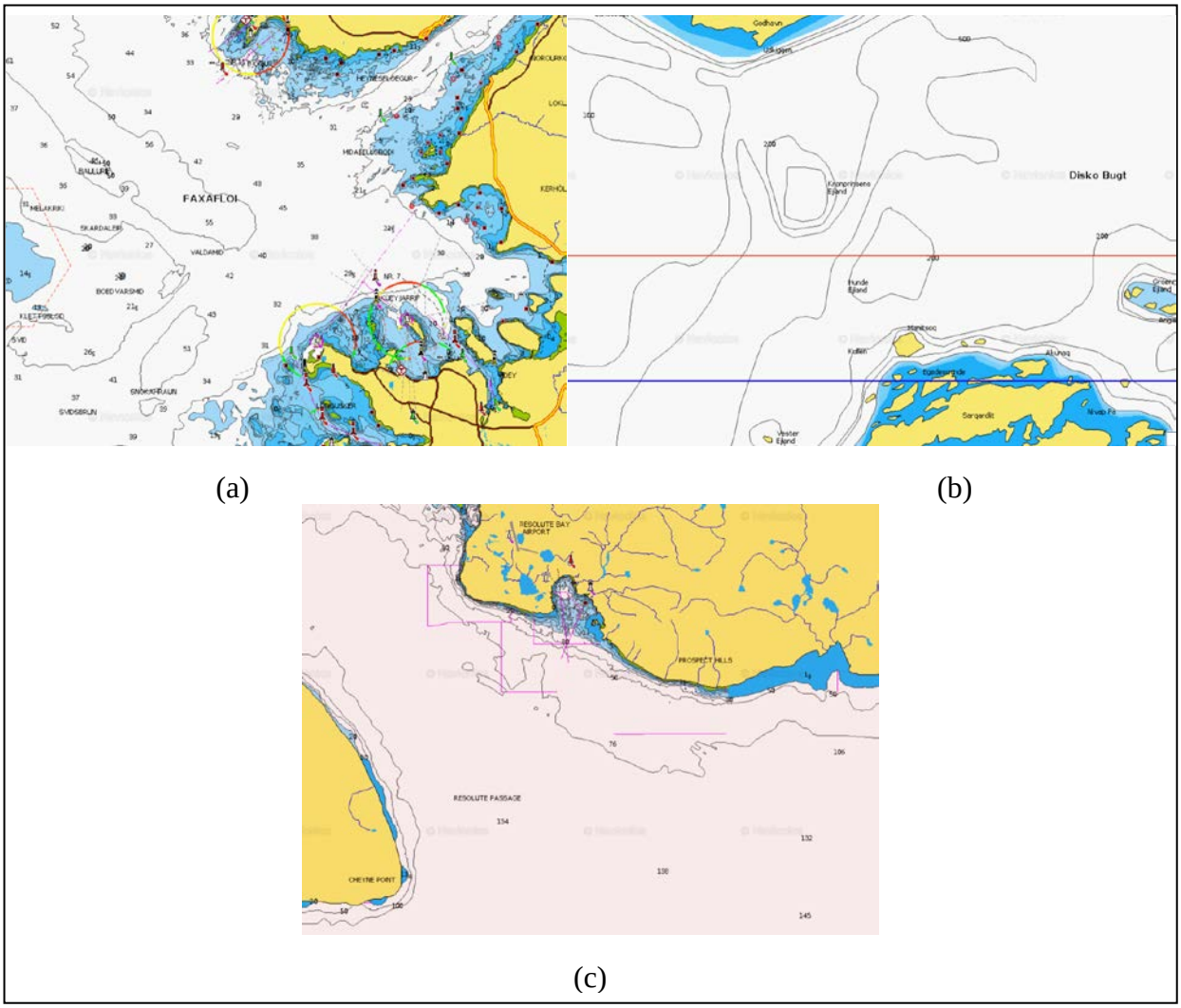

Figure 2.3 Water depth around Reykjavik, Aasiaat, and Resolute. (www.navionics.com)

2.2 Wind

The wind above the ocean seasonally varies in a year, which results in the seasonal variation of wind waves in the sea. Semedo et al. (2018) reported a study on the variation of wind-wave climate from 1979 to 2005. Fig. 2.4~2.7 present the seasonal variation of wind speed (average at 10 m above the sea surface), wave height, wave period, and wave direction, respectively.

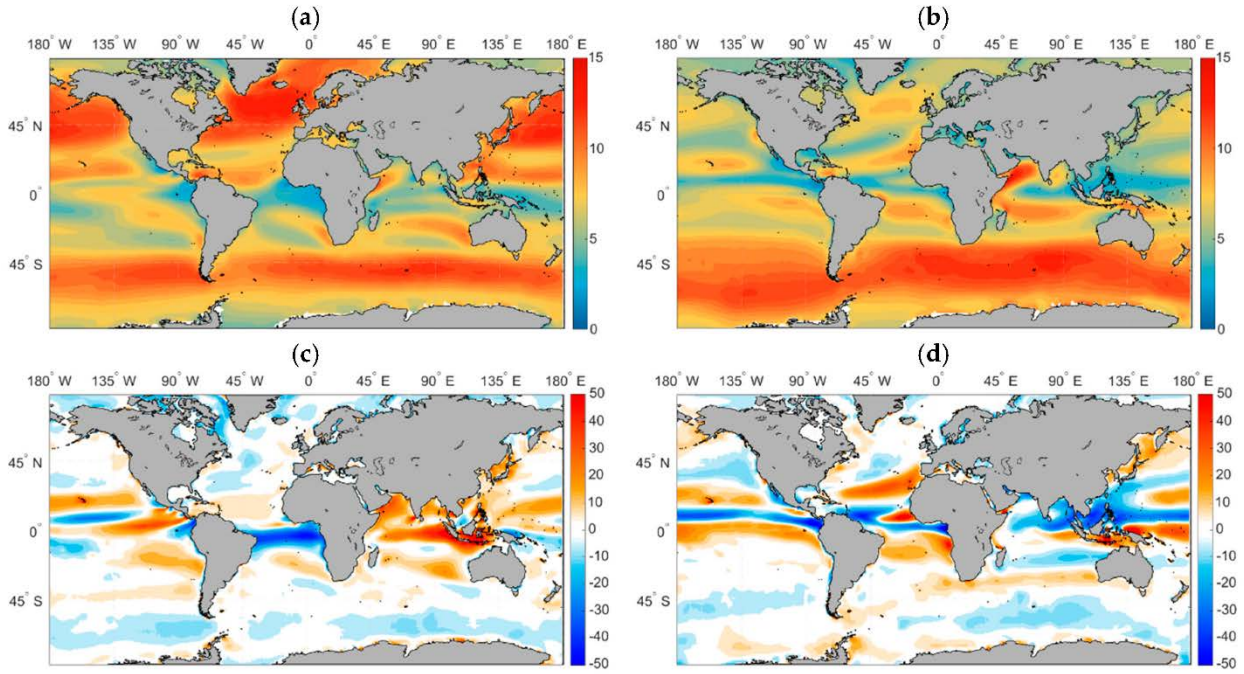

Figure 2.4 PC20-E 1979–2005 seasonal wind speed (U_{10}; s) means for (**a**) DJF and (**b**) JJA. PC20-E *Tm* (s) normalized differences to ERA-Interim (%; PC20-E minus reanalysis normalized by the reanalysis) for (**c**) DJF and (**d**) JJA.

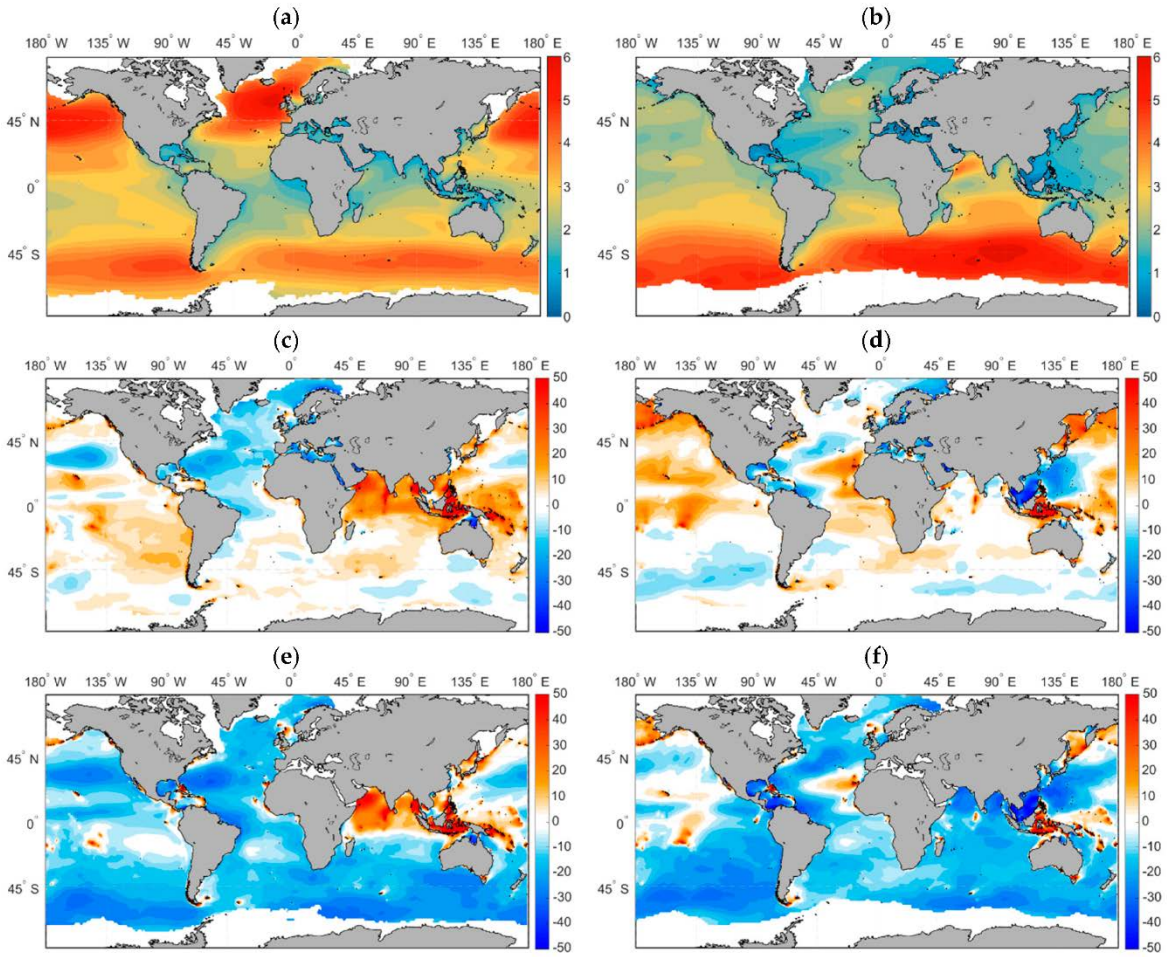

Figure 2.5 Present climate historic ensemble (PC20-E) 1979–2005 seasonal wave height (*Hs*; m) 95% percentile for (**a**) December–February (DJF) and (**b**) June–August (JJA). PC20-E *Hs* (m) normalized differences (%; PC20-E minus reanalysis normalized by the reanalysis) to ERA-Interim for (**c**) DJF and (**d**) JJA, and to Climate Forecast System Reanalysis (CFSR) for (**e**) DJF and (**f**) JJA.

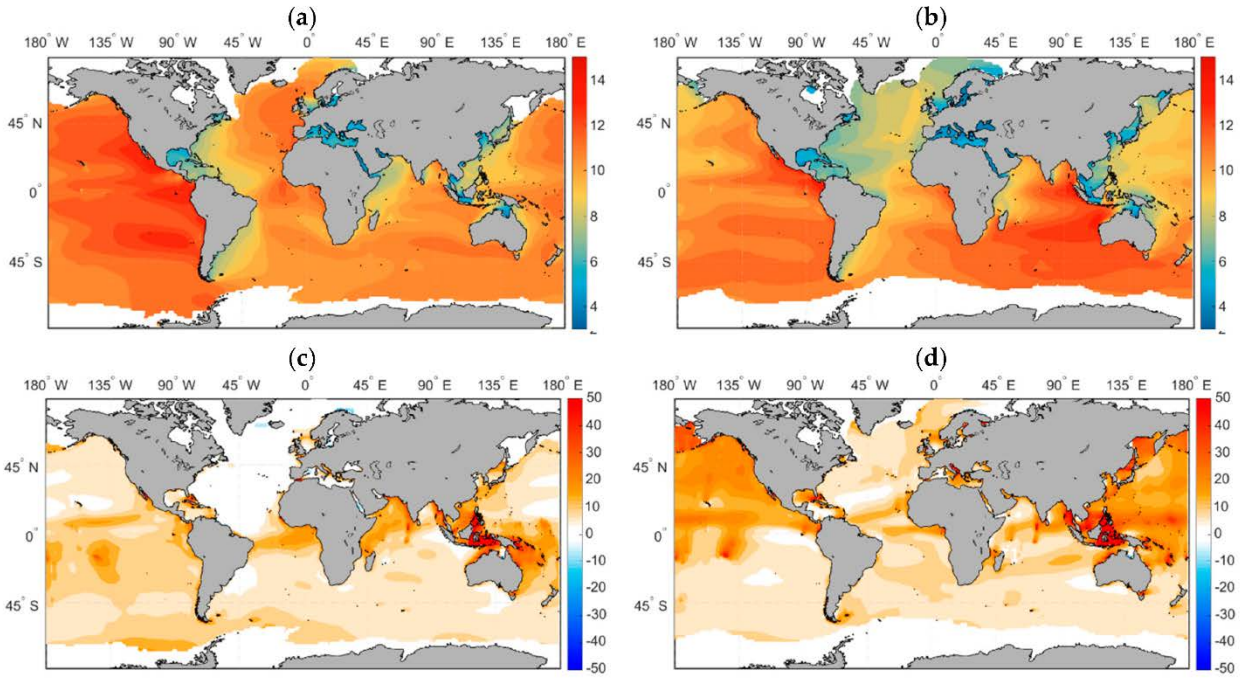

Figure 2.6: PC20-E 1979–2005 seasonal wave period (*Tm*; s) means for (**a**) DJF and (**b**) JJA. PC20-E *Tm* (s) normalized differences to ERA-Interim (%; PC20-E minus reanalysis normalized by the reanalysis) for (**c**) DJF and (**d**) JJA.

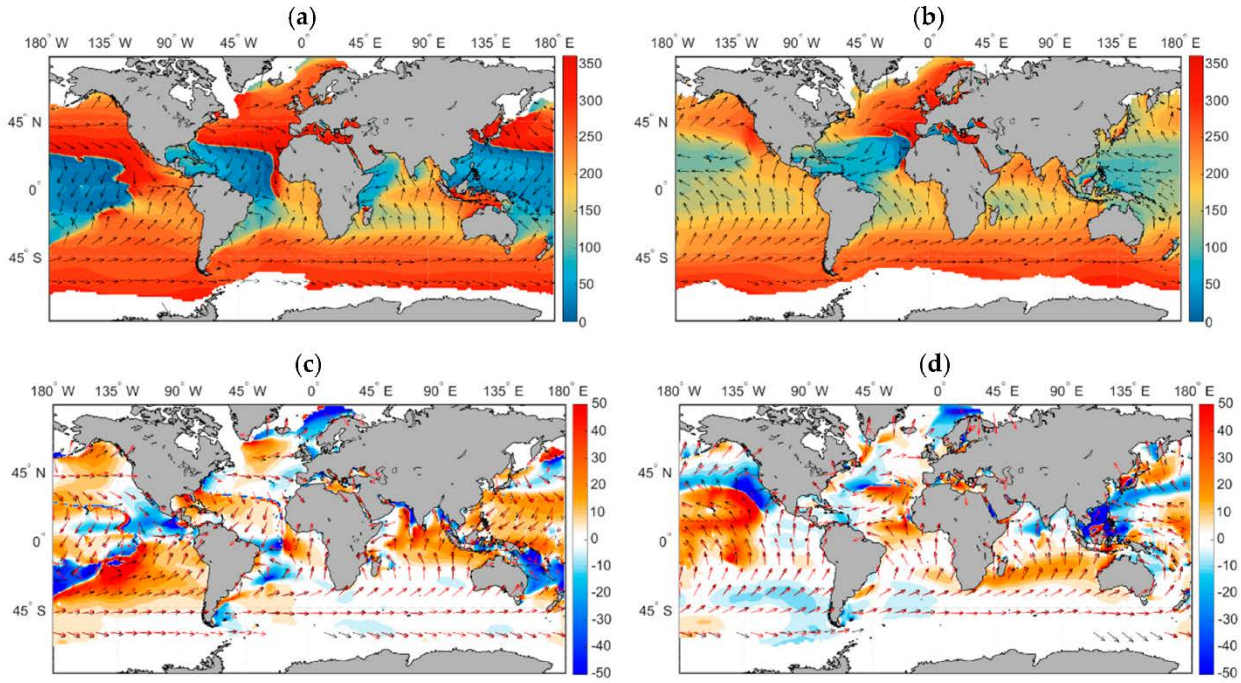

Figure 2.7 PC20-E 1979–2005 seasonal wave direction (θm) means for (**a**) DJF and (**b**) JJA (arrows not scaled). PC20-E differences to ERA-Interim, where positive and negative values represent anti-clockwise and clockwise differences, and black (red) arrows represent PC20-E (ERA-Interim) directions for (**c**) DJF and (**d**) JJA.

Fig. 2.4 ~2.7 show that the wave condition is much more severe from December to February. In addition, there is no wave information in the Baffin Bay during the winter because this area is nearly fully covered with sea ice. Therefore, the design of Khione should be in compliance with the wave condition in the North Atlantic, which is presented in Table 2.2. Thus, the highest wave height is 16.5 m. In addition, the wave period should be considered as well. The natural period of ships motion, especially the natural period of roll, should be designed away from the period of most dangerous sea states, from 10.5 s to 15.5 s. Special considerations should also be given to rogue waves, but as of present, there is no universally accepted design methodology that entails high rogue waves. A crude approach would be to increase the safety margin, but this might easily be too conservative and thus would hinder the performance of the ship.

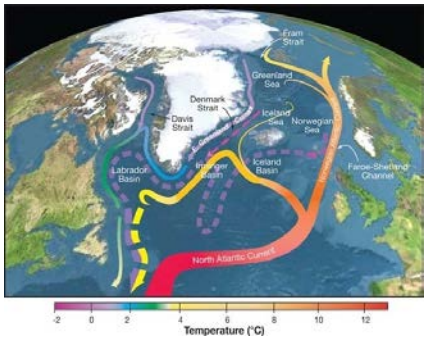

Figure 2.8 North Atlantic current. (Oceanographic Institution Science USGCRP)

2.3 Sea Ice

As to the sea ice, there is no sea ice out of Baffin Bay due to the North Atlantic current, as shown in Fig. 2.8. Therefore, the design only considers the ice condition in the Baffin Bay. By analyzing the ice data from 1981 to 2010, Canada Ice Service provides the annual ice coverage in the Northeast Canada. As shown in Fig. 2.9, the one-year ice exits in the Baffin Bay and the waters close to Resolute from October to the August of next year.

Table 2.2 Wave scatter diagram for the North Atlantic. (DNV, 2010)

Table C-2 Scatter diagram for the North Atlantic

T_Z (s)	3.5	4.5	5.5	6.5	7.5	8.5	9.5	10.5	11.5	12.5	13.5	14.5	15.5	16.5	17.5	18.5	Sum
H_S (m)																	
0.5	1.3	133.7	865.6	1186.0	634.2	186.3	36.9	5.6	0.7	0.1	0.0	0.0	0.0	0.0	0.0	0.0	3050
1.5	0.0	29.3	986.0	4976.0	7738.0	5569.7	2375.7	703.5	160.7	30.5	5.1	0.8	0.1	0.0	0.0	0.0	22575
2.5	0.0	2.2	197.5	2158.8	6230.0	7449.5	4860.4	2066.0	644.5	160.2	33.7	6.3	1.1	0.2	0.0	0.0	23810
3.5	0.0	0.0	34.9	695.5	3226.5	5675.0	5099.1	2838.0	1114.1	337.7	84.3	18.2	3.5	0.6	0.1	0.0	19128
4.5	0.0	0.0	6.0	196.1	1354.3	3288.5	3857.5	2685.5	1275.2	455.1	130.9	31.9	6.9	1.3	0.2	0.0	13289
5.5	0.0	0.0	1.0	51.0	498.4	1602.9	2372.7	2008.3	1126.0	463.6	150.9	41.0	9.7	2.1	0.4	0.1	8328
6.5	0.0	0.0	0.2	12.6	167.0	690.3	1257.9	1268.6	825.9	386.8	140.8	42.2	10.9	2.5	0.5	0.1	4806
7.5	0.0	0.0	0.0	3.0	52.1	270.1	594.4	703.2	524.9	276.7	111.7	36.7	10.2	2.5	0.6	0.1	2586
8.5	0.0	0.0	0.0	0.7	15.4	97.9	255.9	350.6	296.9	174.6	77.6	27.7	8.4	2.2	0.5	0.1	1309
9.5	0.0	0.0	0.0	0.2	4.3	33.2	101.9	159.9	152.2	99.2	48.3	18.7	6.1	1.7	0.4	0.1	626
10.5	0.0	0.0	0.0	0.0	1.2	10.7	37.9	67.5	71.7	51.5	27.3	11.4	4.0	1.2	0.3	0.1	285
11.5	0.0	0.0	0.0	0.0	0.3	3.3	13.3	26.6	31.4	24.7	14.2	6.4	2.4	0.7	0.2	0.1	124
12.5	0.0	0.0	0.0	0.0	0.1	1.0	4.4	9.9	12.8	11.0	6.8	3.3	1.3	0.4	0.1	0.0	51
13.5	0.0	0.0	0.0	0.0	0.0	0.3	1.4	3.5	5.0	4.6	3.1	1.6	0.7	0.2	0.1	0.0	21
14.5	0.0	0.0	0.0	0.0	0.0	0.1	0.4	1.2	1.8	1.8	1.3	0.7	0.3	0.1	0.0	0.0	8
15.5	0.0	0.0	0.0	0.0	0.0	0.0	0.1	0.4	0.6	0.7	0.5	0.3	0.1	0.1	0.0	0.0	3
16.5	0.0	0.0	0.0	0.0	0.0	0.0	0.0	0.1	0.2	0.2	0.2	0.1	0.1	0.0	0.0	0.0	1
Sum	1	165	2091	9280	19922	24879	20870	12898	6245	2479	837	247	66	16	3	1	100000

The H_s and T_z values are class midpoints.

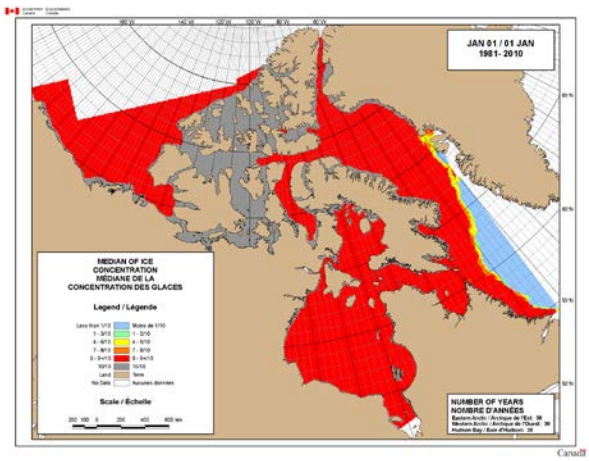
JAN 01 / 01 JAN
1981- 2010
MEDIAN OF ICE CONCENTRATION
MÉDIANE DE LA CONCENTRATION DES GLACES
Legend / Légende
Scale / Échelle
NUMBER OF YEARS
NOMBRE D'ANNÉES

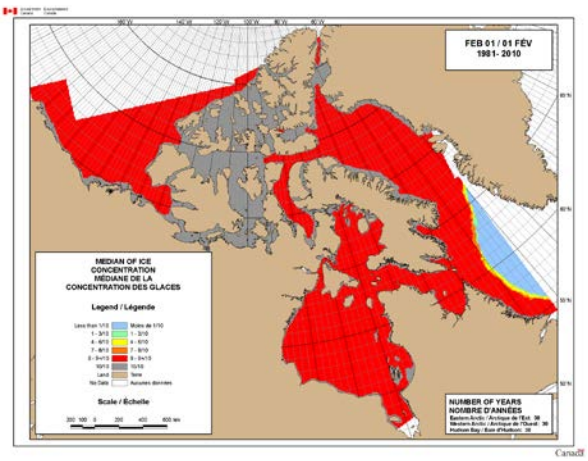
FEB 01 / 01 FÉV
1981- 2010
MEDIAN OF ICE CONCENTRATION
MÉDIANE DE LA CONCENTRATION DES GLACES
Legend / Légende
Scale / Échelle
NUMBER OF YEARS
NOMBRE D'ANNÉES

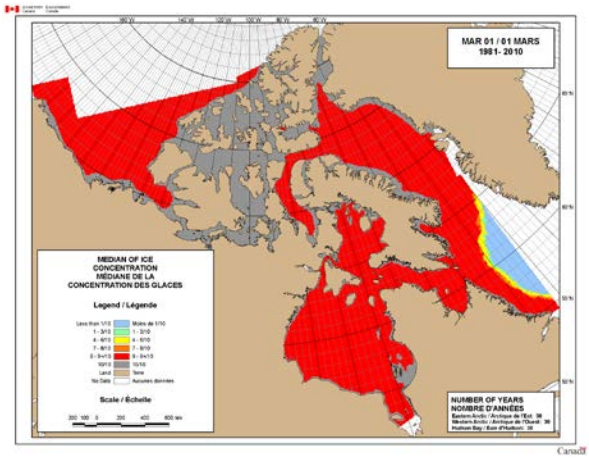
MAR 01 / 01 MARS
1981- 2010
MEDIAN OF ICE CONCENTRATION
MÉDIANE DE LA CONCENTRATION DES GLACES
Legend / Légende
Scale / Échelle
NUMBER OF YEARS
NOMBRE D'ANNÉES

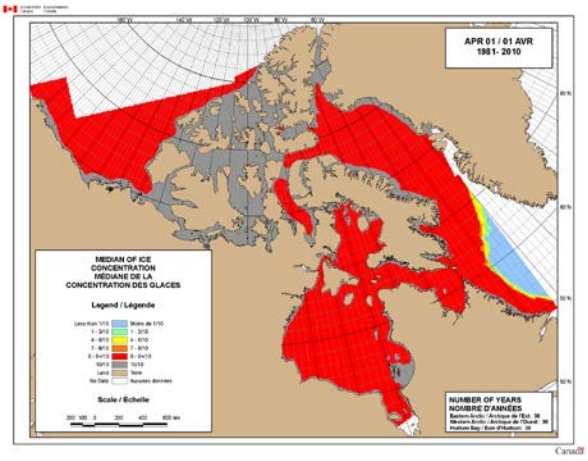
APR 01 / 01 AVR
1981- 2010
MEDIAN OF ICE CONCENTRATION
MÉDIANE DE LA CONCENTRATION DES GLACES
Legend / Légende
Scale / Échelle
NUMBER OF YEARS
NOMBRE D'ANNÉES

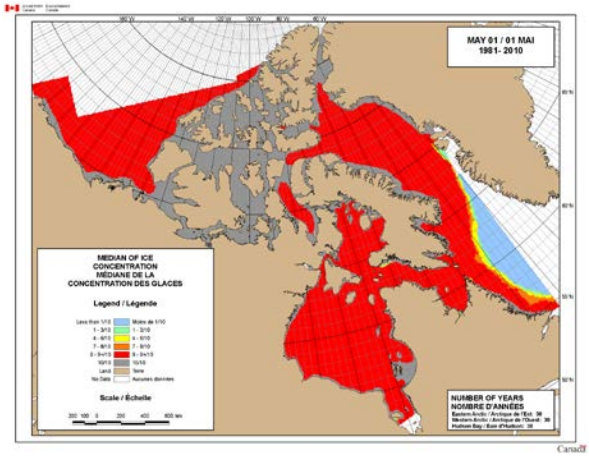
MAY 01 / 01 MAI
1981- 2010
MEDIAN OF ICE CONCENTRATION
MÉDIANE DE LA CONCENTRATION DES GLACES
Legend / Légende
Scale / Échelle
NUMBER OF YEARS
NOMBRE D'ANNÉES

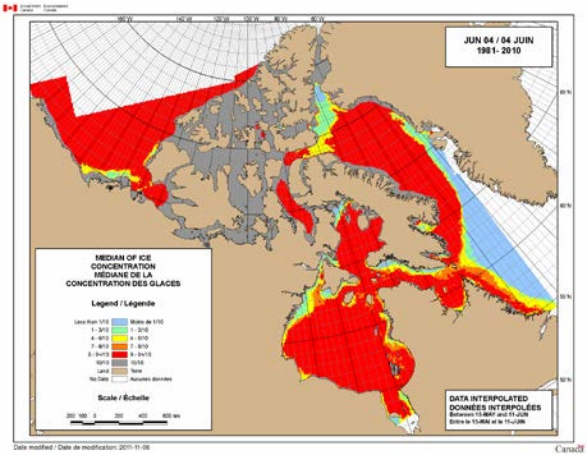
JUN 04 / 04 JUIN
1981- 2010
MEDIAN OF ICE CONCENTRATION
MÉDIANE DE LA CONCENTRATION DES GLACES
Legend / Légende
Scale / Échelle
DATA INTERPOLATED
DONNÉES INTERPOLÉES

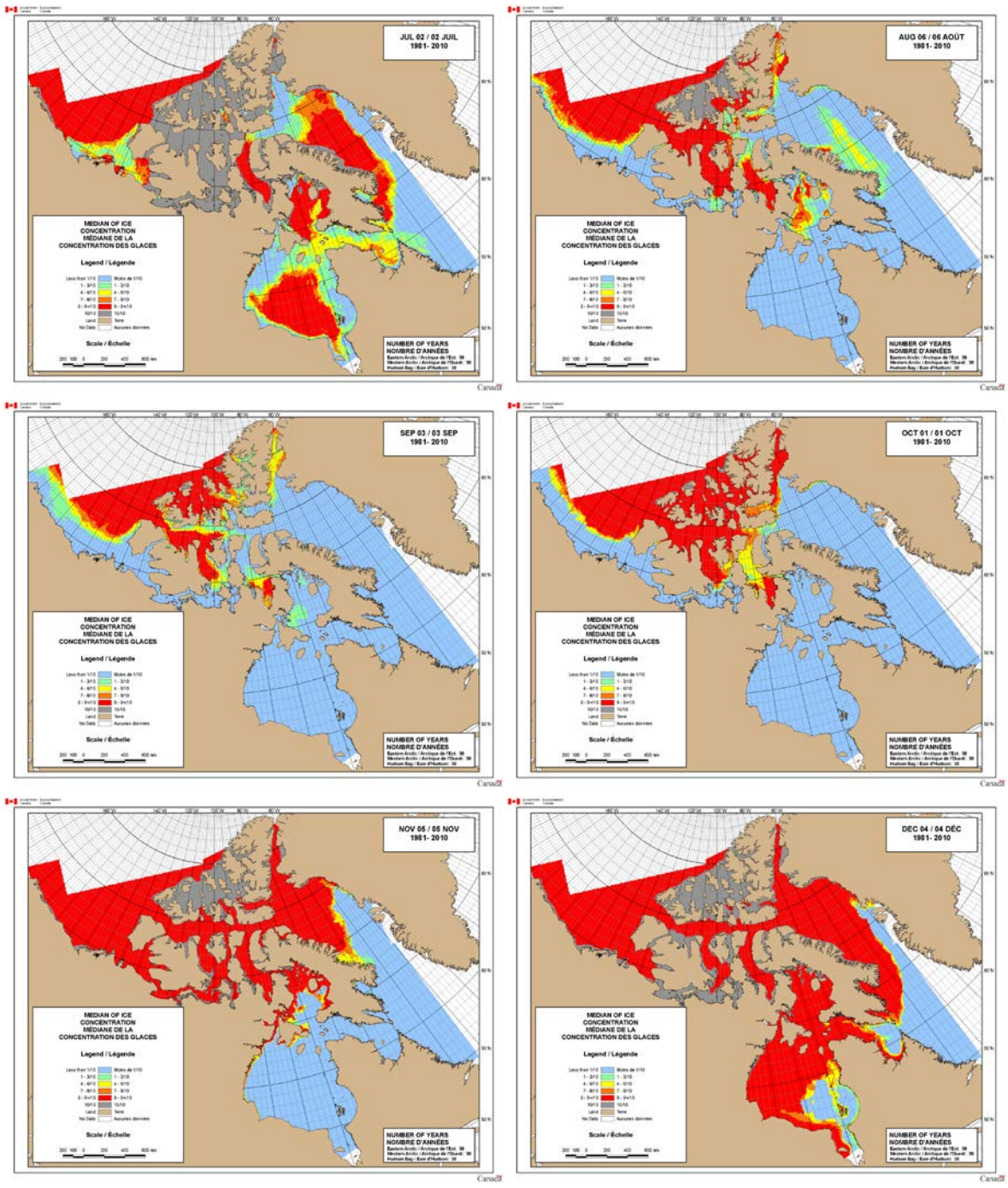

Figure 2.9 Ice concentration in the Northeast Canada (Canada Ice Service, 2020)

According to the annual arctic report of Canada Ice Service, the maximum ice thickness is over 1.2 m at the fast ice around Resolute, as shown in Fig. 2.10. Khione's ice breaking capability is designed as 1.65 m so she is capable of serving in the waters of Northeast Canada.

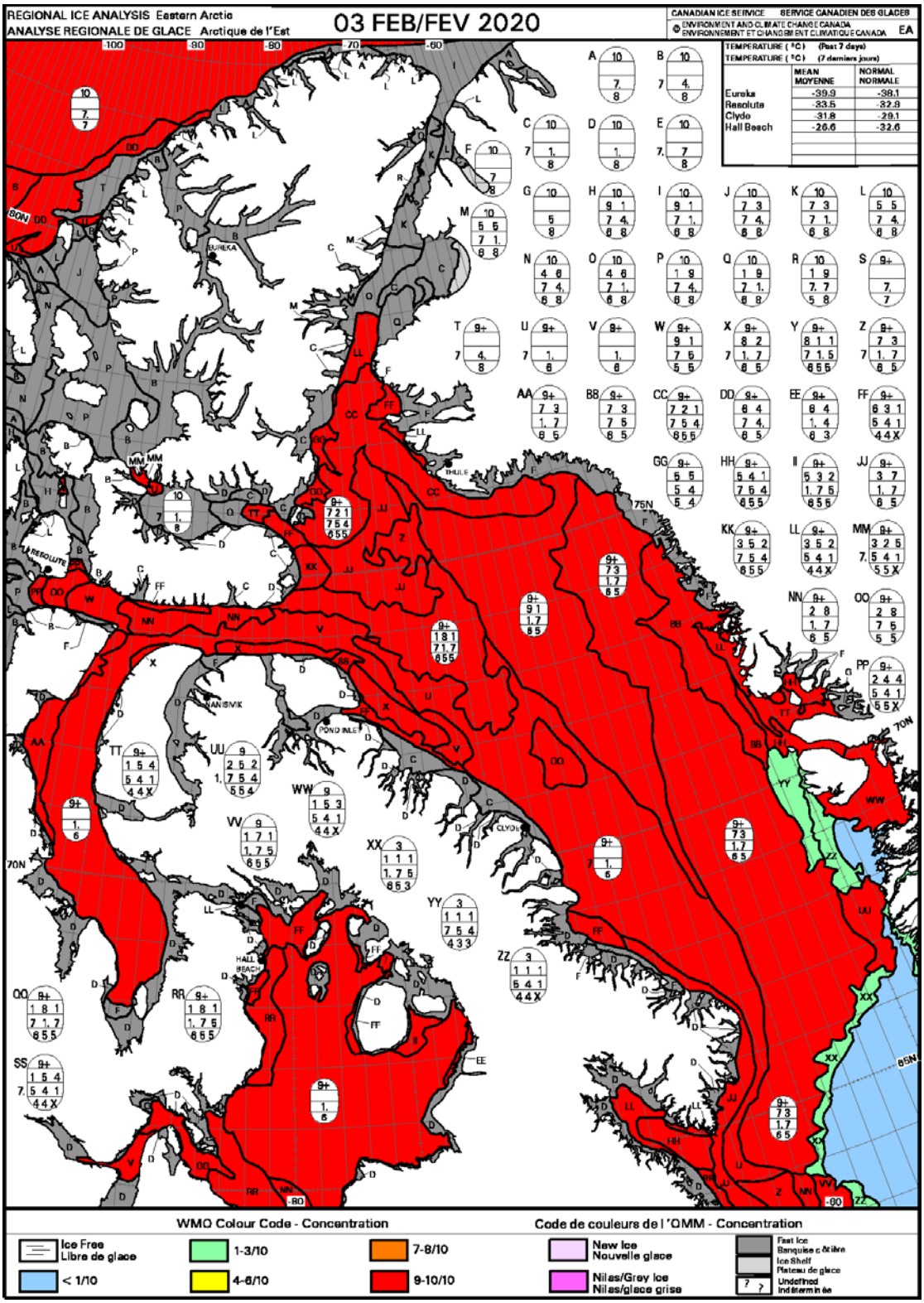

Figure 2.10 Sea ice chart in February 2020. (Canada Ice Service, 2020)

2.4 Shallow and Deep Water Waves

During a typical journey between Resolute and Reykjavik one encounters both deep and shallow water waves. Both types of waves can be estimated using linear wave theory. The biggest difference between linear waves in shallow and deep water is that in shallow water the wavelength depends only on the water depth "d" while in deep water the wavelength depends on the wave period "T". In particular:

$$\lambda_{shallow} = 2\pi d \tag{2.1}$$

$$\lambda_{deep} = \frac{gT^2}{2\pi} \tag{2.2}$$

The wavelength can then be used to calculate the wave number "k", which in turn can be used to find a sinusoidal equation for the water elevation "ζ" as shown below:

$$k = \frac{2\pi}{\lambda} \tag{2.3}$$

$$\zeta(x) = \zeta_0 sin(kx) \tag{2.4}$$

In which "ζ_0" is the wave amplitude, which is half the significant wave height. Data on the significant wave height around the world is gathered in the "Global Wave Statistics" by the BMT Group (BMT, 1986). This data is presented in the form of different measured wave heights their zero down period in different areas around the world, presented in Fig. 2.11. In the case of Khione the relevant areas are 2, 3, 8 and 9, which are all part of the North Atlantic.

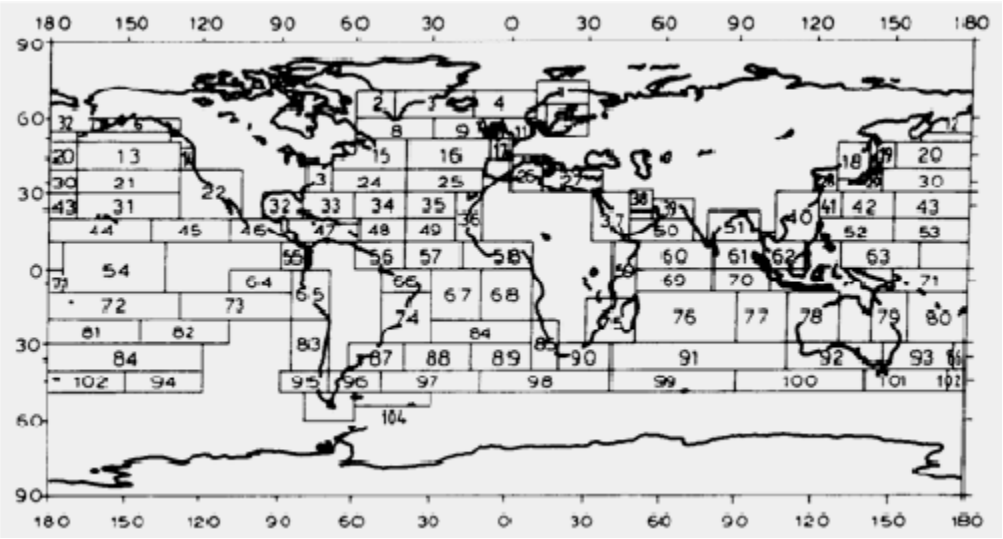

Figure 2.11 Global Wave Statistics zone designation (Hogben, et al., 1986).

Shallow Water Waves

In Fig. 2.12 a number of shallow water waves are sketched, based on the water depths presented in Fig. 2.3. The wave height for all these waves is 13 m, which is the maximum wave height in area 3, around Reykjavik, according to BMT. This is likely an overestimation of the true wave height, because the BMT wave heights may have been measured in deep water and not shallow waters.

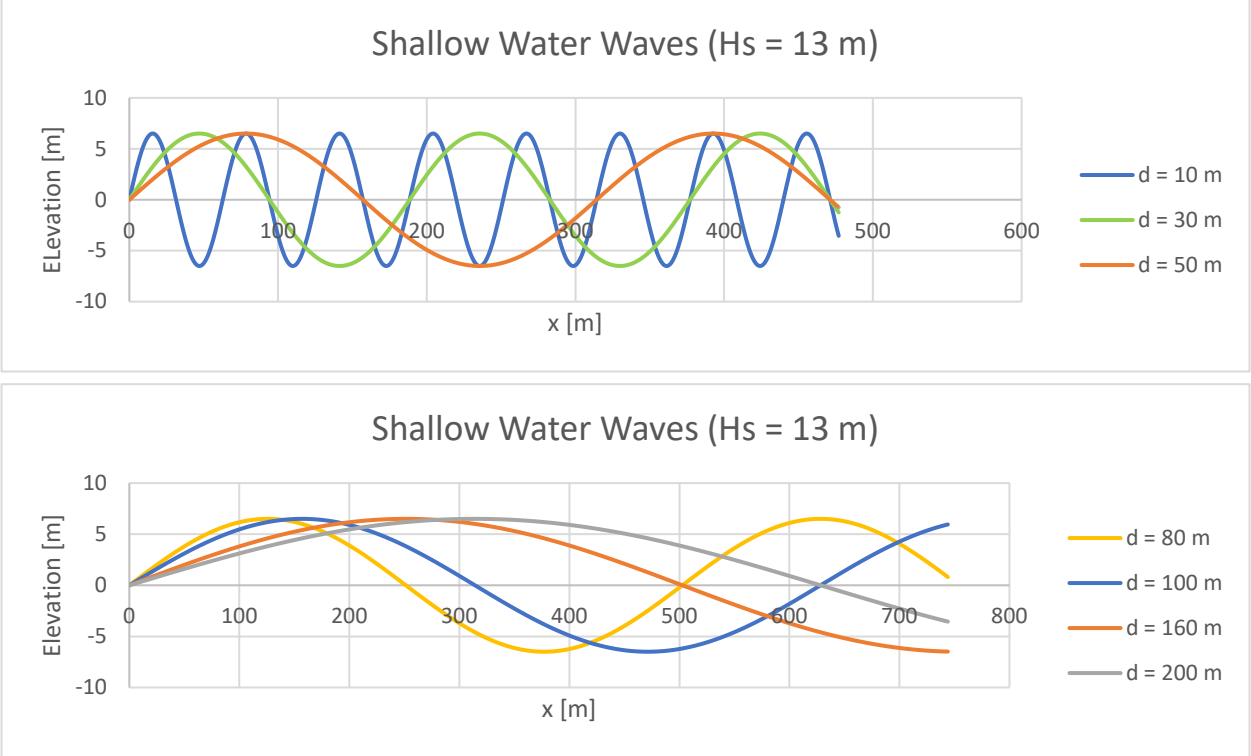

Figure 2.12 Shallow water waves based on depths found in Figure 2.3. Wave height is highest in area 3 (around Iceland). (BMT, 1986)

Deep water waves

For deep water waves the BMT Global Wave Statistics are directly used, assuming that all the BMT waves measured were measured in deep water. This is likely true, as area 8 and 9 are nearly entirely open sea and the depths in area 2 and 3 are shown to be mostly over 500 m in Fig. 2.13 and Fig. 2.2 respectively. Fig. 2.14 shows the highest wave height and associated period in area 9 at different seasons, the highest waves occurring in winter. Fig. 2.15 shows the annual highest wave height in area 2, 3, 8 and 9, their associated period and the seasons at which they occur. The highest wave heights of area 3, 8 and 9 are the same, being 13 m but the period of these waves is different.

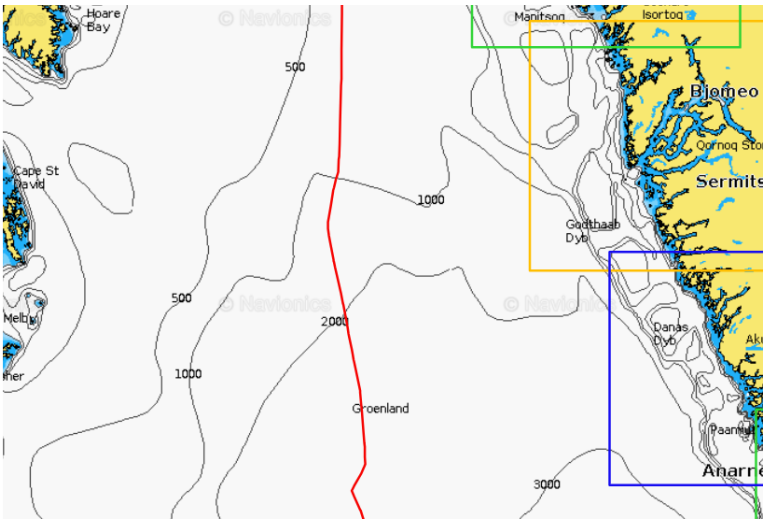

Figure 2.13 Water depth around Greenland in BMT area 2. (www.navionics.com)

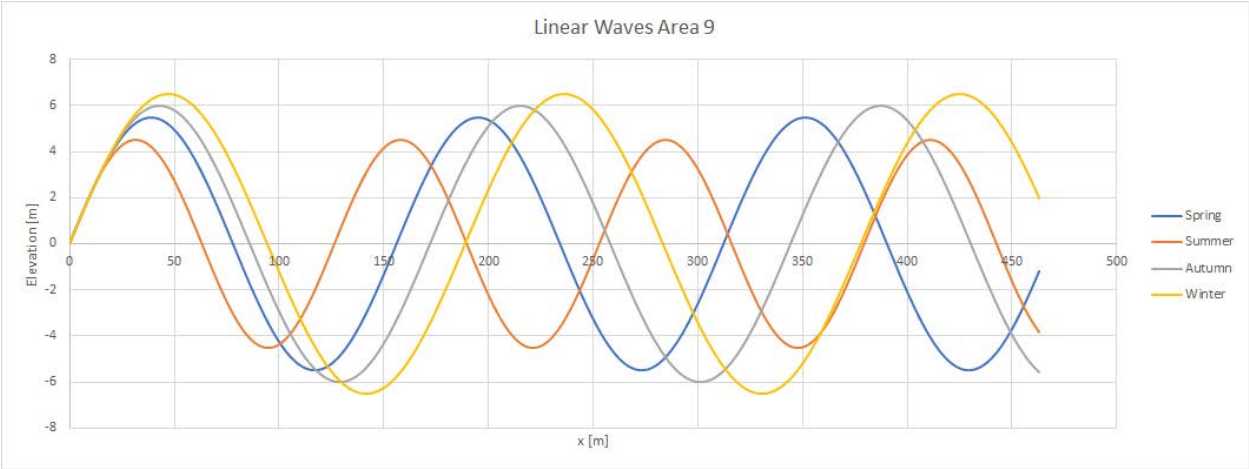

Figure 2.14 Linear waves in area 9 for different seasons. The wave height is the highest in that season, the period is based on the zero crossing period associated to the highest wave height. (BMT, 1986).

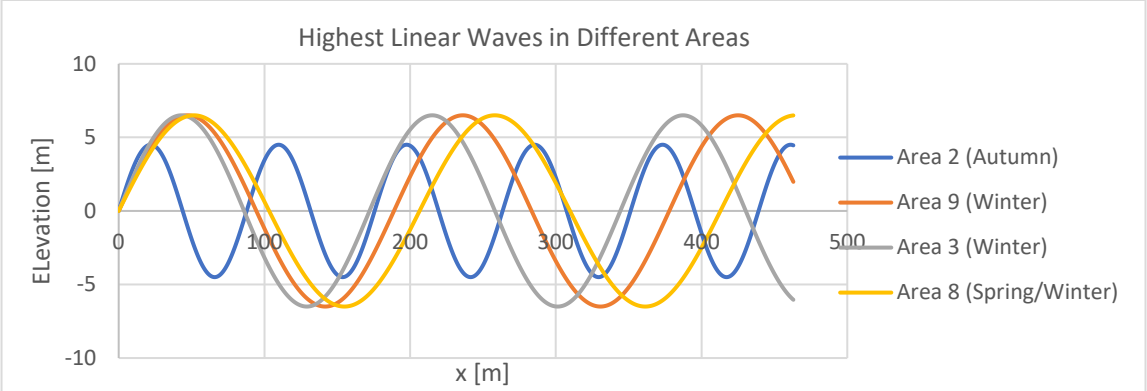

Figure 2.15 Linear waves in area 2, 3, 8 and 9 for different seasons. The wave height is the highest in that area during the entire year, the period is based on the zero crossing period associated to the highest wave height. (BMT, 1986)

Now one may note that the highest waves presented in Fig. 2.15 are 13 m, while the highest waves in the North Atlantic were mentioned to be 16.5 m in Section 2.2. This is probably because area 2, 3, 8 and 9 do not encompass the entire North Atlantic an these higher waves may have been measured in another area. For completeness and because the ship will be designed for 16.5 meters high waves, the highest waves in area 9 and the highest wave in the North Atlantic are shown in Fig. 2.16.

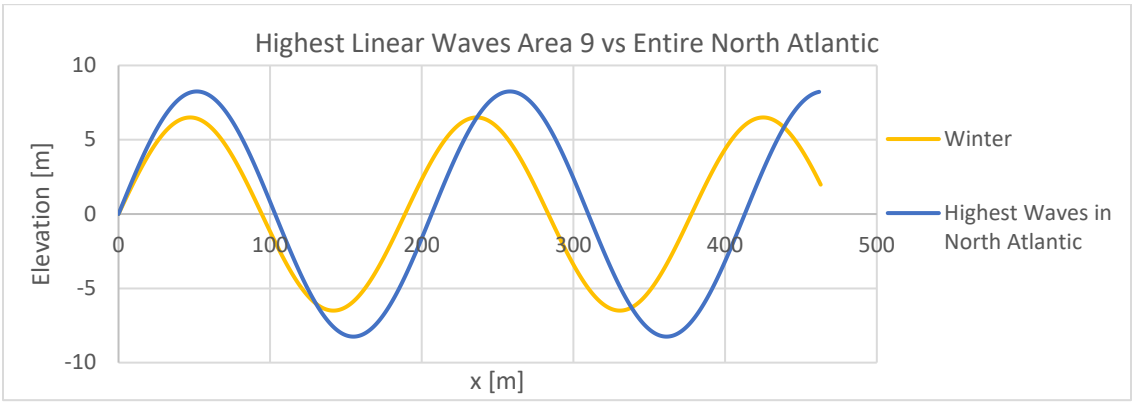

Figure 2.16 Highest linear wave in area 9 and entire North Atlantic. (BMT, 1986) and (DNV, 2010)

2.5 Wave spectra

Ocean waves are random and difficult to describe and analyze. To ease the analysis, time series of the waves are converted into frequency domain. Forming wave spectra is more practical for engineering purposes than the original time series. However, ocean waves are complicated and very variable, which causes challenges for the wave spectra formation. In order to solve this problem, so called idealized wave spectra have been developed. These spectra attempt to describe the ocean wave spectra based on variables like wind speed, fetch, characteristic period and

significant wave height. Typically, deep seas and constant wind speeds are assumed (Holthuijsen, 2007).

Commonly used idealized wave spectrums are Pierson-Moskowitz spectra, including its modifications like ISSC spectra, and JONSWAP spectra. Selection of suitable spectra for each ship should be done based on operational profile of the vessel. In case of our ship, the operational profile is varying because of the nature of the ship's mission. In purpose to make the ship suitable for all ocean areas, assessment of the ship in terms of most harsh i.e., North Atlantic sea conditions should be considered. Thus, in choosing of the suitable idealized wave spectra for the ship, features of the North Atlantic must be considered.

Pierson-Moskowitz spectrum assumes constant wind blowing steadily over large area, thus assuming fully developed conditions. Only parameter for the wave spectrum is wind speed. This spectrum has been derived based on measurements in the Northern Atlantic Ocean. On other hand, JONSWAP (Joint North Sea Wave Observation Project) spectrum is derived on basis of the North Sea. In case of limited fetch conditions, differing from Pierson-Moskowitz, JONSWAP spectrum should be considered. The purpose of the spectrum is to represent wave conditions in areas with limited fetch. The difference between the spectrums is that JONSWAP assumes that sea state is never completely developed, and the shape of the spectrum varies as a function of fetch. Fig. 2.17 illustrates the difference between Pierson-Moskowitz spectrum and JONSWAP spectrum. JONSWAP has more pronounced peak which grows with the fetch. Effect of the fetch illustrated in Fig. 2.18.

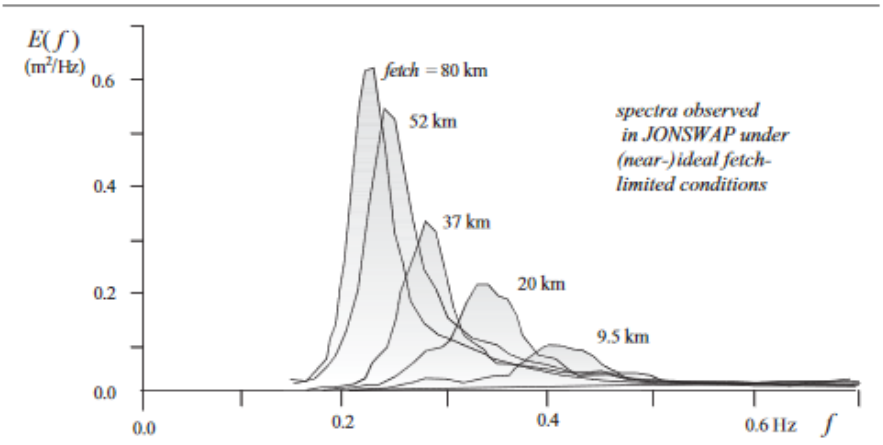

Figure 2.17 Comparison of wave spectrums. (Abankawa, et al., 2015)

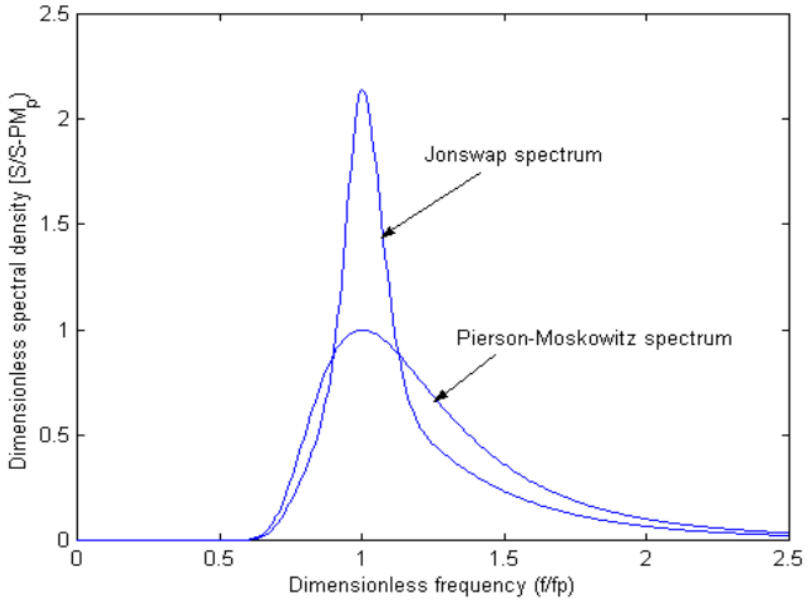

Figure 2.18 Influence of fetch on JONSWAP. (Holthuijsen, 2007)

Holthuijsen (2007) states that in idealized conditions Pierson-Moskowitz should be used for fully developed seas and JONSWAP for young seas. As we want to analyze performance of our ship in worst case scenario, the North Atlantic is chosen as a benchmark for the wave spectrum selection. In North Atlantic fetch is sufficiently large to be not relevant and thus the sea is considered as fully developed (Holthuijsen, 2007). The ocean in the North Atlantic region is also sufficiently deep to not have influence on waves. Based on previous reasoning sensible choice for us is spectrum developed for the Northern Atlantic fully developed conditions i.e., Pierson-Moskowitz spectra.

2.6 Literature Review

2.6.1. Book Chapter: Ochi (2005) – Ocean waves: stochastic approach, Chapter 5: Sea severity

The sea severity is a key concept related to design loads of marine structures. The most relevant theories and principles of the field for Khione are presented below.

Sea severity is used to measure quantities of the ocean waves that affect the design of marine systems. The designer must be aware of the severest (and the rarest) conditions that can occur in the system's lifetime. In addition to this, for systems prone to fatigue effects, one greatly benefits knowing the frequency of occurrence of all sea conditions, not just the severest. The most important and readily available quantity is the significant wave height H_s, and other quantities include average zero-crossing period T_0, wind speed etc.

Crudely, the stochastic approach in conducted as follows: the first step is to collect long term data to obtain the frequency of different significant wave heights and periods. In practice, measurement buoys measure the highest waves for period of hours. This means that the presentation of short-term effects is skewed, from frequency point of view. After the data has been collected, a suitable probability distribution function is developed and fitted into data. The statistical properties of the developed function can then be exploited to obtain the extreme event that the system will experience in its lifetime as well as the load distribution of milder events.

Wave height distributions

In his book, Ochi has picked a 3-year, 5000-sample observation data from the North Sea as an example case. He and various others have then developed models that fit this particular data. Corollary, said models are valid only for North Sea and they cannot be generalized elsewhere.

The simplest model is called the log-normal distribution, which fits a straight line to logarithmic cumulative wave height data. The validity of the model can be examined by plotting it with the observed data (Fig. 2.19). It is clear, that while it agrees well in lower wave heights, more extreme events deviate heavily from it; exactly the events that dictate the worst-case scenario of the system.

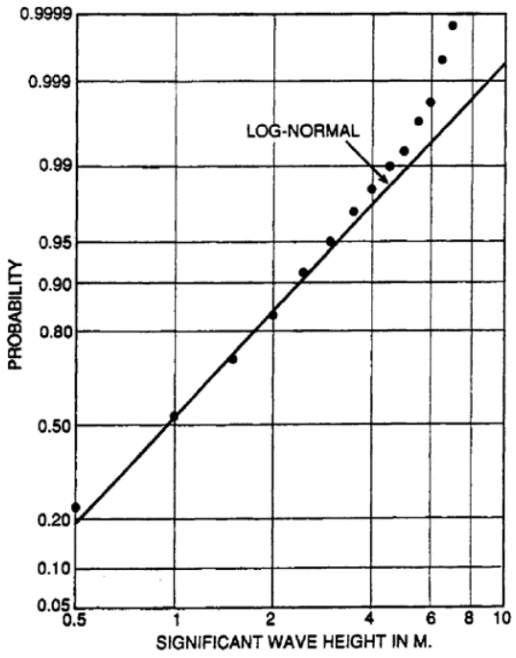

Figure 2.19 Cumulative log-normal distribution against measured data.

On the other hand, Weibull distribution gives a good agreement of extreme side but overestimates the frequency of lower energy waves (Fig. 2.20). Weibull distribution can be improved by adopting additional parameters; however, tuning these parameters is challenging and thus the results should not be taken as a gospel.

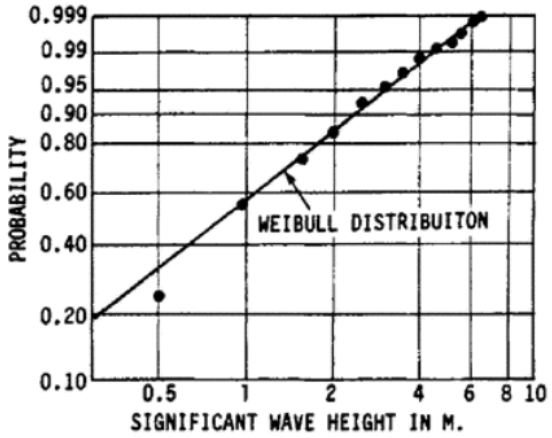

Figure 2.20 Cumulative Weibull distribution against measured data.

A generalized, 3-parameter gamma distribution function has been developed to fix the shortcomings of aforementioned models. Fig. 2.21 describes it plotted against the North Sea weather data. Parameters m, λ, c are chosen by equating the moments of the data and the gamma distribution.

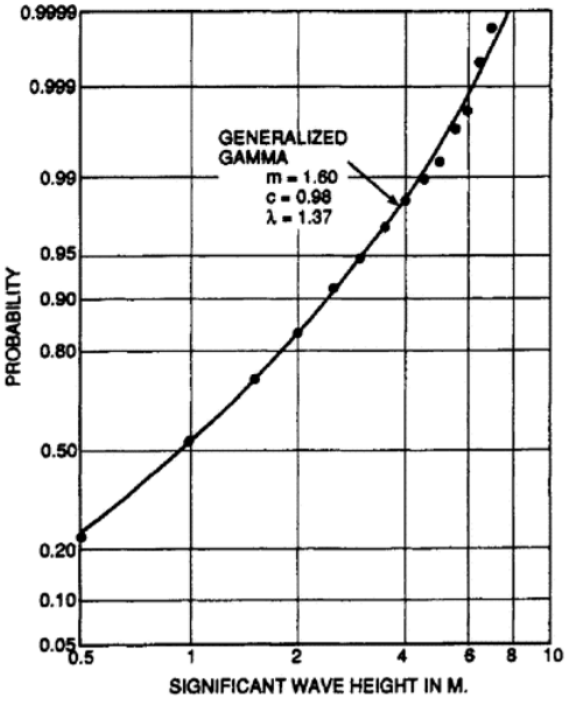

Figure 2.21 Cumulative gamma distribution against measured data.

These models can then be used to statistically estimate the probability of occurrence of severe sea states those already measured in the data, as well as limited, conservative extrapolation to even

higher wave heights. More reliable use is to evaluate the spectrum of significant wave heights and use it to model fatigue loads to the structure.

Joint distributions

Not all wave heights are equally dangerous: a short period, aggressive wave will lead to much stronger response that long-period swell. Based on this, two-dimensional joint probability functions have been developed to provide a more reliable method of evaluating the marine system's environment. Naturally, more richer 2-parameter measurement data is required for this method. As the mathematics behind the statistics get increasingly complicated, only a brief overview is presented below.

The idea is to define a probability of each discrete $H_s - T_o$ combination. The joint probability function is assembled from previously developed H_s distribution and from a conditional $T_0|H_s$ - distribution: for each significant wave height, a probability distribution of wave period is defined. Fig. 2.22 illustrates this joint probability distribution for data obtained in the North Sea. The overlaid numbers represent actual occurences, while the contour envelope certain amounts of the distributions. We can note that the resolution is fairly poor for predicting exact quanitites. However, it is more than sufficient for the prediction of global distribution. Numerical tables such as these are available for the most relevant sea areas around the globe, as shown in lecture notes.

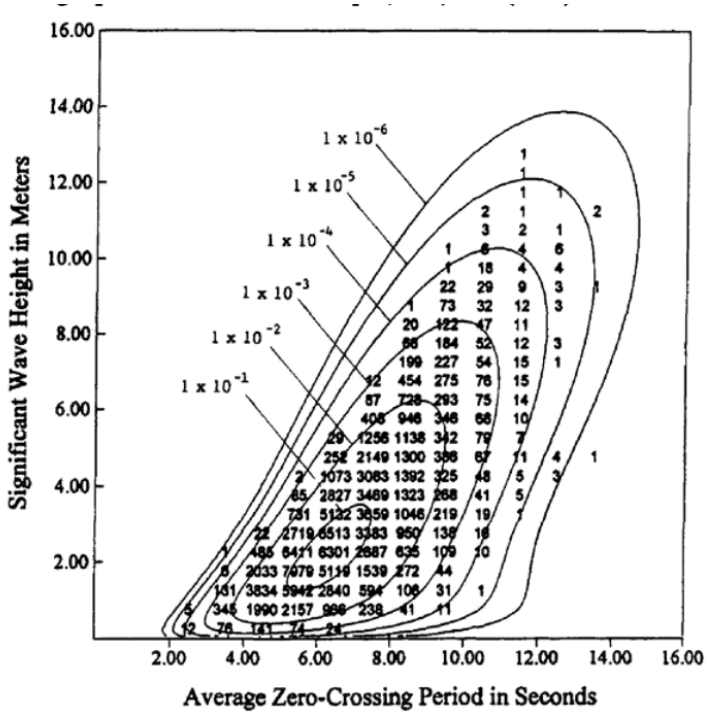

Figure 2.22 Joint probability function (contours) and measured tabular data.

On time series and hurricane seas

In addition to severity parameter distributions, the sea state can be evaluate temporally. Time series analysis aims to uncover seasonal variations in data; that is, it is to be used as an auxiliary tool for more relevant distribution models. Figure 2.23 represents the annual variation of H_s and T_0, expressed through the coefficient used in corresponding probability distributions. Time series analysis can be used to evaluate the validity of wave height and period data; how are the harshest conditions represented by them.

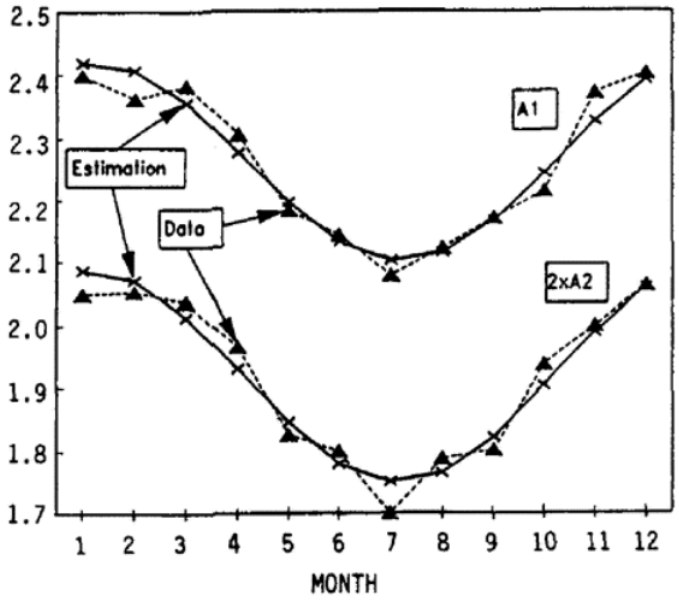

Figure 2.23 Seasonal variability of wave heights and periods, given as parameter of distribution functions.

The sea states so far have assumed to originate from fairly constant and long-blowing winds. Hurricanes, in contrast, exhibit heavily time-dependent wind conditions as well as dependence on parameters such as vicinity of the storm's eye, movement of the storm etc. Another problem of the hurricanes is their unique nature: data obtained from one hurricane might poorly predict the next, even on the same area. Interesting quanitites we can deduce from the limited include wind speed-wave height -relationship and spectral energy distribution. Figure 2.24 represents the energy spectra of ELOISE hurricane and an assortment of ordinary wind-generated harsh seas at the same significant wave height.

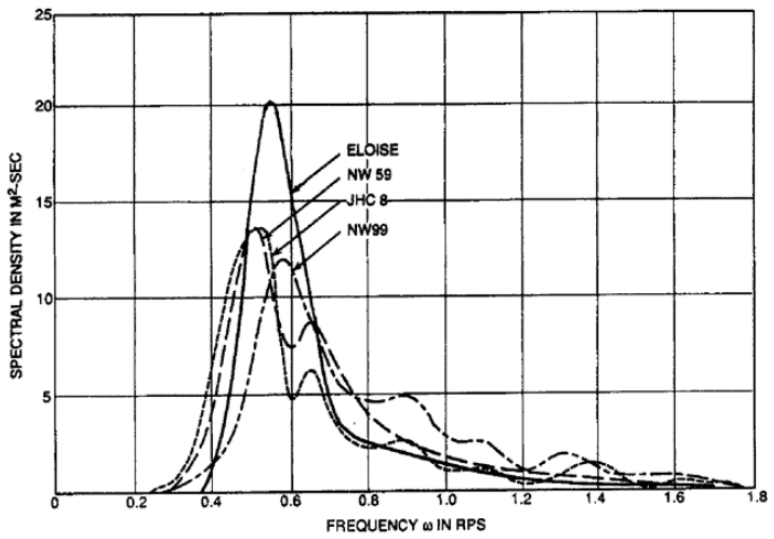

Figure 2.24 Hurricane and ordinary storm energy spectra.

We can see that a short-term nature of the hurricane concentrates energy heavily into peak frequency, while ordinary storms have much more dispersed spectra and multiple separate peaks.

2.6.2. Book Chapter: Ochi (1993): Marine environment and its impact on design of ships and marine structures

For ships, marine environment mostly translates to waves. High ships and ships with large cross-sectional area also experience considerable dynamical loads from winds, though this is of less concern for Khione. She will be travelling in northern Atlantic, so the ship must endure hurricane-associated sea states.

Wind

Mean wind speed needs no introduction: it is easy to measure over long periods of time and is used mostly for analysis of static responses . Mean long-term wind speed is also connected to sea severity. The roughness of the sea surface reduces mean wind speed, but increases the turbulent gust speed. According to Ochi, the wind loading can be divided to three different components: mean linear wind, turbulent linear, and turbulent non-linear. To obtain these components, one of course needs to have an access to turbulent windspeed data collected at sea (which Ochi notes, is substantially different to terrestial wind data). The paper concludes that turbulent non-linear wind loading is negligible compared to other terms, only longitudal variation of mean wind needs to be considered and that measured low-frequency spectral components of wind differ from simulated, such that extra caution is needed for structures prone to resonance. When considering hurricanes, one should note that the rapidly increasing wind speeds are not reflected in sea severity; the sudden onset of the storm ensures that wind doesn’t have enough time to transfer its energy on the sea.

Figure 2.25 represents the relation of wind speed and significant wave height at the growing stage of the storm. It should be noted that this function was developed based on single hurricane: it cannot be unconditionally generalized.

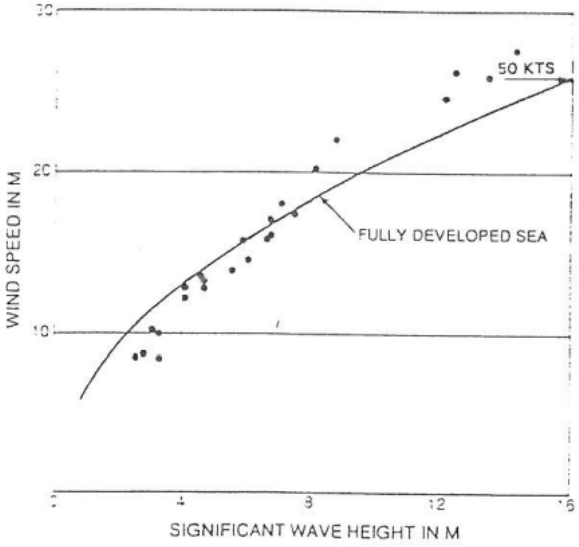

Figure 2.25 Wind speed and significant wave height during the growing stage of hurricane.

The extent of wind effects on Khione is still an open question: it certainly is not the most vulnerable vessel, but the effect cannot be naively discarded as negligible. Further investigations will ensue.

Waves

Thanks to its operation area, Khione will be subjected to some of the most severe sea states on earth. Estimating the highest loads endured by the ship during her lifetime aswell as the cumulative loads are possible by exploiting statistical properties of distributions fitted to measured data. Thankfully, North Atlantic has been historically very frequently monitored, and data is readily available along with wave spectrums, such as Pierson-Moscowitz.

The generalized gamma probability distribution has been adopted as the best choice when evaluating H_s distributions. This is in line with the results of the book review. Equation 1 describes the cumulative probabilty distribution. Given this distribution, one can evaluate the severest probable sea state, that is, highest probable H_s during the vessels lifetime for given risk parameter with Equation 2.

$$F(x) = \Gamma\left\{m, (\lambda x)^c\right\} / \Gamma(m) \tag{2.5}$$

$$\frac{1}{1 - \frac{\Gamma\left\{m, (\lambda y_n)^c\right\}}{\Gamma(m)}} = \frac{N}{\alpha} \tag{2.6}$$

The general and bounded gamma functions are defined as below:

$$\Gamma(z) = \int_0^\infty e^{-t} t^{z-1} dt \tag{2.7}$$

$$\Gamma(s, x) = \int_x^\infty t^{s-1} \exp(-t) dt \tag{2.8}$$

For North Atlantic, a widely used and reliable spectrum is the Pierson-Moscowitz. During hurricanes, the wave energy spectrum can be represented more faithfully with JONSWAP spectrum, albeit with different parameters than in ordinary storms. Evaluating the extreme event with this spectra could be useful; however it should be noted that hurricane sea measurements are far from general and hefty risk parameters should be used.

Ochi presents a detailed spreading function developed by Longuet-Higgins, aimed to bring the unidirectional idealized sea closer to the chaotic reality. For our design purposes, the simplified ITTC spreading function (Eq.5) would prove sufficient:

$$D(\omega, \theta) = \frac{2}{\pi} \cos^2 \theta\,,\ abs(\theta) \leq \frac{\pi}{2} \tag{2.9}$$

Ochi suggests that the design wave height, based on Rayleigh distribution, is given by:

$$\left(\begin{array}{c}\text{Design extreme} \\ \text{amplitude}\end{array}\right) = \sqrt{2 \ln\left\{\frac{(60)^2 T}{2\pi\alpha}\sqrt{\frac{m_2}{m_0}}\right\}}\sqrt{m_0}\,, \tag{2.10}$$

where T is the lifetime in hours, α is the risk parameter, m0 is the area under the wave spectrum and m2 the second moment of the spectrum.

Unlike with single variable distributions, joint distributions are a bit trickier to work with. The most relevant is the the wave zero-crossing period T_0 as a function of H_s. The most damaging, and thus the design $T_0 - H_s$ -combination depends heavily on the size and the geometry of the system in question, and such no single extreme event formula is presented. By detecting the resonant frequencies of the ship's dynamical response (parametric roll etc.) one can refer to the

joint distribution and evaluate the safety of the design. Figure 2.26 represents the dimensionless Longuet-Higgins distribution. Whereas the practice with H_s distributions has been to evaluate the severest geographical area, with joint distributions it may not suffice anymore. For given structure, the high waves of North Sea might not be as dangerous as lower, but more resonant waves of other locations.

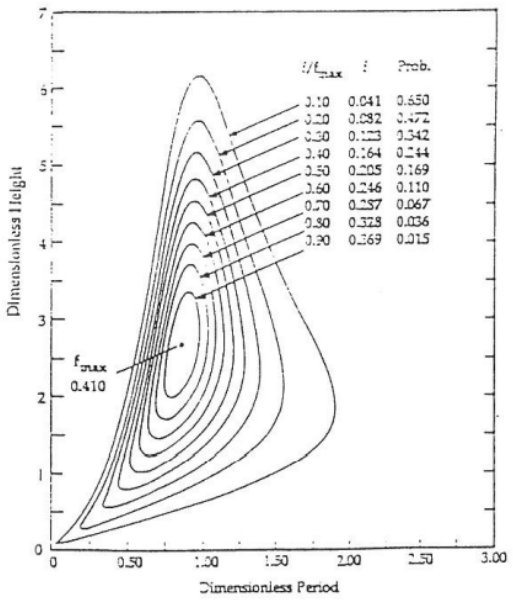

Figure 2.26 An example waveheight-period distribution.

When considering the impact of high waves on the marine structure, it is naturally important to consider the shape of the wave. In particular, waves with high H_s/T_0 -ratio are prone to breaking. Breaking waves cause heavy slamming loads due to their more vertical character. In addition, they might also flood the deck with green water. Ochi presents a simple check for checking whether the waves break or not, given by wave height H and period T:

$$H \geq 0.02gT^2 \tag{2.11}$$

Despite the sea being a very chaotic process, sometimes surprising intermittent burst of order may emerge from the chaos. In context of waves, these are called group waves, and they are characterized by uniform wave period. Group waves occur at all heights, but of course only the highest are actually of concern for the designer. Ochi does not present any formulas for designing for extreme group waves during the marine structure's lifetime. The notion of group wave is not rigorously defined, but it can be solved from the wave spectrum and joint probability distributions which, though, as Ochi notes, is extremely difficult. Figure 2.27 represents a group wave probabilistic distribution, based on measurement data from North Sea, for specific frequency of

0.42 rps. After deducing the critical resonance components of Khione, a group wave distribution for such frequency can be used to evaluate the worst possible case during her lifetime.

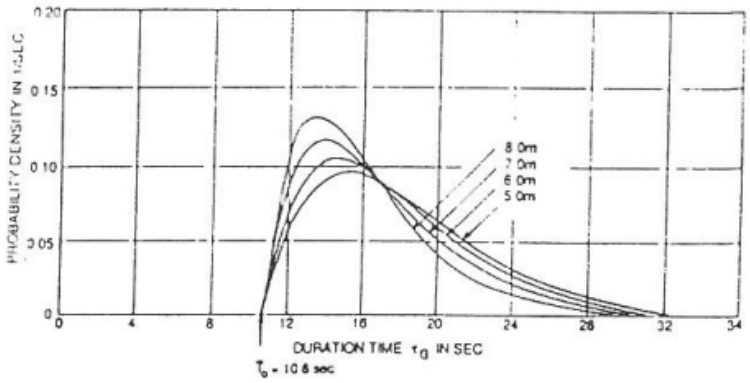

Figure 2.27 Group wave distribution with a cutoff period of 10 seconds.

The paper also touches on subject on wave induced local design loads and currents, but focuses heavily on offshore structures, such as tension-leg platforms. Thus, these areas are of little interest for Khione. However, Ochi states that when evaluating the extreme loads, it is sufficient to consider only the short time periods containing the most extreme events, unless the structure is particularly prone to fatigue, such as an aluminum vessel is.

2.6.3. Cherneva, Guedos Soarez (2014): Time–frequency analysis of the sea state with the Andrea freak wave

The freak waves are characterized by high degree of non-linearity: that is, they are not predicted by extreme tail events of idealized wave spectra. The idea of this paper is to investigate the time and frequency domains of the sea around the measurement of Andrea freak wave. Owing to its capability of demonstrating non-linear effects, the Wigner spectrum is fitted to measured data and the resultant wave energy spectrum is analyzed. The Fourier transforms used in the formation of the spectrum allow the spectrum to have high resolution – a necessary trait to capture the interesting events in such a short duration. It should be noted that the spectrum is not an idealized one such as Pierson-Moscowitz – it is a transform.

The peak wave energy spectrum, amplitude and time-frequency spectrum is presented in Figure 2.28.

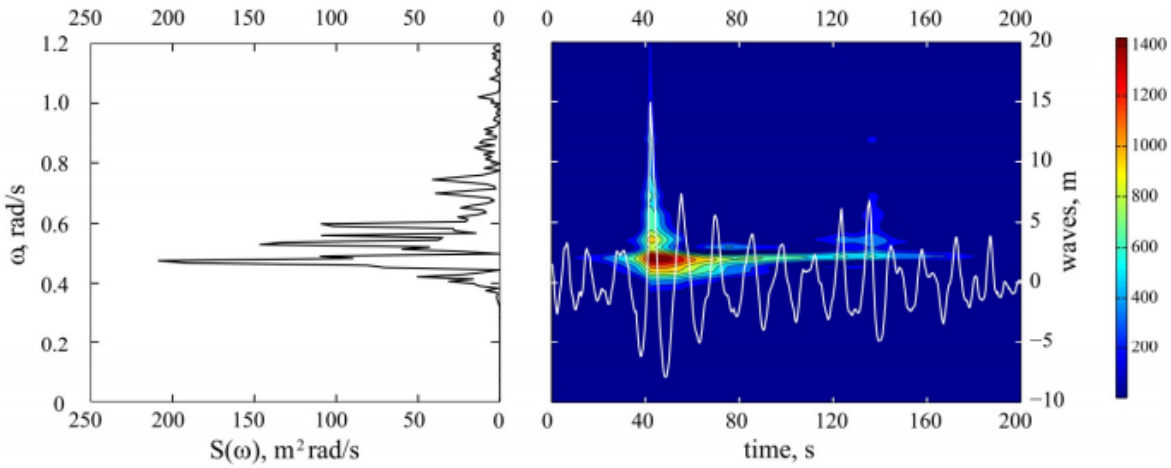

Figure 2.28 Energy spectrum and time-frequency spectrum of the Andrea group.

The paper makes a number of remarks about the time-frequency spectrum. The most obvious observation is the sharply focused energy on certain frequency. Before the wave, there is a gradual build-up of energy exactly at the peak frequency. During the peak period, higher frequencies suddenly build up energy and dissipate quickly while the main frequency remains at high energy for some 100 seconds.

Additionally, they argued that downshifting to a lower sideband of the spectral peak also appears in the absence of breaking and showed the significant role of the balance between momentum losses and energy dissipation in the exchange of energy between the sidebands.

The prospect of frequent freak waves is catastrophic for linear wave theory: the design guidelines given by Ochi are based on real measurements, which assume a certain distribution of wave height probabilities. However, as demonstrated here, thanks to their non-linear nature, freak waves occur much more commonly than regular high waves born of interference, and often are precisely the tail event that marine structures are designed to withstand.

The article by Cherneva and Guedos Soarez is a step towards understanding the mechanisms of non-linear seas; thus, a step towards the development of a more reliable model that predicts the extreme events more accurately.

3 Wave Induced Motions in Regular and Irregular Waves

3.1 Equations of Motion

When considering ship motions from perspective of safety and comfort, we are usually interested of those motions that cause risk to stability, excessive structural loading and high accelerations. The most critical degree of freedom is that of roll, arising naturally from the elongated shape of the ship's hull. Excessive rolling may cause discomfort to personnel onboard and in extreme cases, capsizing. Small amplitude roll motion is governed by equation 1:

$$\left(J_{xx} + I_{\varphi\varphi}(\omega)\right)\ddot{\varphi} + N_{\varphi\varphi}(\omega)\dot{\varphi} + C_{\varphi\varphi}\varphi = K_{\varphi}(t) \tag{3.1}$$

where $K_{\varphi}(t)$ is excitation by waves, φ is the roll angle, J_{xx} is the longitudal moment of inertia, $I_{\varphi\varphi}$ is added inertia due to viscocity, $C_{\varphi\varphi}$ is hydrostatic roll restoring coefficient and $N_{\varphi\varphi}$ is roll damping coefficient.

Heave motion is governed by classic Newton equation:

$$\left(M_{zz} + m_{zz}(\dot{z})\right)\ddot{z} + N_{zz}(\dot{z})\dot{z} + C_{zz}z = F_{z}(t) \tag{3.2}$$

where right side is pressure-induced resultant force, M_{zz} + m_{zz} is the ship's mass plus the added mass, N_{zz} is the damping term (again due to energy transfer to medium) and C_{zz} is restoring force (responsible for free vibration).

Finally, pitch motion is similarly governed by modified Newton:

$$\left(J_{yy} + I_{vv}(\dot{v})\right)\ddot{v} + N_{vv}(\dot{v})\dot{v} + C_{vv}v = M_{v}(t) \tag{3.3}$$

where $M_{v}(t)$ is the pitch excitation vector, J_{yy} is the pitch moment of inertia, I_{vv} is the added mass moment of inertia, N_{vv} is the pitch damping coefficient and C_{vv} is the pitch restoring moment.

3.2 Khione's parameters affecting the equations of motion

3.2.1 Hull form

Hull form and main particulars play a role on every parameter in equations above. Breadth and draught directly affect the moment of inertia J_{xx}: the larger the particulars, the lower the resonant wave frequency. In the same manner, the length plays a big role in J_{yy}. The fairness of hull lines in breadthwise direction govern how much water is dragged along the hull in roll motion, that is, the added mass term $I_{\varphi\varphi}$. The damping term $N_{\varphi\varphi}$ relates closely to $I_{\varphi\varphi}$, however it is a measure of how vorticity induced by hull motion bleeds the roll energy. The same story is true for

corresponding parameters in both heave and pitch motions, albeit for these degrees of freedom the amplitude is usually much lower and therefore not as critical. As Khione's hull is fairly streamlined, especially at bow and stern, it is likely that heave damping N_{zz} and pitch damping N_{vv} are lower than those of more box-like ships. A V-shaped section creates less pressure/suction and vorticity during horizontal movement.

Khione is lacking external anti-roll devices, so only hull shape plays a role in damping. Characteristic for icebreaker, the bow ice plow acts as bilge keel in roll motion. In addition, the box-like midship and stern contribute to $I_{\varphi\varphi}$ and $N_{\varphi\varphi}$. Icebreaking features at the bow, such as high flare and waterline angle, also tend to lead lower heave and pitch motions in the seaway (Moton, 1991). Compared to high C_B vessels, the spoon bow may lead to unusual hydrostatic restoring moment curve and thus introduce increased restoring moment to $C_{\varphi\varphi}$ at high roll amplitudes. The reasoning is that parts of the bow (and stern) might be immersed and emerged during the roll motion. In pitch motion, keel emergence, immersion and slamming all introduce local stresses and nonlinearities to pitch restoring moment curve C_{vv}.

In reality, there is a strong coupling between pitch and heave motions, and lesser coupling with other degrees of freedom. One important application for such coupled equation is the determination of vertical translation of the bow using pitch v. If the wave environment is known, one can evaluate the risk of deck wetness and bow flare slamming.

Hull form determines the metacentric height G_{M0}, which is a quantity related to the roll restoring moment $C_{\varphi\varphi}$. The metacentric height should be high enough to prevent capsizing, but low enough that the accelerations in top deck are not excessive and/or the natural frequency does not coincide with highest amplitude wave frequency of scatter diagram. Longitudal metacentric height relates to the restoring moment C_{vv}, which may lead to structurally critical hull girder moments, especially when wavelength of $M_v(t)$ is about the length of the ship.

3.2.2 Operation profile

In this context, operational profile describes the wave excitation, namely the amplitude and the period. The most important task of the ship designer is to ensure that the natural frequencies of the ship won't match the frequency of highest waves given by scatter diagram. It may be meaningful to think about the most probable direction of waves and thus the encounter frequency during Khione's voyage in North Atlantic. The operational profile also links into wave shape: at low depth regions the wave excitation is different than at high seas due to failure of linear wave theory.

3.2.3 General arrangement

Within the context of ship motions, General arrangement is mainly about weight distribution. We assume that no cargo translation takes place, given the fragile nature of scientific equipment. However, fuel tanks for both the vessel and the helicopters ask for a dynamic approach. The general arrangement of Khione is presented below.

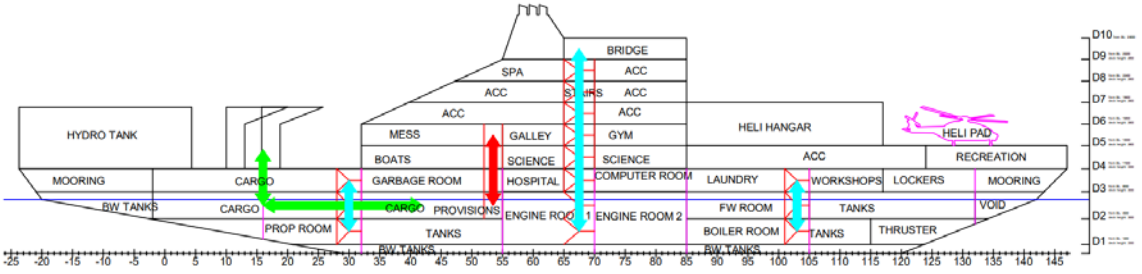

Figure 3.1 General arrangment.

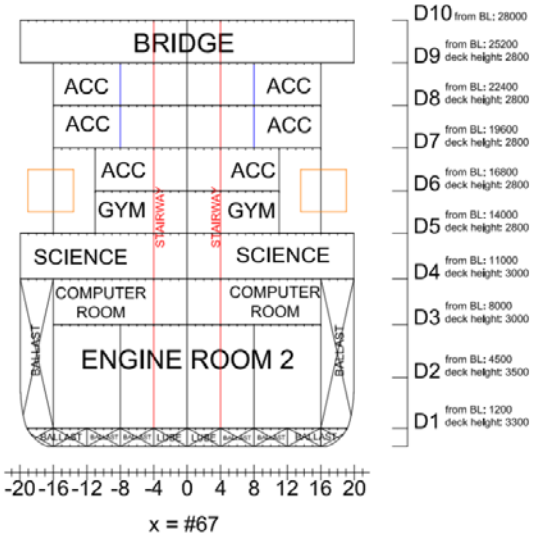

Figure 3.2 General arrangement.

With respect to roll motion, the vertical center of gravity is the metric to pay attention to. It is the opposing moment to G_{M0}, and together they determine the response and restoring moment. Heavy scientific equipment and fluid tanks on the sides and away from midships also increase longitudal moment of inertia J_{xx} in Eq. 3.1 and transverse moment of inertia J_{vv} in Eq. 3.2. Azimuth propulsion and bow thrusters increase the damping and added mass terms for all degrees of freedom. While unrelated to equations of motion, the weight distribution in relation to buoyancy distribution introduces static hull girder moments that can be alleviated by tweaking the general arrangement.

The remaining three degrees of freedom, namely surge, sway and yaw, do not have any restoring forces associated to them and as such, are not at risk of becoming resonant. Additionally, the magnitude of these motions is comparatively small and thus they are considered somewhat negligible, especially with respect to hull design workflow. It is worth noting that situations that lead to sway motion, such as beam waves slamming into hull, can be critical in terms of structural loading.

3.2.4 Mission

Khione is a semi-autonomous research vessel that controls itself using range of sensing equipment. The ship uses radar to identify obstacles above water and GPS to determine its position. Sonar is used for identifying underwater obstacles as well as research such as ocean mapping. Sonar and radar work by transmitting sound or electromagnetic waves respectively and measuring the time it takes for the waves to return to the receiver. From this data an object's location and speed can be determined. Often the transmitter and receiver are part of the same antenna. Ideally, the location of the antenna does not change in the time between transmission and receival of a sonar wave, because this changes the distance the signal must travel as well as the angle at which the signal is received. The result is that obstacles will be determined to be in a different place than they really are. This is not a problem for radar, as radar is practically instantaneous.

Waves induce motions in ships and indeed Schothorst (1975), has shown that the motions in high seas "...may cause a severe degradation of the sonar detection performance." in ships looking for submarines. For a semi-autonomous ship that is entirely reliant on sonar to locate underwater obstacles, a misdetection could be a severe collision hazard. By slowing down the ship's motion, specifically roll, the signal degradation can be reduced. This can be achieved by increasing the inertial terms, J_{xx} and $I_{\varphi\varphi}$, or decreasing the roll stiffness, $C_{\varphi\varphi}$ in Eq. 3.1.

Ship motions not only degrade the sonar signal received, but it also makes aiming a sonar signal harder. This is problematic when researchers want to map a specific region of the ocean. Rollmotion tends to have the highest frequency and so damping out the roll motion of the ship is advantageous. This can be done be increasing the damping coefficient, $N_{\varphi\varphi}$, in Eq. 3.1.

Khione has two helicopters on its upper deck as well as a helicopter landing pad. Needless to say, it is dangerous to land a helicopter on a landing pad that is rapidly moving. This rapid motion is associated with the stiffness term in the roll and heave equations. The greater the stiffness, the faster the ship tries to return to its upright position. If the helicopter is close to the deck when the ship suddenly rolls back upright or heaves upwards at high speed, the helicopter may crash into the deck. Furthermore, rapid restoring motions can induce sea sickness in both the researchers and the crew, as well as making desk work harder.

Not every of these potential problems is equally likely. It is likely that the high seas that would become dangerous for helicopters would be caused by winds that would make helicopter flying impossible anyway. But sea sickness due to roll, pitch and heave are always a problem and reason to limit the stiffness coefficients $C_{\varphi\varphi}$ (roll), C_{vv} (pitch), C_{zz} (heave) in Eq. 3.1, 3.3 and 3.2 respectively.

Being an icebreaker, Khione will travel through seas covered in broken ice as part of its research mission. In general, ice cover on seas tends attenuate the wave amplitude (Keller, 1998). In the equations of motion, this manifests itself as a decrease in amplitude of the forcing terms. As a result, any method to reduce ship motions in open water to acceptable levels should be sufficient in ice as well.

So far, the solution to many of the mission related problems has been to decrease the roll stiffness. While this is possible, it can only be done to a certain limit since decreasing the roll stiffness to far could lead the ship to capsize. Thus this lower limit must be evaluated and respected.

3.3 Seakeeping analysis

Seakeeping analysis was performed using both NAPA, AQWA, and Hydrostar. Basic theories behind the seakeeping analysis were strip theory and panel theory. Seakeeping analysis was performed to achieve maximum response motions based on generated RAOs and wave spectra.

Strip theory is a linear seakeeping analysis method which divides the ship into slices with constant cross-section. The analysis is essentially two-dimensional for each slice and the physical responses are obtained by integrating slices over the ship's length. Areas with high longitudinal curvature, such as bow and stern, require much denser slicing to achieve faithful representation. Due to wall-sided slicing, the only effect of forward speed is the change in encounter frequency. Strip theory assumes that the responses are simply linear with regards to excitation, the hull is completely displacement-type and viscous damping is decoupled from responses. The obvious shortcomings of this method are alleviated by applying independent correction constants and functions, such as in the case of damping.

Panel method or Green function method constructs a mesh of the ship's wetted surface and the pressure, forces and moments are calculated for each mesh element. This method is truly three-dimensional, eliminating some inherent simplifications related to strip theory. The method is still linear, so the effects of varying waterplane area (parametric roll) and non-linear restoring forces are not captured.

3.4 Motions of Khione in regular waves

The motions of Khione in regular waves are calculated by using two potential flow theory, which are presented with the Response Amplitude of Response (RAO). The RAO represents the motions

induced by the regular waves with 1 m wave height. It also considers the wave direction and wave frequency. The wave directions consist of 0, 45, 90, 135 and 180 degrees. 0 degree denotes the waves propagate in the direction same with the heading of ship. 90 degree denotes the waves propagate from the starboard. The wave frequencies range from 0.2 rad/s to 1.58 rad/s. For this calculation, three advancing speeds are taken into account: 0 knot, 3 kn, and 13 kn. 3 kn is the minimum speed in the ice breaking condition. 13 kn is the cruising speed.

The roll motion takes a critical position in the wave induced motions because of the features of hull section and roll itself. As show in Fig. 3.1, the hull moves tangentially relative to the fluid in the roll motion, so the roll damping is much small comparing to the damping of the other motions. The potential roll damping is even smaller because the potential theory ignores the viscosity of water. Therefore, it is reasonable to add additional roll damping to the calculation. ITTC (2011) recommends that the roll damping has five components: wave damping, lift damping, frictional damping, eddy damping and appendage damping. The wave and lift components are linear components which are proportional to roll angular velocity. The friction, eddy and appendage components are nonlinear components. Hydrostar user manual (BV, 2020) recommends the additional linear roll damping is 3% ~8% of critical damping, which depends on the hull forms. The quadratic damping in absolute value

$$B_Q = 0.5\rho C_D L B^4 \tag{3.4}$$

where:

ρ is the water density, C_D is a coefficient which scales around 0.1 ~ 0.2, L is the ship length, and B is the ship width. This calculation uses the recommended method of Hydrostar.

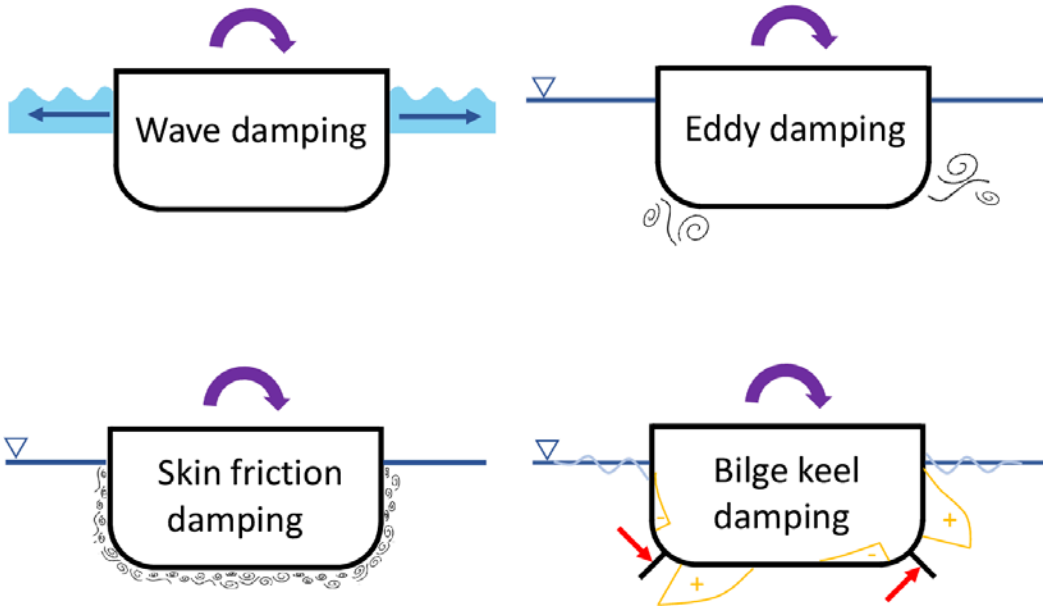

Figure 3.3 Roll damping components of ship (Borgenhov, 2017)

3.4.1 RAO from AQWA and Hydrostar

The RAOs of motions are calculated by using AQWA (AQ) and Hydrostar (HS). Figure 3.4 shows the mesh of calculation. The results are presents in the Fig. 3.5 ~ 3. 22.

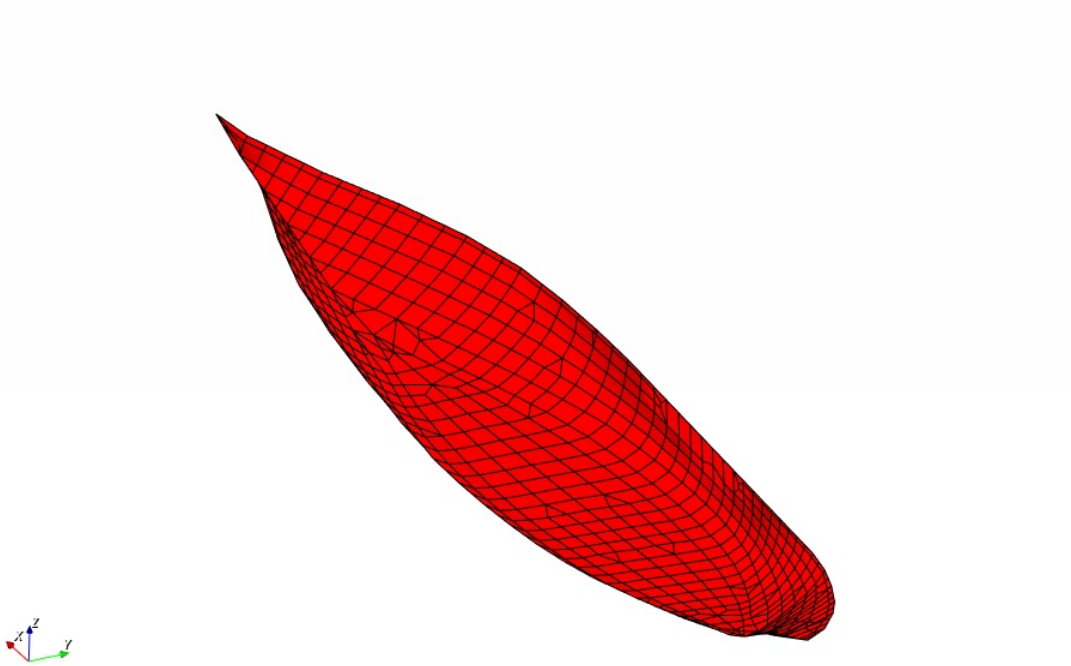

Figure 3.4 Mesh of hull

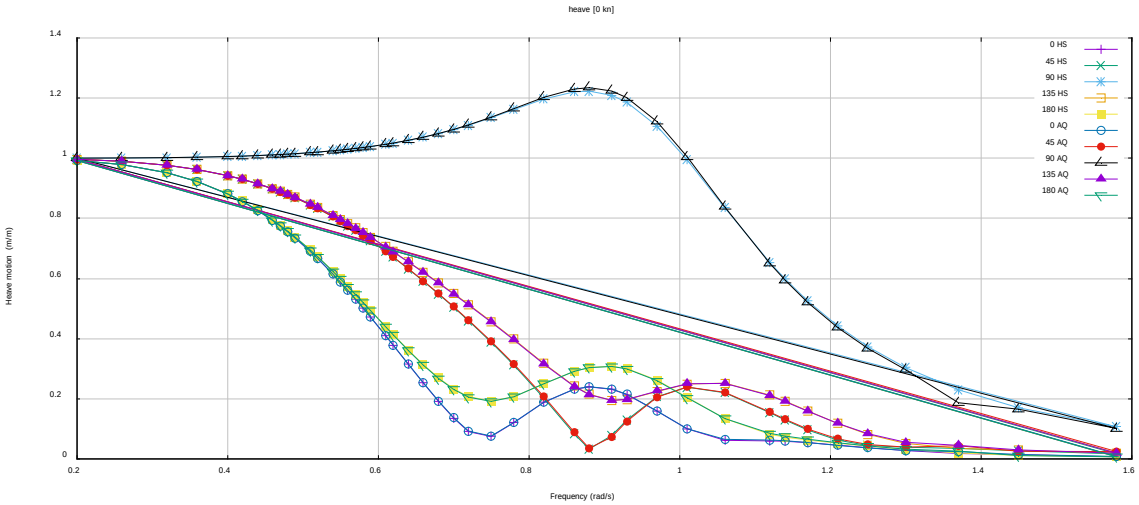

Figure 3.5 Heave RAO at 0 kn

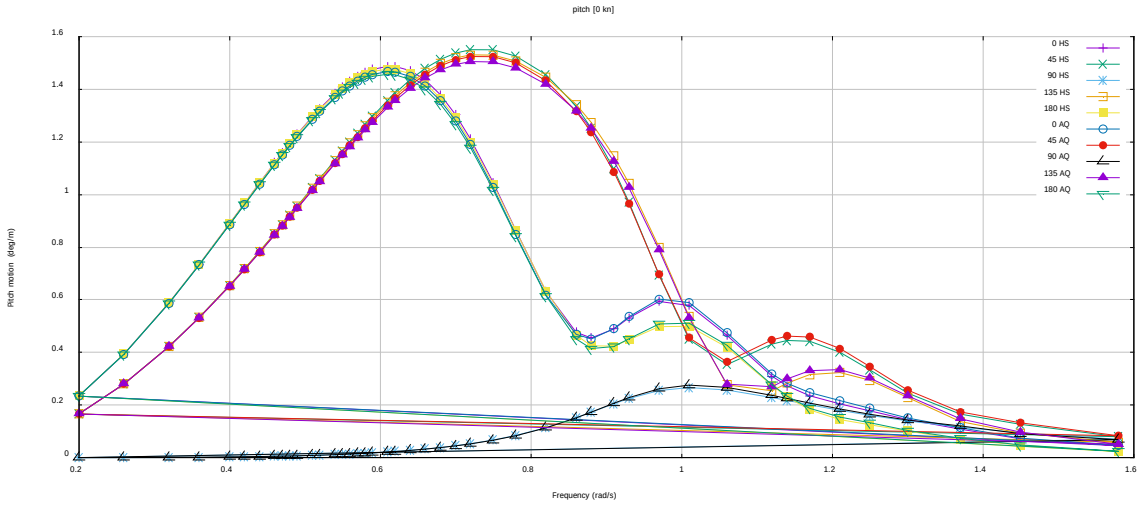

Figure 3.6 Pitch RAO at 0 kn

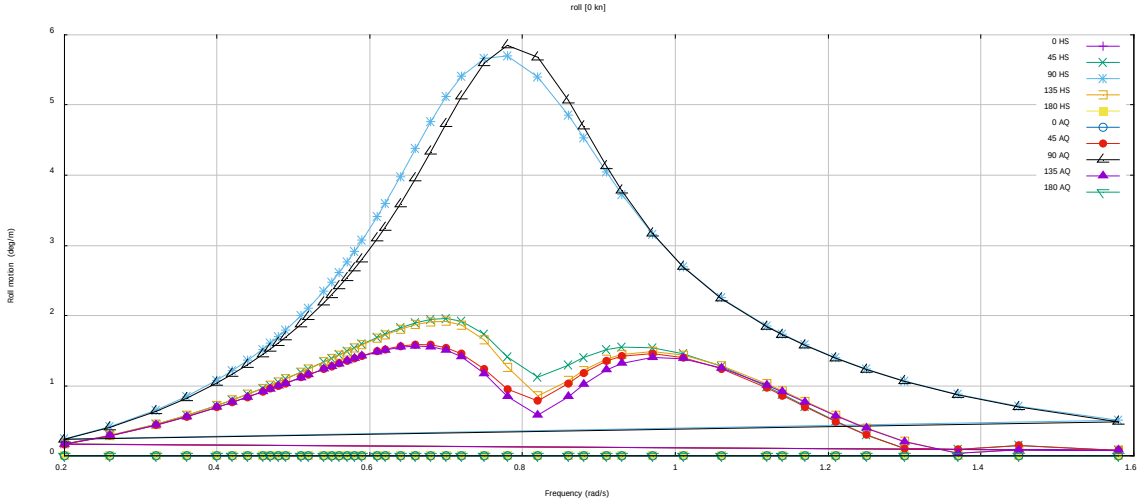

Figure 3.7 Roll RAO at 0 kn

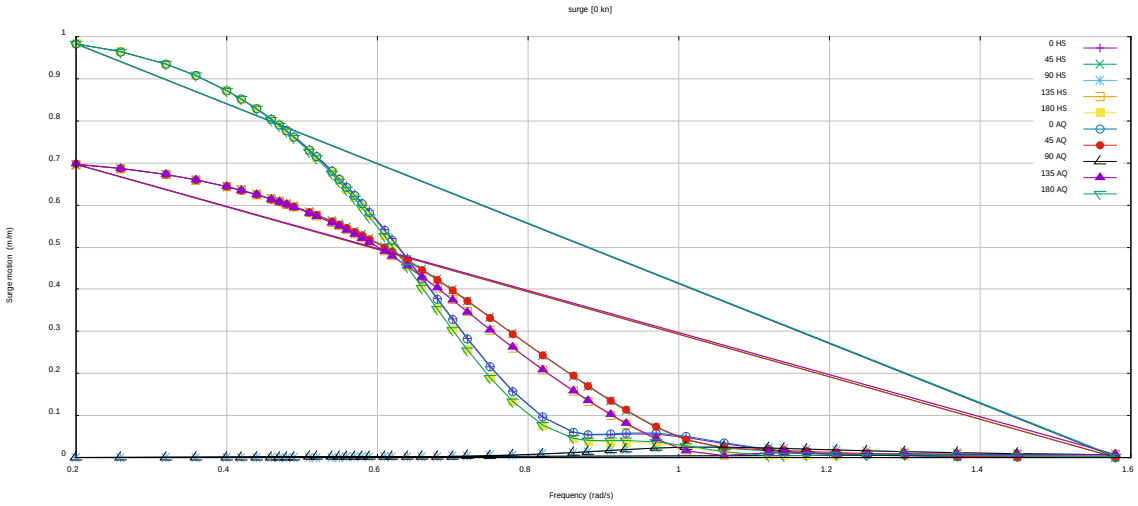

Figure 3.8 Surge RAO at 0 kn

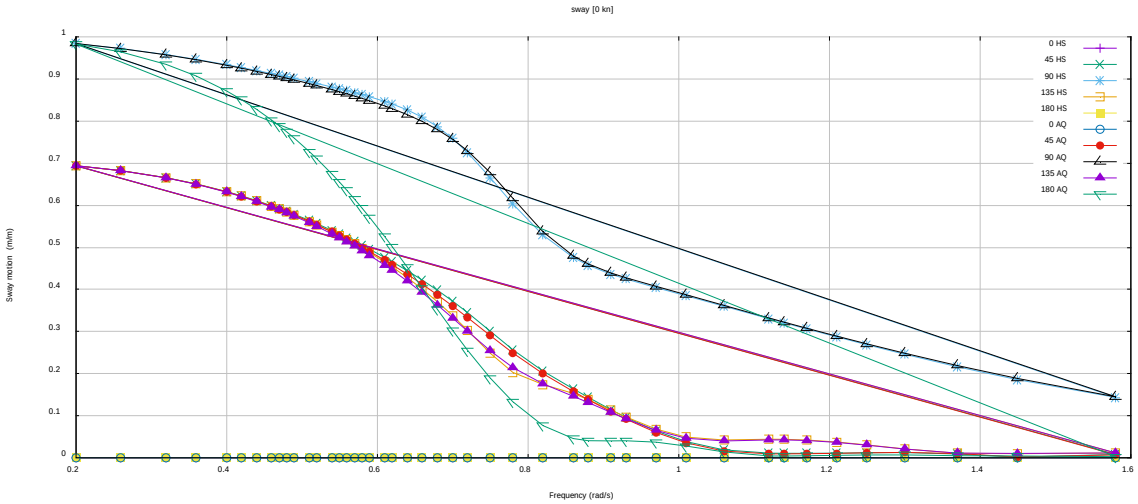

Figure 3.9 Sway RAO at 0 kn

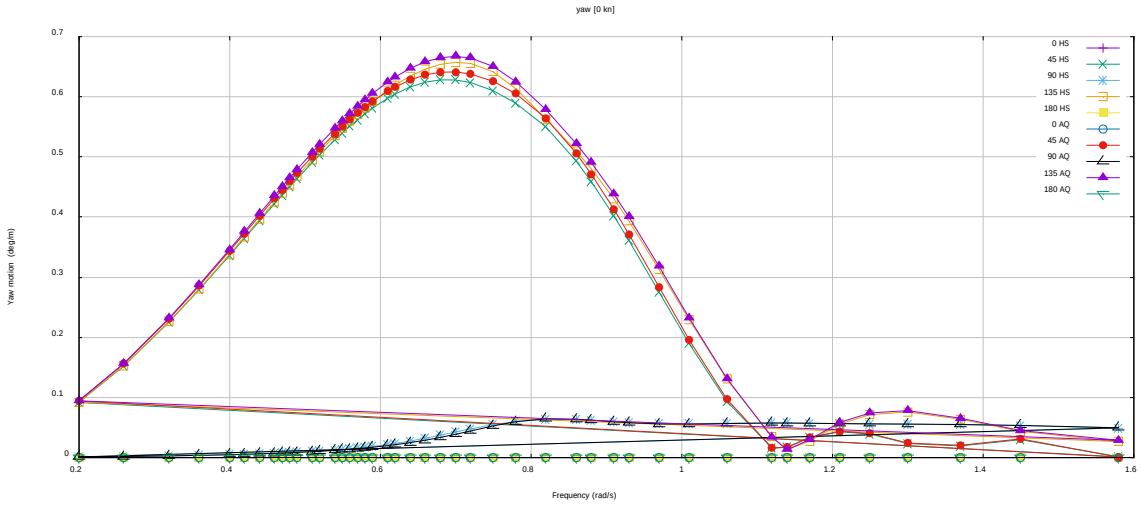

Figure 3.10 Yaw RAO at 0 kn

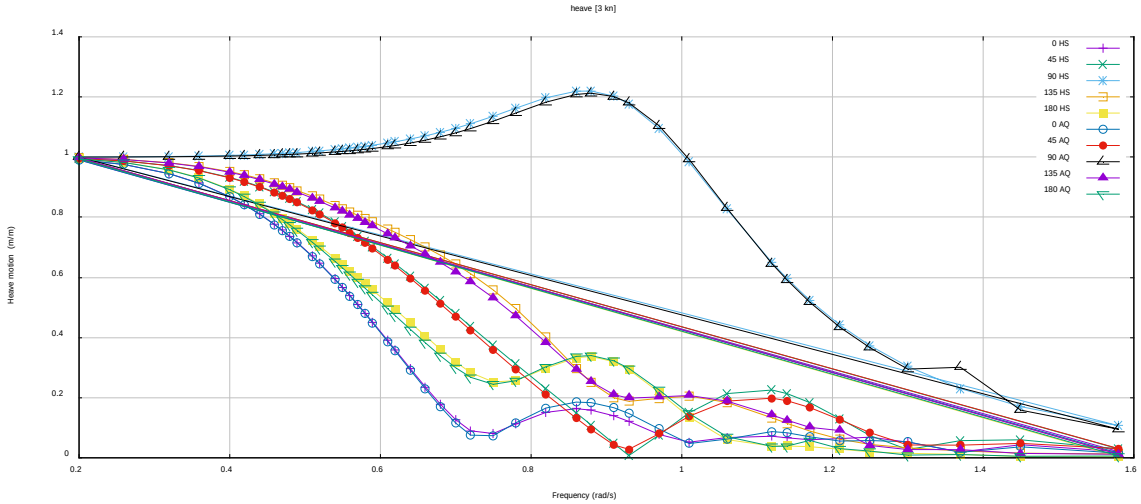

Figure 3.11 Heave RAO at 3 kn

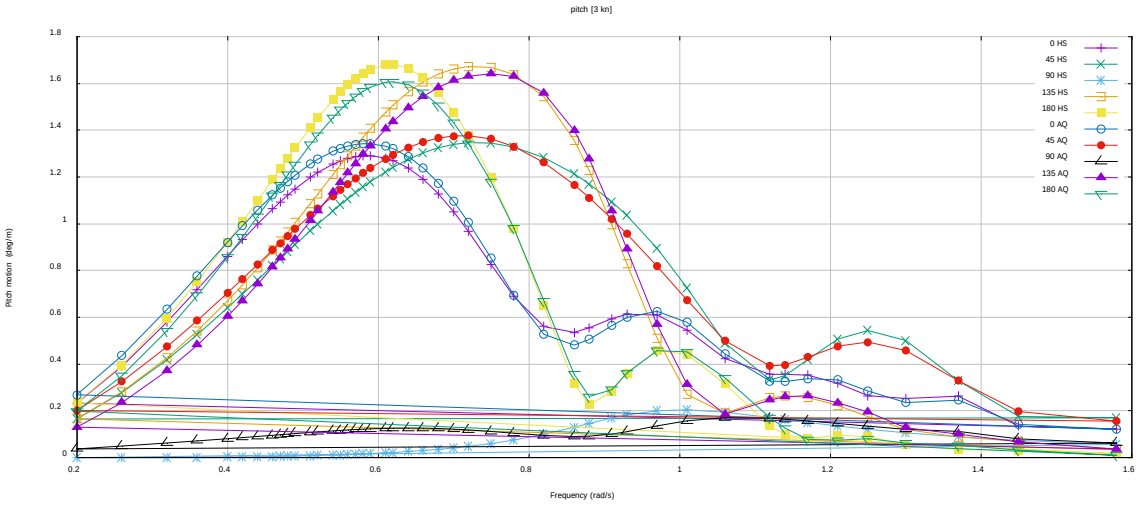

Figure 3.12 Pitch RAO at 3 kn

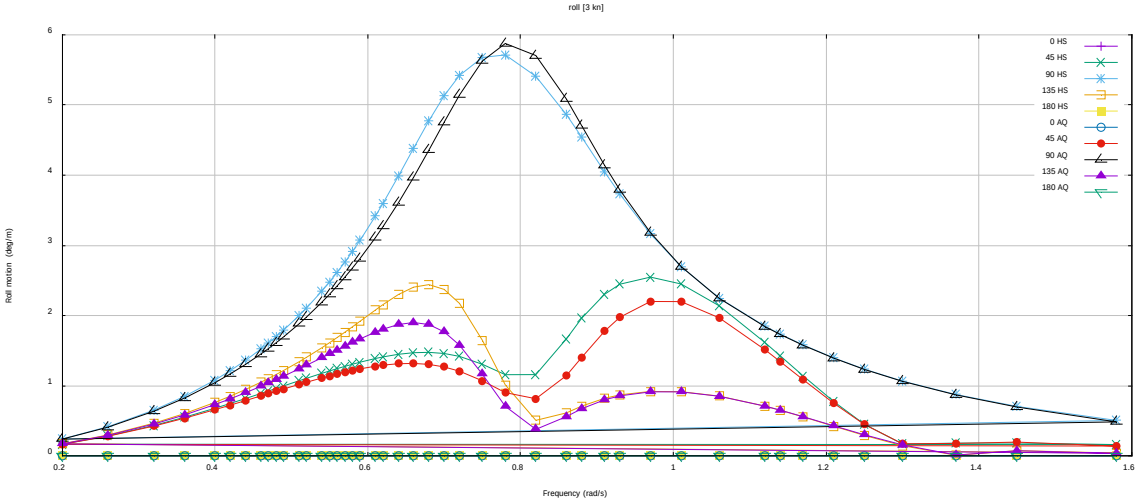

Figure 3.13 Roll RAO at 3 kn

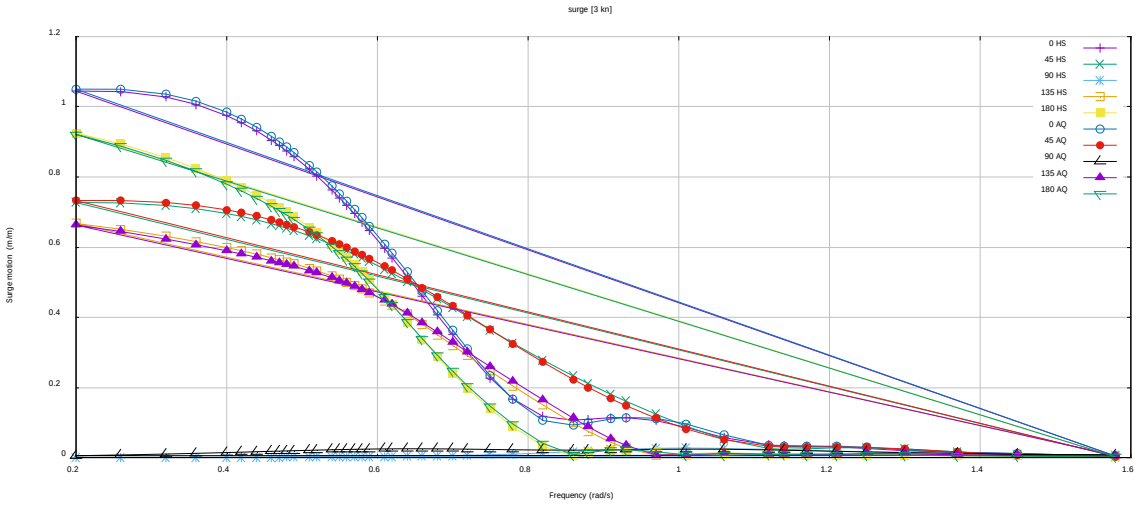

Figure 3.14 Surge RAO at 3 kn

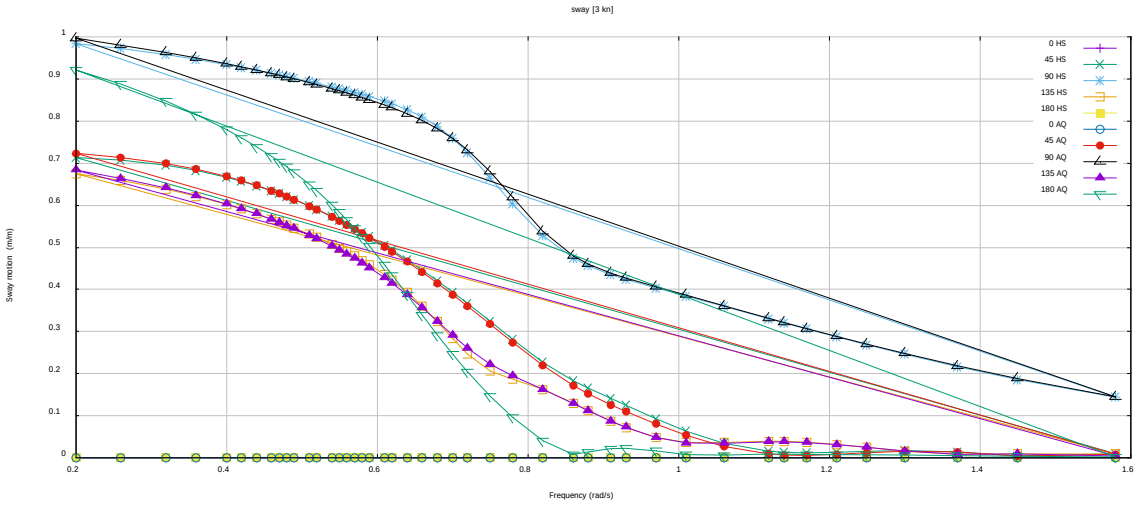

Figure 3.15 Sway RAO at 3 kn

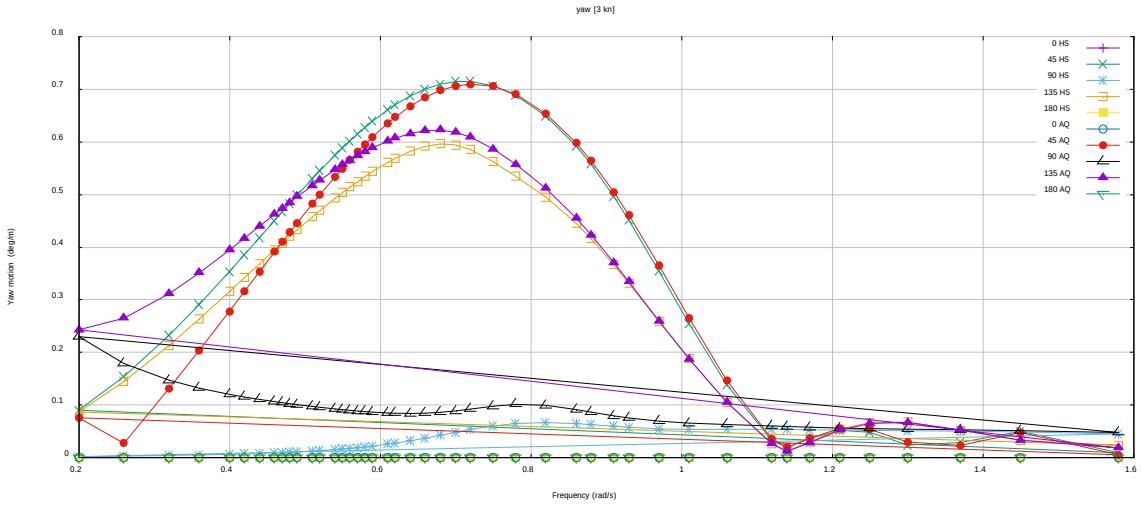

Figure 3.16 Yaw RAO at 3 kn

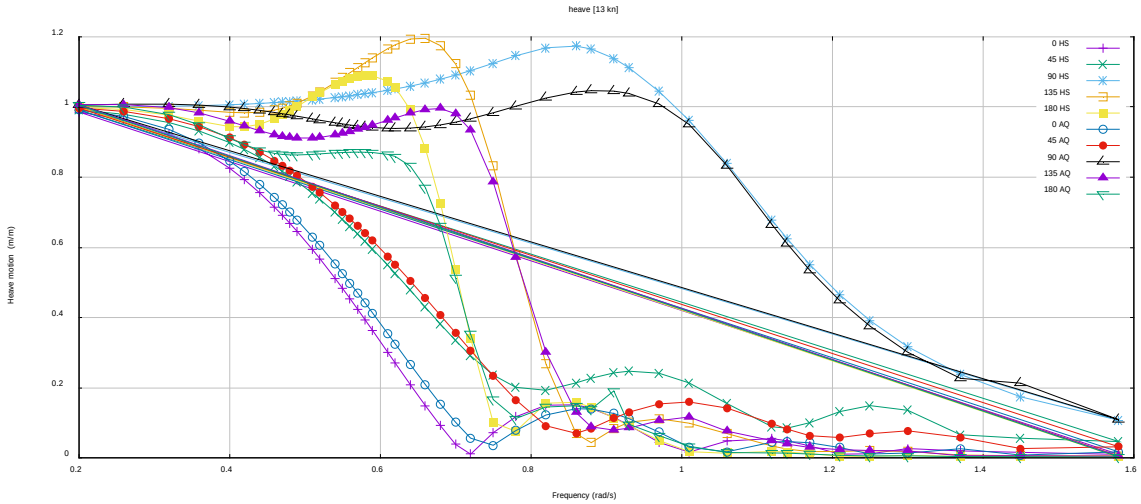

Figure 3.17 Heave RAO at 13 kn

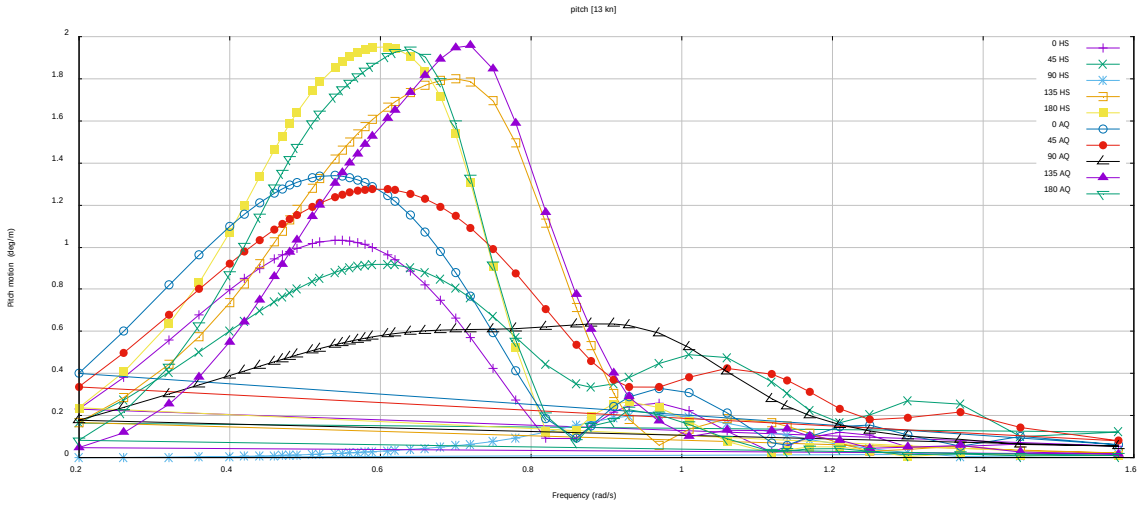

Figure 3.18 Pitch RAO at 13 kn

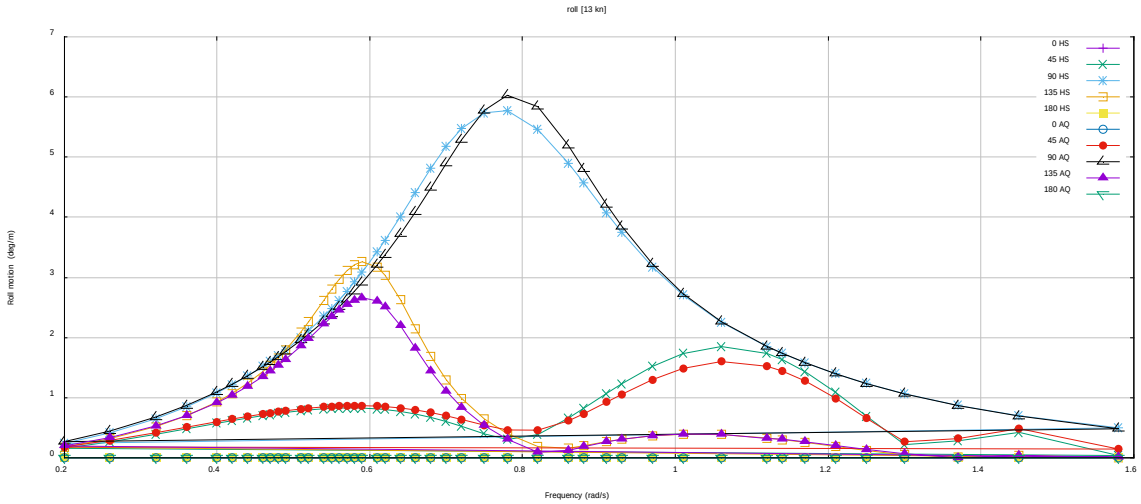

Figure 3.19 Roll RAO at 13 kn

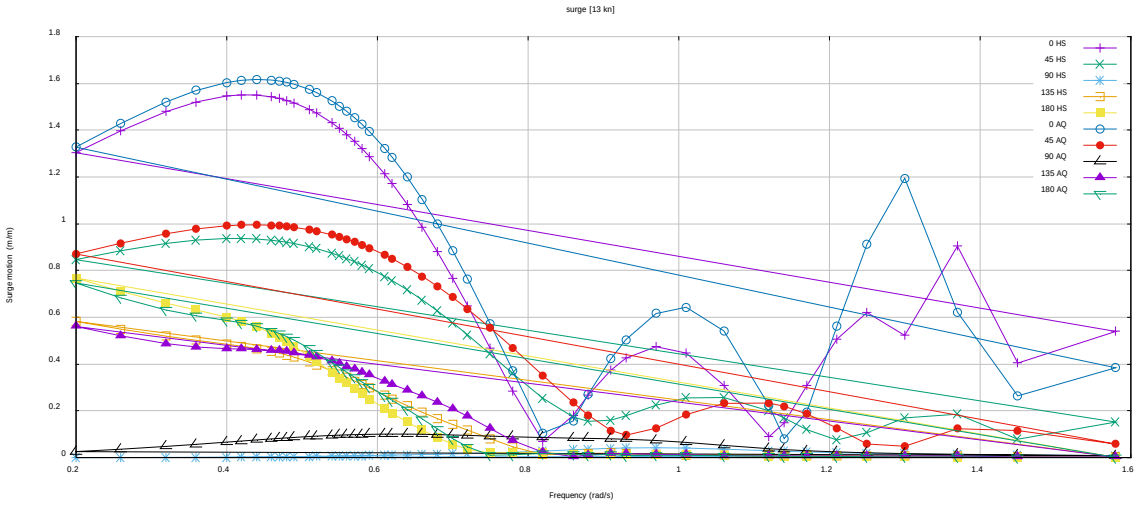

Figure 3.20 Surge RAO at 13 kn

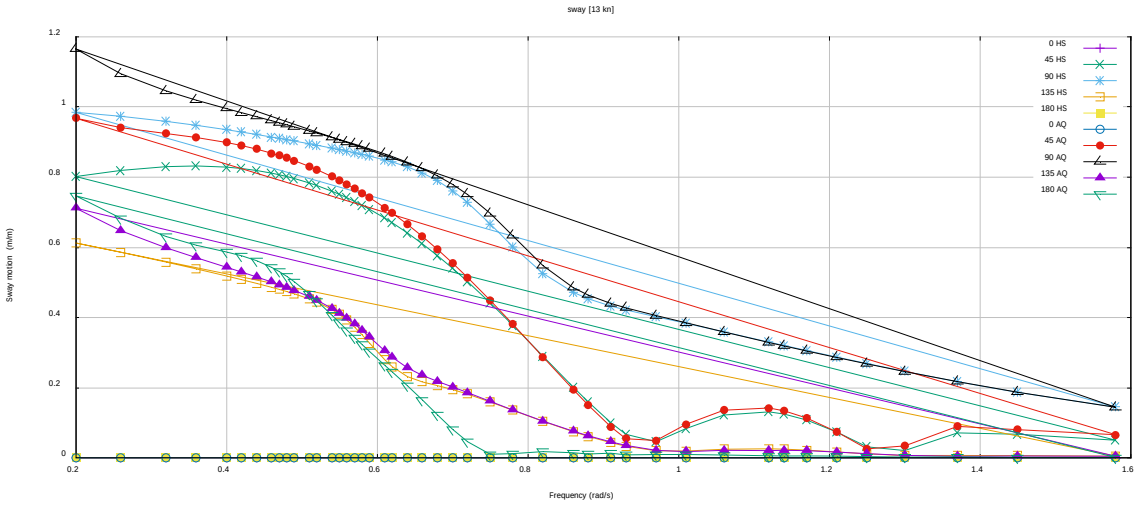

Figure 3.21 Sway RAO at 13 kn

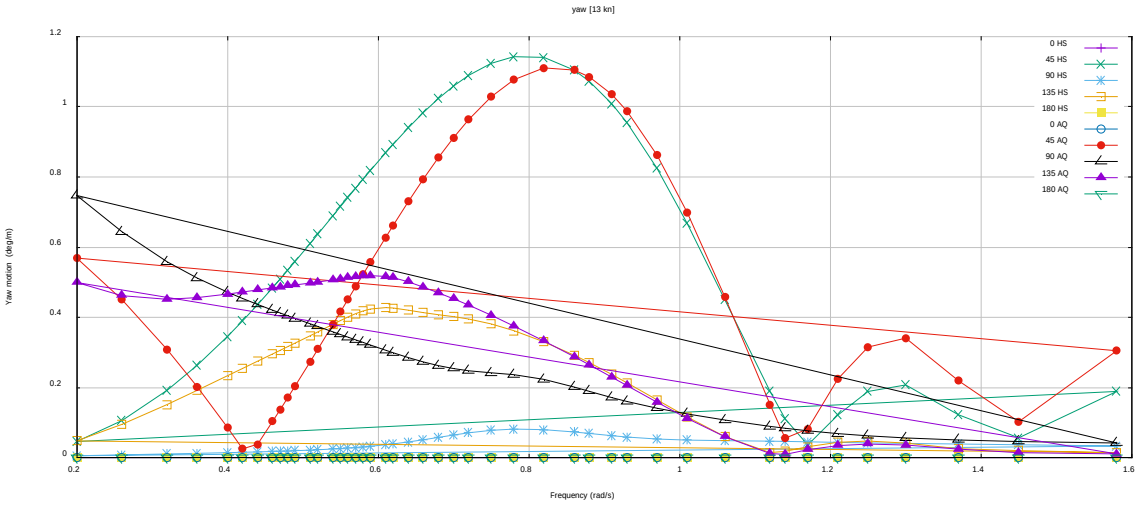

Figure 3.22 Yaw RAO at 13 kn

Heave

At the left end of the curves of heave RAO, the amplitudes are all close to one. This means the hull moves with the wave elevation when the wave is long enough (the wave length is much larger than the ship dimension in the wave direction) and the wave period is large enough. Because the ship length is much larger than the width, the heave is intensively influenced by the wave direction. The heave RAO in beam sea is apparently larger than those in the other wave directions. In addition, the heave RAO amplitude is not affected by the advancing velocity because the wave direction is perpendicular to the direction of advancing velocity. In the following sea and quartering sea, the advancing velocity can decrease the heave RAO amplitude. However, the advancing velocity increases the amplitude in the bow sea and head sea. The peak of heave RAO in the bow sea is even larger than the peak in the beam sea when the velocity reaches 13 knots.

Roll

The roll is intensively influenced by the wave direction. The roll RAO in beam sea is apparently larger than those in the other wave directions. The roll RAO curve only has one peak in the beam sea, but it has two peaks in the following sea and bow sea. The roll RAO is influenced by the advancing velocity in the following sea and bow sea. In the bow sea, the speed increases the amplitude of left peak and decreases the right peak. The influence is proportional to the magnitude of speed. However, the influence of speed is more complicated in the following sea. The speed can reduce the height of left peak and its influence is proportional to the magnitude of speed. The speed dose not always increase the right peak. The heigh of right peaks are close at the speed of 0 and 13 knots. Nevertheless, the height of right peak is higher at the speed of 3 knots.

The peak of roll response amplitude operator is heavily dependent of the natural frequency of the ship under rolling oscillation. The paper by Chen & He (2020) studies the responses of 153m icebreaker, calculated with MAXSURF software. Interestingly enough, as illustrated by figure 3.23, the peak of the RAO is at considerably lower frequency for the icebreaker. Khione appears to exhibit much milder response for both stern- and bow-quartering waves.

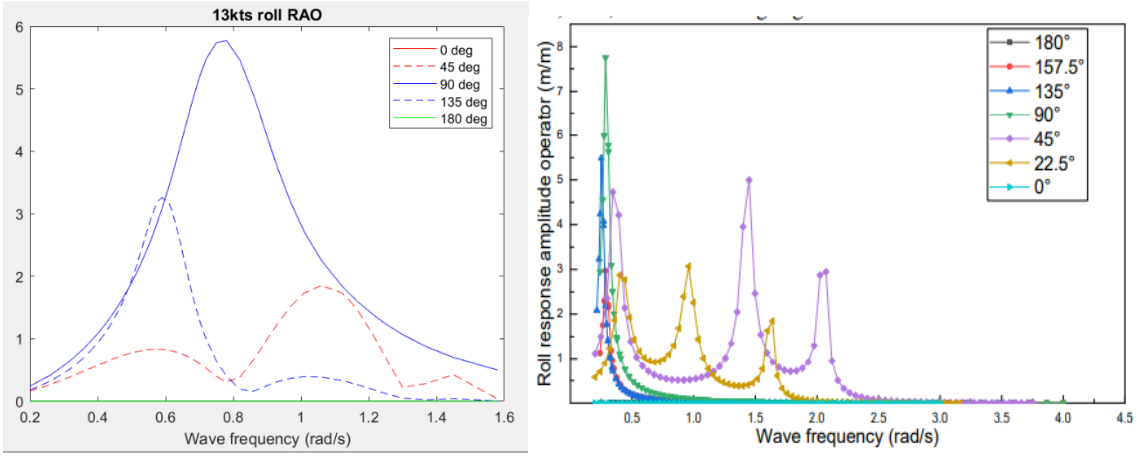

Figure 3.23. Left: Roll RAO of Khione with the speed of 13 knots. Right: Roll RAO of the icebreaker studied by Chen & He for 15 knots speed.

Pitch

The peak frequency of pitch RAO is affected by the wave direction. As shown in the pitch RAO figure, the peak frequency is around 0.6 rad/s at 0^o and 180^o, 0.8 rad/s at 45^o and 135^o, 1.0 rad/s at 90^o. The advancing speed has slight influence on the peak frequency of pitch RAO, but strong influence on the amplitude of pitch RAO. In the following sea and quartering sea, the speed decreases the amplitude of pitch RAO. On the opposite, the speed increases the amplitude of pitch RAO. The pitch RAO is not zero in the beam sea because the hull geometry is not symmetrical to the Y axis.

Maximum pitch response should be achieved at wavelengths comparable to ship length, as is evident in papers from Ghassemi et al (2015) and Chen & He. Figure 3.24 compares Khione's pitch RAO to pitch RAO of the icebreaker studied by Chen & He.

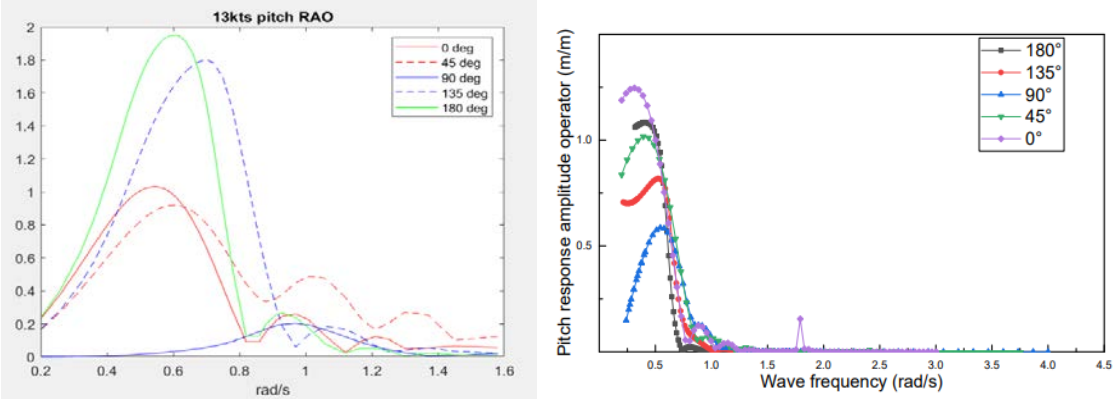

Figure 3.24 Left: Khione's pitch RAO for speed of 13 knots, obtained from Hydrostar. Right: Pitch RAO for 153m icebreaker for speed of 15 knots.

We can observe that for both vessels the RAO peaks at around 0.5-0.7 range, depending on wave direction. For both cases stern waves yield the high RAO maximums. Acknowledging the differences of the studied ships, the qualitative agreement is fair and it suggests that no major errors are present in our calculations.

Ghassemi et al have calculated the pitch and heave RAOs for S60 hull, which with respect to length and block coefficient, is remarkably similar to Khione's hull. They have used parametric Bretschneider spectrum and focused only in head seas condition. For Fn = 0.2, the peak of the pitch RAO is at around **160** meters wavelength, while Khione shows the peak at **170m** for same head seas condition. With respect to peak wavelength, the behavior of heave RAO is almost identical to pitch.

Yaw

Khione only has obvious yaw motion in the bow and quartering sea. The hull is symmetrical to the X axis and approximately symmetrical to the Y axis, so it is reasonable that the yaw motion is zero or closely zero in the following, head and beam sea. The advancing speed increases the yaw RAO in the quartering sea and decrease the yaw RAO in the bow sea. This is opposite to its influence on the pitch RAO.

Surge

The wave direction has strong influence on the surge RAO. The amplitude of surge RAO in the following and head sea is larger than that in the quartering and bow sea. The surge RAO is close to zero in the beam sea. This shows that the surge motion is mainly determined by the incoming wave loads and diffraction wave loads. The advancing speed increases the increases the surge RAO in the following and quartering sea and decreases the surge RAO in the bow and head sea.

Sway

The sway response has the similar feature as the surge except the influence of wave direction. The sway response is the largest in the beam sea.

Accuracy of the obtain results

The accuracy of the method used in this report is good enough for the engineering application. However, there is still some factors undermining the accuracy.

First, the potential flow theory ignores the viscosity of water and consequently ignore the rotation of water particle.

Second, the boundary element model only considers the mean wet surface. The hull motions do not change the wet surface. In addition, the model uses flat panels to replace the accurate geometry of the hull. Thus, the model does not represent the hull.

Third, the mass distribution and COG of Khione is not well known at this design stage. This firstly affects the calculation of wave induced motions. Secondly, this affects the calculation of hull girder loads.

3.4.2 RAO from NAPA

Panel method was used in seakeeping analysis in NAPA. Wetted surface of the hull was modelled with around 400 panels for the calculations. RAOs for every direction of motion were obtained for three different velocities of the ship: 0 knots, 3 knots and 13 knots. Y-axis is presented as m/m for translation motions and deg/m for rotational motions. X-axis is presented as non-dimensional wavelength, where L_{pp} is length between perpendiculars and Lam is wavelength. RAOs obtained from NAPA presented below.

Figure 3.25 Explanation of function colors

Heave

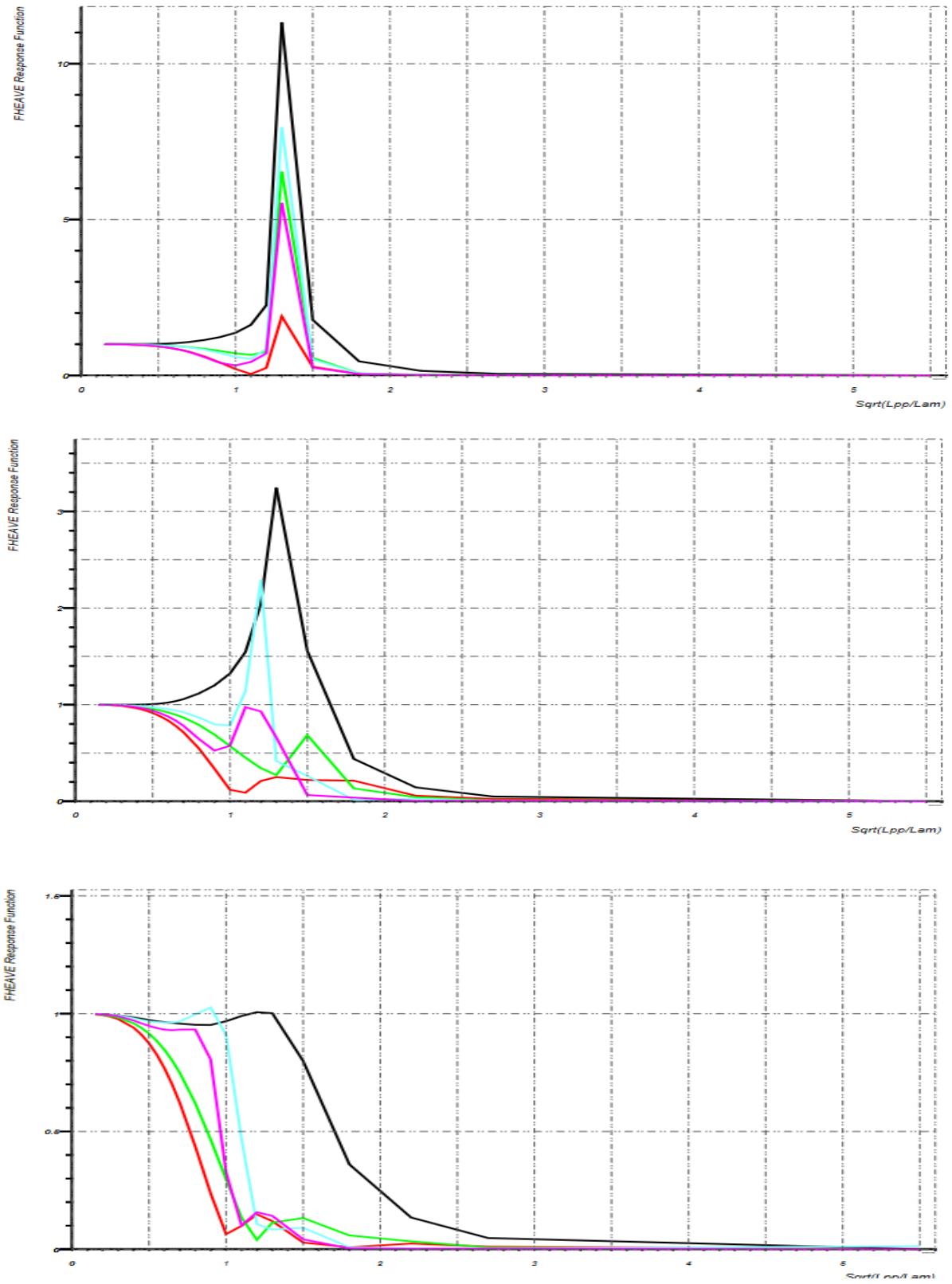

Figure 3.26 Heave RAOs from top to bottom at 0, 3 and 13 knots

Sway

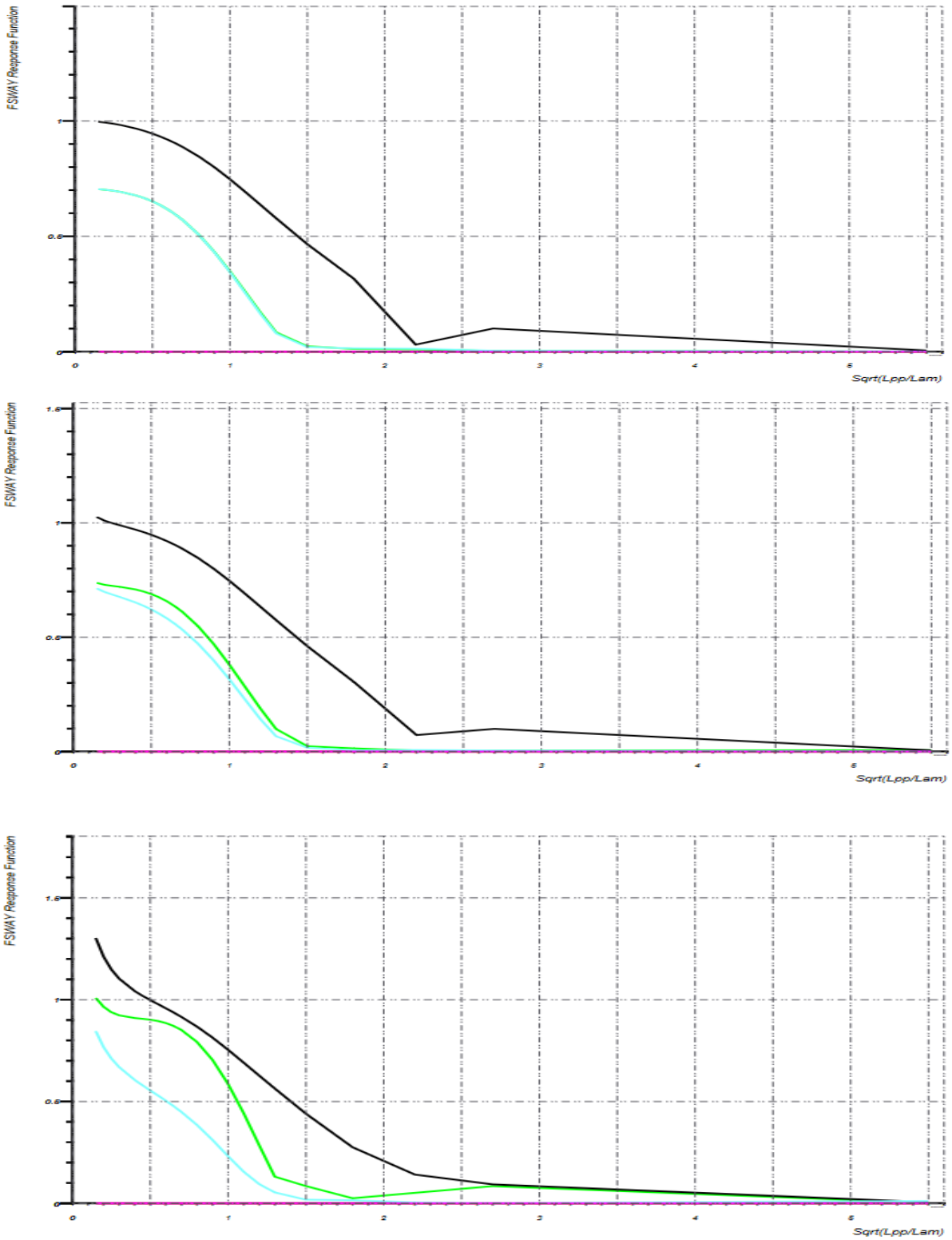

Figure 3.27 Sway RAOs from top to bottom at 0, 3 and 13 knots

Roll

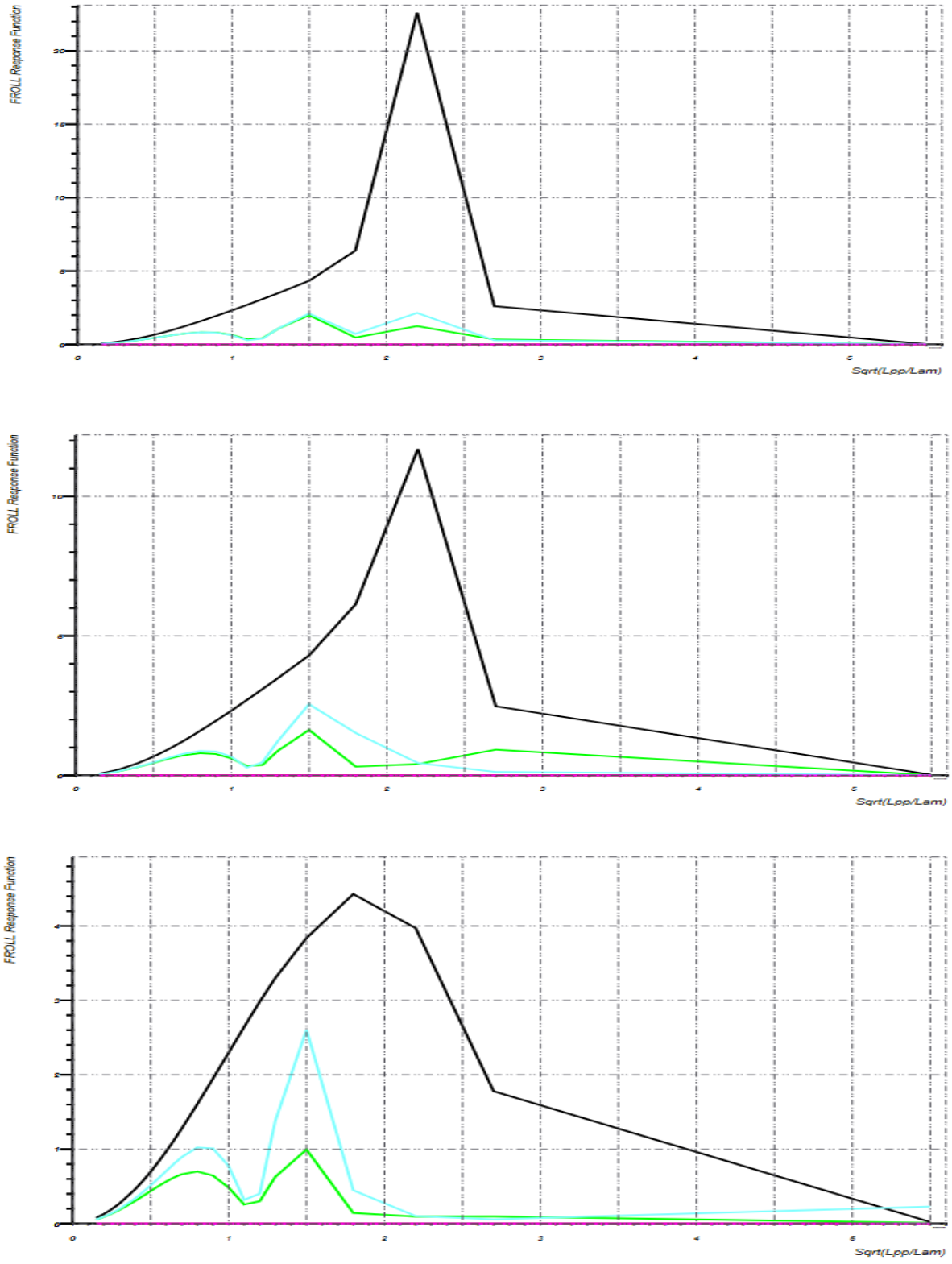

Figure 3.28 Roll RAOs from top to bottom at 0, 3 and 13 knots

Pitch

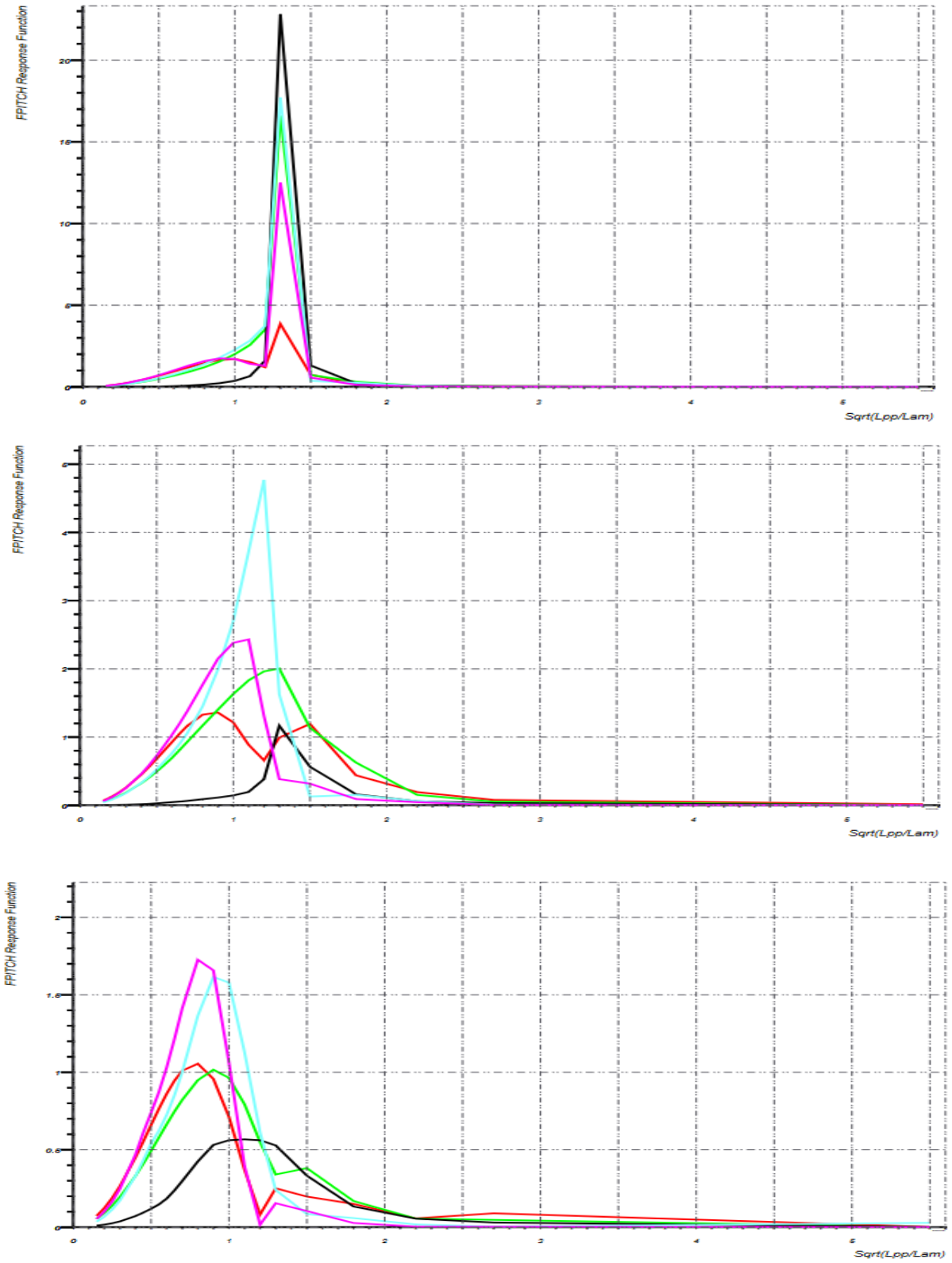

Figure 3.29 Pitch RAOs from top to bottom at 0, 3 and 13 knots

Surge

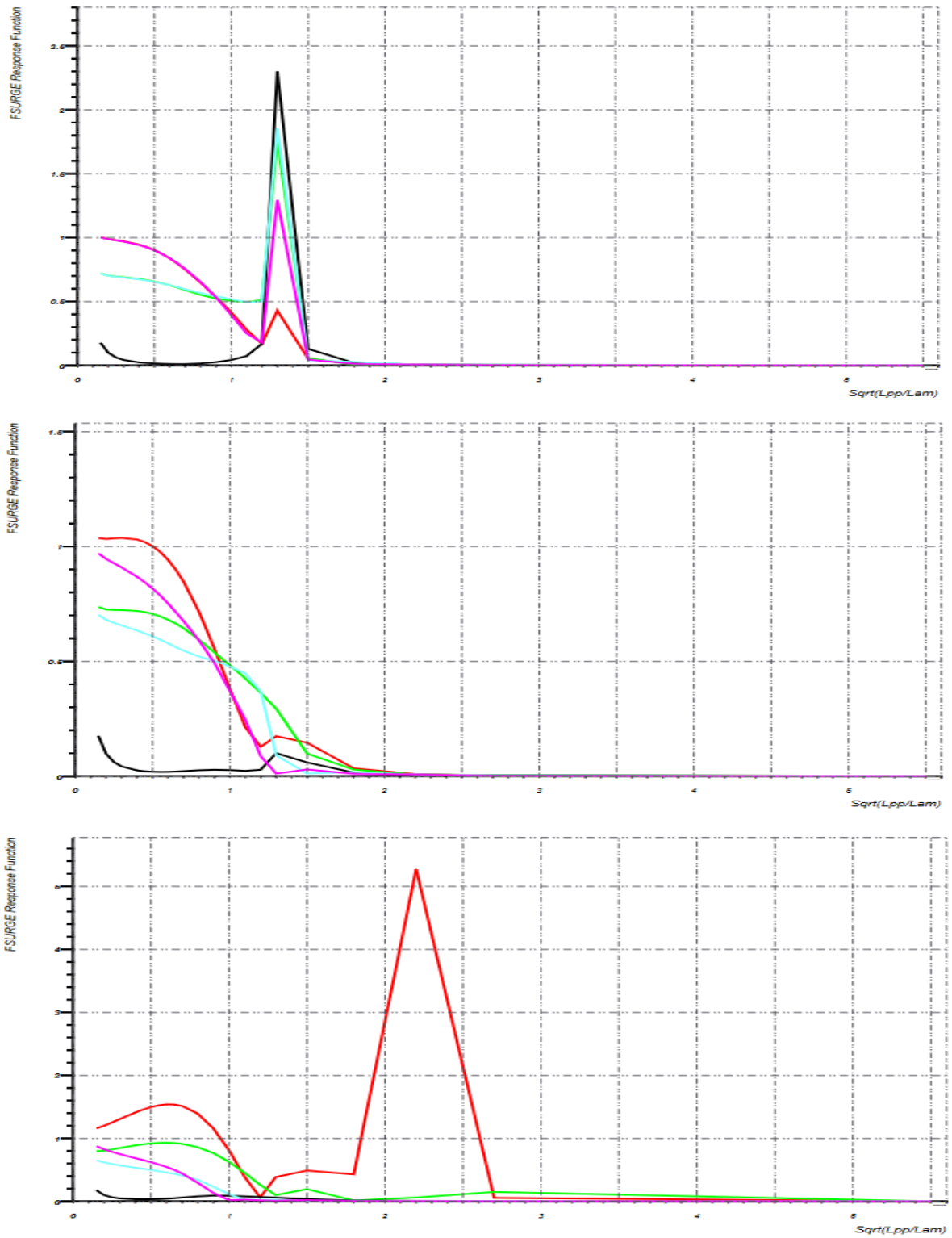

Figure 3.30 Surge RAOs from top to bottom at 0, 3 and 13 knots

Yaw

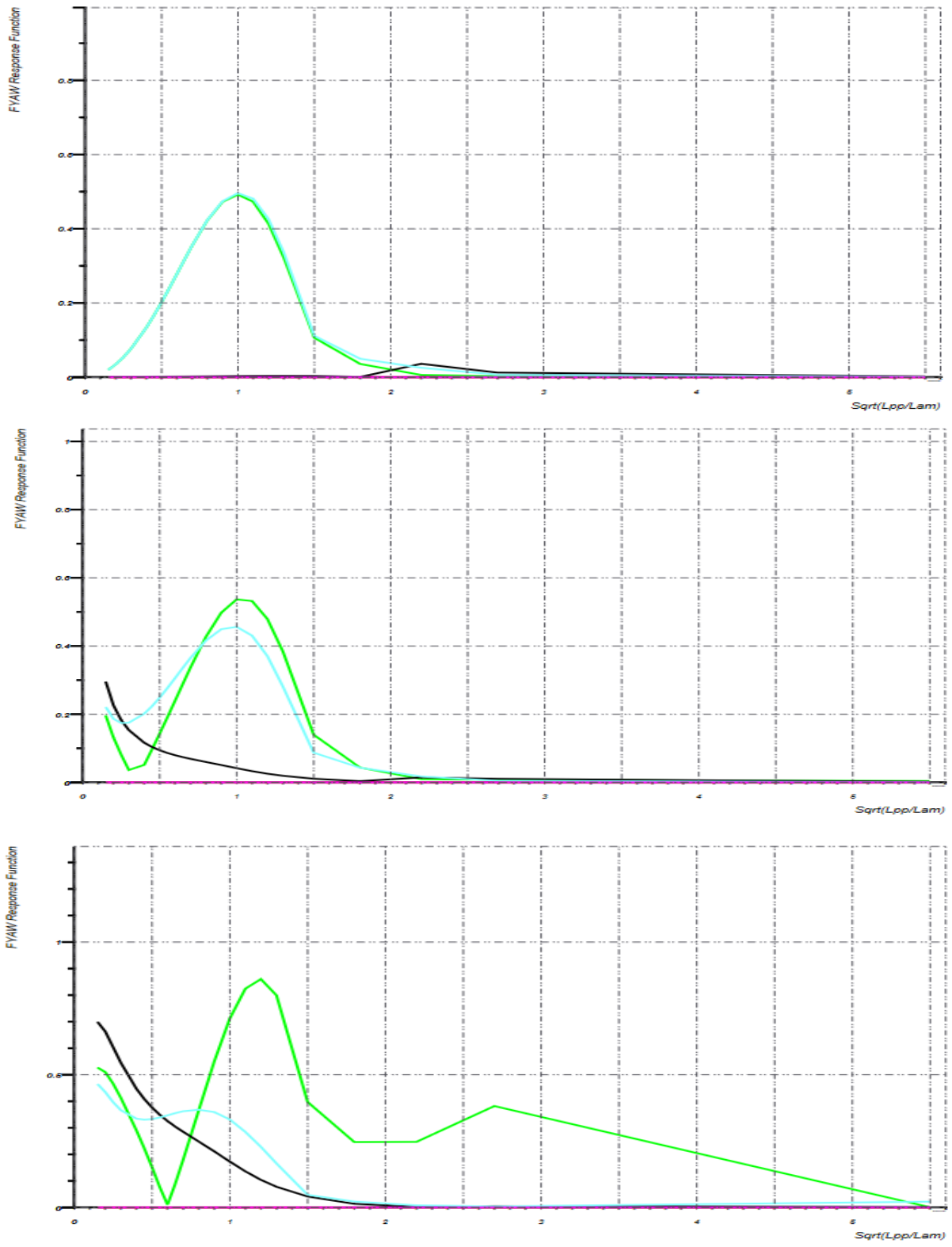

Figure 3.31 Yaw RAOs from top to bottom at 0, 3 and 13 knots

3.5 Motion response in irregular waves

Prediction of significant motions was done by matching peak periods of RAOs and wave spectrums. The wave spectra of selected sea states are shown in Fig. 3.32. Only vertical motions are shown in this section.

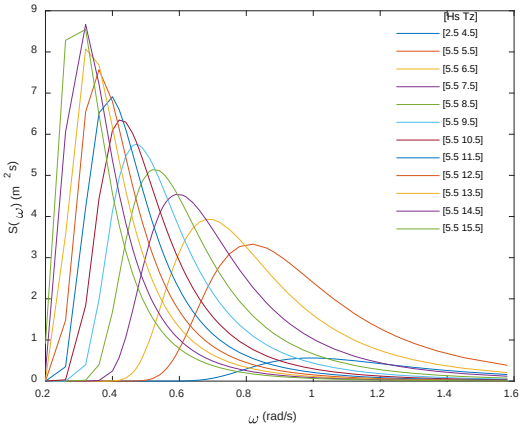

Figure 3.32 Spectra of selected sea states

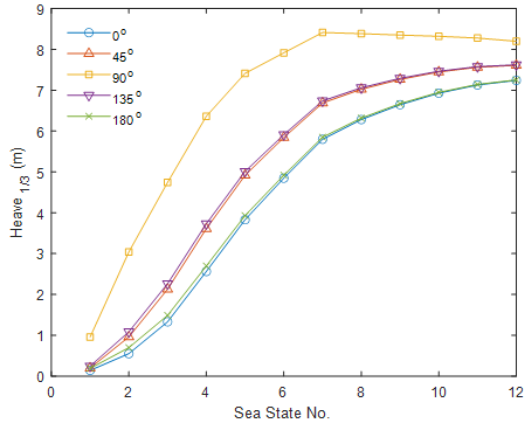
0°
45°
90°
135°
180°
Heave 1/3 (m)
Sea State No.

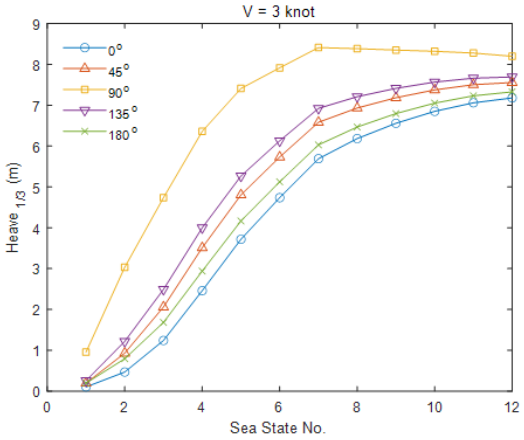
V = 3 knot
0°
45°
90°
135°
180°
Heave 1/3 (m)
Sea State No.

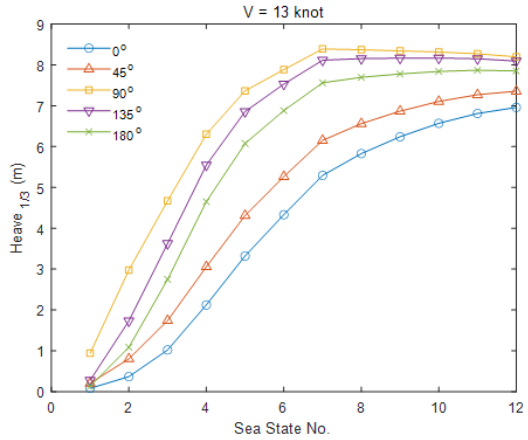
V = 13 knot
0°
45°
90°
135°
180°
Heave 1/3 (m)
Sea State No.

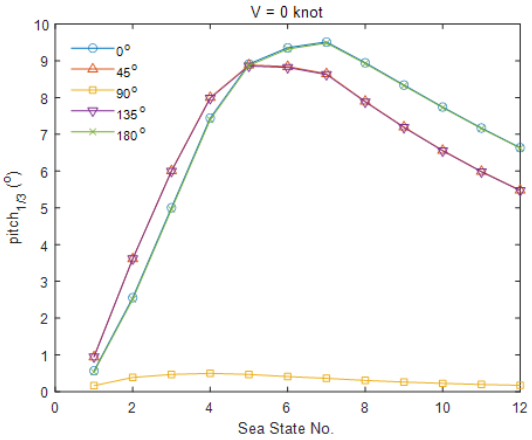
V = 0 knot
0°
45°
90°
135°
180°
pitch1/3 (°)
Sea State No.

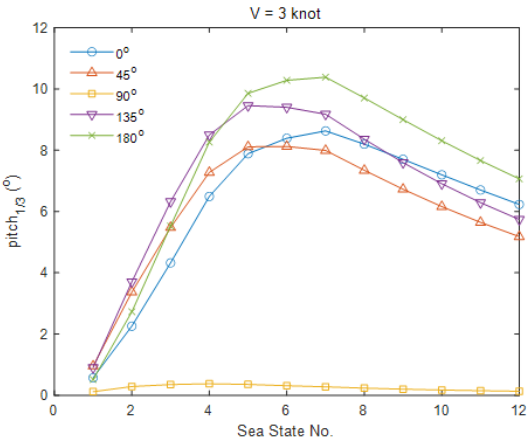
V = 3 knot
0°
45°
90°
135°
180°
pitch1/3 (°)
Sea State No.

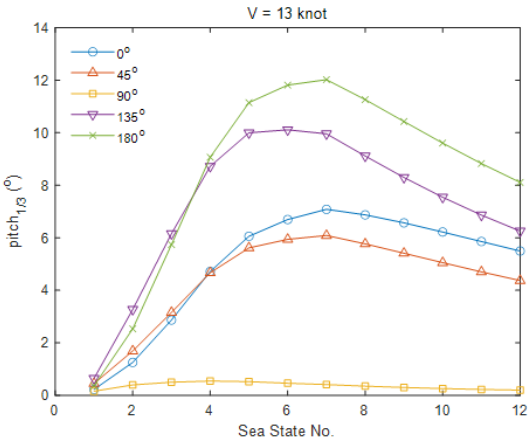
V = 13 knot
0°
45°
90°
135°
180°
pitch1/3 (°)
Sea State No.

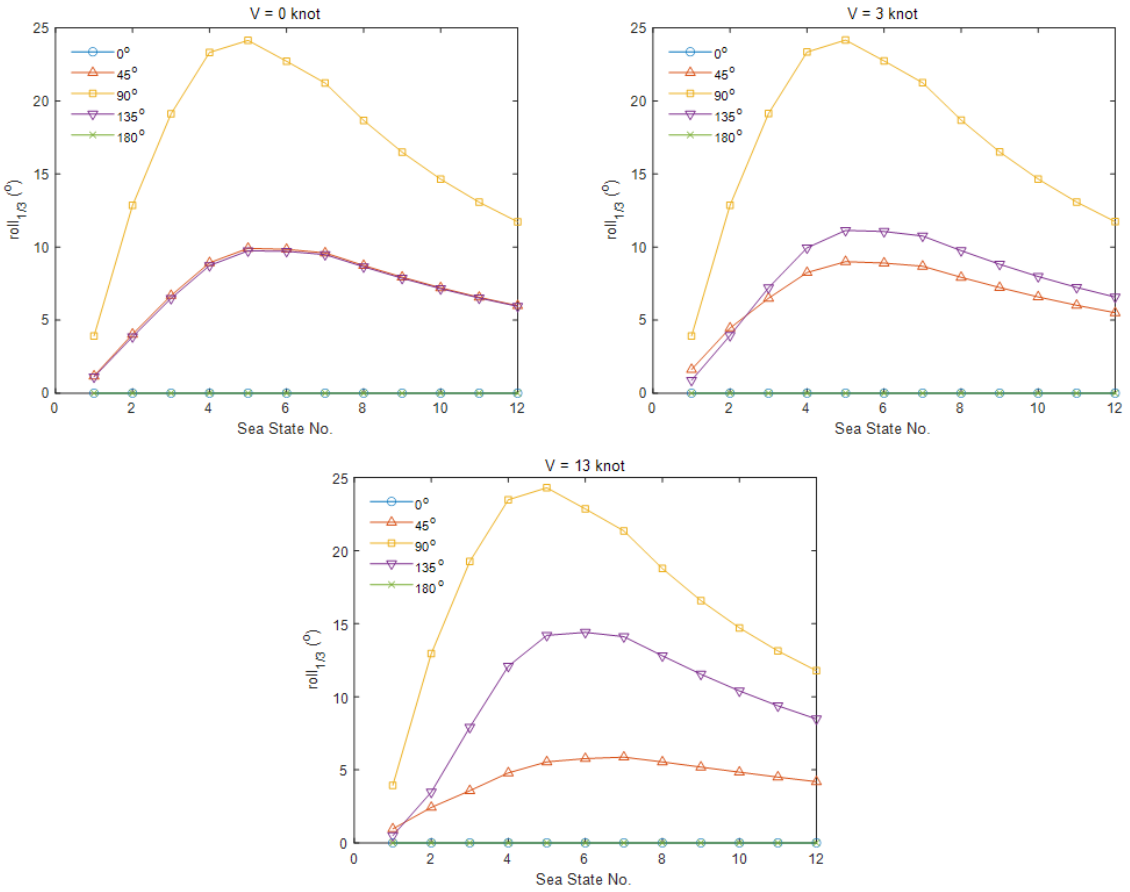

Figure 3.33 Significant value of heave, pitch, and roll motion in 12 sea states

As to the heave motion in irregular waves, the significant values are also higher in the beam sea. It is easy to understand because the heave RAO is higher at most wave frequencies in the beam sea. At zero speed, the heave response is similar in the head sea and following sea. When the speed is larger than zero, it makes the heave response larger in the head sea and the influence is proportional to the magnitude of the speed. The situation in the bow sea is same with the situation in the head sea.

As to the roll motion in irregular waves, the roll response reaches the maximum when the peak of wave spectrum is close to the peak of roll RAO in the beam sea. In this case, the roll response is the largest in the sea state with 8.5 s mean zero crossing period. That is because the roll motion has small damping and relatively small restoring moment. When the wave period is close to the natural period of roll, it is easy to induce resonance with large amplitude motion. The speed can increase the roll response in the bow and head sea and decrease the roll response in the following and quartering sea. The influence is proportional to the magnitude of speed.

As to the pitch motion in irregular waves, the pitch response is large when the peak frequency of wave spectrum is close to the peak frequency of pitch RAO. The advancing speed decreases the pitch response in the following and quartering sea but increases the pitch response in the bow and head sea.

From the aspect of seakeeping, the design of Khione is good in heave and pitch. The largest significant value of heave is about 8.5 meters in the severest sea state. The largest significant value of pitch is about 12 degrees in the severest sea state. However, the largest roll is about 25 degrees. The possible solution is to decrease the vertical center of gravity. This can increase the stiffness in the roll motion, and consequently, the peak frequency of RAO curve will increase and move apart from the wave spectrum of severe sea states. As a result, the significant roll will be reduced. One problem is this solution could reduce the comfortable level of ship crew. Other options are to increase the width of hull, or using the passive/positive anti-rolling tank.

3.6 Literature review

3.6.1 Book chapter, Jerzy Matusiak, Dynamics of a Rigid Ship: Chapter 4, General form of equations of motions

The book chapter General form of equations of motions by Jerzy Matusiak, from book Dynamics of a Rigid ship, explains the general equations of motion of a rigid body by two vector equations. According to the chapter equation of motions can be divided into equations for translational motion and equations for angular motion.

For the equations of motion, chapter states that it is easier and more logical to express external forces acting on a ship in coordinate system moving with the ship, instead of co-ordinate system in internal XYZ co-ordinate system. This coordinate system, which is moving with the ship is called body-fixed system. Often body-fixed coordinate systems are defined at the center of gravity of the ship, but Matusiak states that sometimes it is convenient to locate the coordinate system elsewhere, for example to the intersection of main frame, center plane and waterplane. In the chapter, Matusiak shows step by step how the equations of translation are derived from simple form of Newton's second law:

$$\boldsymbol{F} = \boldsymbol{m}\frac{d\boldsymbol{U}}{dt} \tag{3.5}$$

, where **F** is the vector of external forces, **m** is mass and **U** is the velocity of the center of gravity. Final form of the equations of translation motions depends on the coordinate system. Number of the formulating equations is three, because of all possible translation directions. Translation motion equations are cross-coupled to angular motion of the ship.

In case of the angular motion Matusiak states that governing vector is of a following form:

$$\boldsymbol{G} = \frac{d\boldsymbol{h}}{dt} \tag{3.6}$$

, where **G** is the moment of external forces around the center of gravity and **h** is the angular momentum. Forming angular motion equations depend on mass moment of inertia of body and angular velocity components. Formulating equations depends on used coordinate system. Resulting three angular motion equations are the final equations to complete the ship degrees of freedom equations for the ship.

3.6.2 Comparative study on the time-domain analysis of non-linear ship motions and loads

Article was about performed study that compared predictions of different non-linear time-domain codes applied to investigate the wave-induced vertical bending moment in a container ship. Analysis was done for wave of different steepness. Article was published in 1999 and addressed many issues of that time, when the computer power was significantly less than nowadays. Assessment of wave-induced loads on ships have been done for long times based on linear strip theory. It is known to be good engineering tool for the purpose, but it is also known that it has some limitations. One significant limitation is very much fundamental: the linear nature. The linear strip theory is, or at least was, commonly used, even it has been shown that different codes based on the theory can result in different predictions of the wave-induced loads on the ships. Obviously, this is causing uncertainty for designers.

For the first time concerns about the uncertainty of the linear theory raised as long time ago as in 1966. Concerns raised after Smith performed measurements of wave-induced loads in full-scale. Measurements were done on destroyer ships and results clearly showed that experienced sagging moments of the ship are much larger than the experienced hogging moments. This observation has triggered many attempts to develop theory that is able to present these non-linear features. Two main types of approaches to solve these non-linearities are: approach that attempts to model detailed and accurately all forms of non-linearities, and another that attempts to just account for the most significant contributions. At the time of the publication of the article computation power was very much weaker than nowadays so it was stated that first approach is not very suitable for design purposes. Possibly and probably nowadays the computing power has raised to level that the approach is also suitable for design use.

Article states that many of the non-linear load predictions are based on time-domain simulation. These simulations typically were carried at extreme wave conditions. Article divides the time-domain simulations in two main groups: simulations performed in time-domain and simulations performed mostly in frequency domain. In the frequency domain approach, the linear and non-linear terms are joined together in equations of motions, to achieve the non-linear responses. Hydrodynamic problem is assumed linear in this approach. This article focuses on these simplified

frequency-based methods of analyzing non-linear loads in ships. Methods were compared within each other and the adequacy of each methods is evaluated by comparing its predicted loads to experimental results. However, it is stated that conclusions of the accuracy of the methods cannot be done based on the comparison between the predictions and experimental results, but the indication about uncertainty of the non-linear prediction will be seen.

Article stated numerous numbers of methods. However, only limited number of codes ended up being compared. Even so, comparison clearly indicated that all the tested non-linear methods give Because of lack of time only few of the non-linear codes were used in comparison. All the methods gave results that are in line with the linear predictions in the low wave height region. In high wave region the similarity tented to become less. Reason behind this is increased role of the elastic behavior of the ship. Eventually, it seems like comparison between non-linear procedures and experimental or measured data was not done and is considered as the next step for deciding whether the non-linear methods are valid or not.

Performed study can be considered old and is possibly outdated. Assumingly, the time-domain simulations, which require more computing power are more in use nowadays. Wave induced loads are not yet considered in our ship design project. It would be interesting to find out if the linear approach for the load predicting is till the main design tool or are the non-linear simulations overtaken them.

3.6.3 Quick Strip Theory Calculations in Ship Design

The paper describes calculation method that delivers information about ship motions and added resistance in a very short computation time. This calculation method is based on a strip theory. The results of this method are compared to results of more accurate computation program for validation. The article is published in 1992, so possibly some information is already outdated.

The article states that ship design is mainly focused on still water performance. However, designer needs, in many cases, also information about variables like local motions, accelerations, added resistance, bow slamming and green water. Model experiments are one way to get this information, but unfortunately it is very expensive and time consuming, making it non-practical. Since about 1970 it has been possible to incorporate these previously mentioned seakeeping variables by use of numerical methods. One of these methods is the linear strip theory. Article states that non-linear theories will become available for design purposes too, so apparently at time of the publishing of the paper they were not in use yet.

At the time of publishing many, strip theory based, ship motion programs were occasionally used during the design process of ships. Article states that in many cases during the iterative design process these programs are too complicated and slow to use. To tackle this program, quick and human-error-safe method was developed. Tool was made on basis of strip theory and

comprehensive database with potential hydrodynamic coefficients in sway, heave and roll for a very wide range of monohulls. Eventually calculated responses for several ship types for all six degrees of freedom by this quick method were compared to accurate strip theory calculations.

At the time computer aided ship design tools were studied and discussed, but in article by Faltinsen and Svensen in 1990 it was stated that despite the limitation, the strip theory is still best alternative for practical and successful calculations of the wave induced motions of the ship in the early design stage (Faltinsen & Svensen, 1990). That is why comparison of the new quick methods to the strip theory at that time was sensible. However, it is shown that strip theory is very well effective for certain ship bodies. Best suitable hulls for the strip theory are slender hulls with length to breadth ratio less than 3. Downsides of the strip theory is low accuracy in extreme sea states, and because it is based on potential flow theory, it does not consider viscous effects. Neglecting the viscous effects can cause serious problems in predicting roll motions at resonance frequencies.

Based on performed comparison of the quick method and the strip theory it concluded that the quick method can be used for conventional monohull ships at least at early stage of design. Quick method had basically the same limitations as the strip theory i.e., non-slender or non-conventional hulls, high-speed vessels, and extreme sea states.

During last thirty years since the article was published a lot of progress has been seen in computing capacity and software. Nowadays the need for such quick method is possibly not anymore so needed. However, basic linear strip method is still used for predicting the wave induced motions and loads in the software like NAPA and Maxsurf.

4. Global Loads in Irregular Waves

4.1 Calculation of global loads

Analysis of global loads included analysis of shear forces and bending moments experienced by Khione. Analysis was performed with two different software, like in analysis of RAOs and ship motions. NAPA and Hydrostar were used. BY using Hydrostar, the global loads on hull girder are calculated at three advancing speeds: 0 knot, 3 knots, and 13 knots. Five wave directions are considered: 0°, 45°, 90°, 135°, and 180°. Four typical sea states are used to generate the significant value of vertical bending moment and shear force. Table 4.1 shows the significant wave height and mean zero crossing period of these four sea states. The value is derived from Table C-2, Scatter diagram for the North Atlantic, of DNV RP C205. Pierson-Moskowitz spectrum is used to represent the sea states.

Table 2.1 Parameters of sea states

Sea state no.	1	2	3	4
Hs [m]	9.5	14.5	16.5	16.5
Tz [s]	6.5	8.5	10.5	12.5

For calculating the bending moments and shear forces, 22 cross sections are established along with the hull girder. The normal vector of these sections is parallel to the X axis of the hull girder. The mass of ship is distributed at these sections, which is shown in Fig. 4.1.

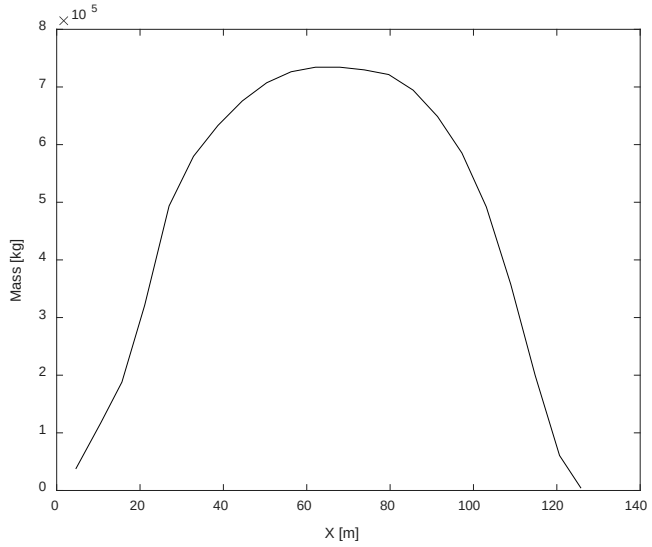

Figure 4.1 Mass distribution at the cross sections

Figures 4.2 ~ 4.7 show the significant value of vertical bending moment and shear force at each section.

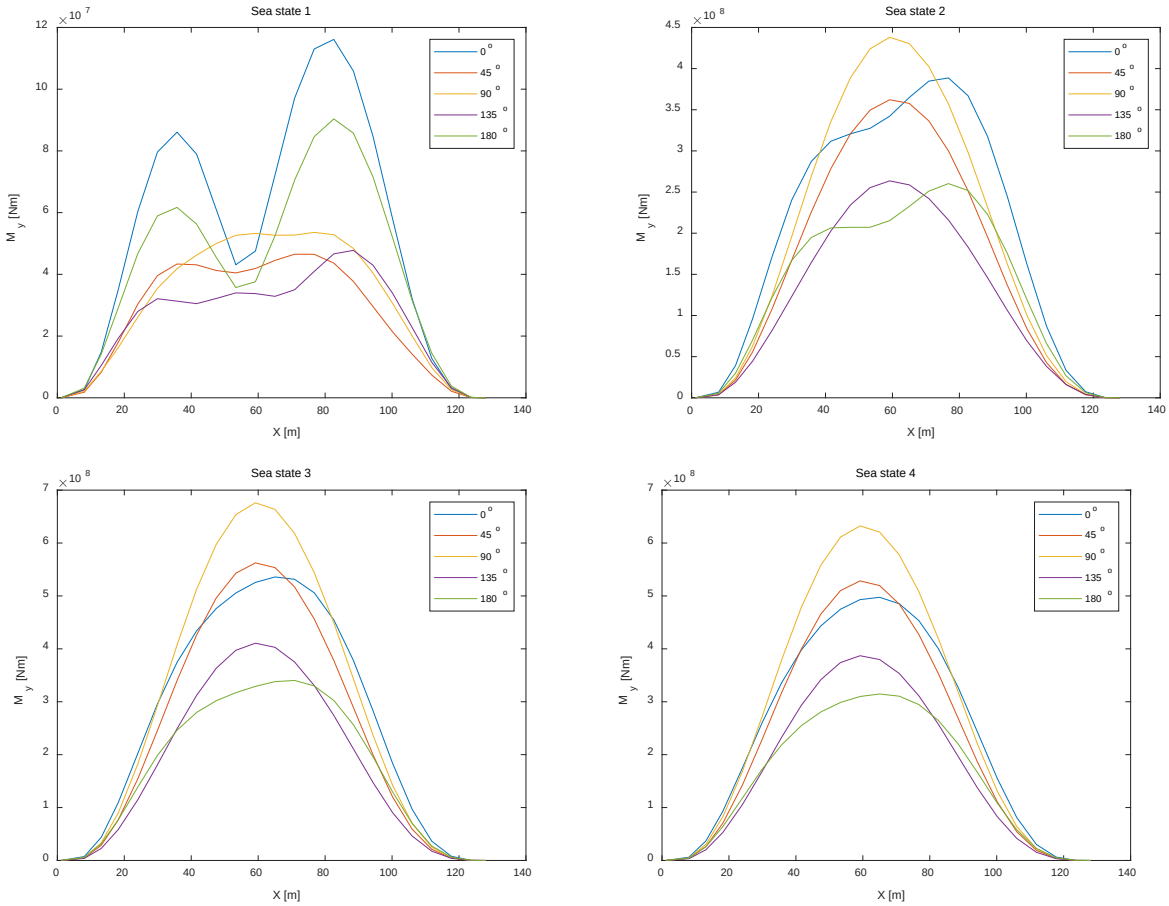

Figure 4.2 Vertical bending moment, V = 0 knot

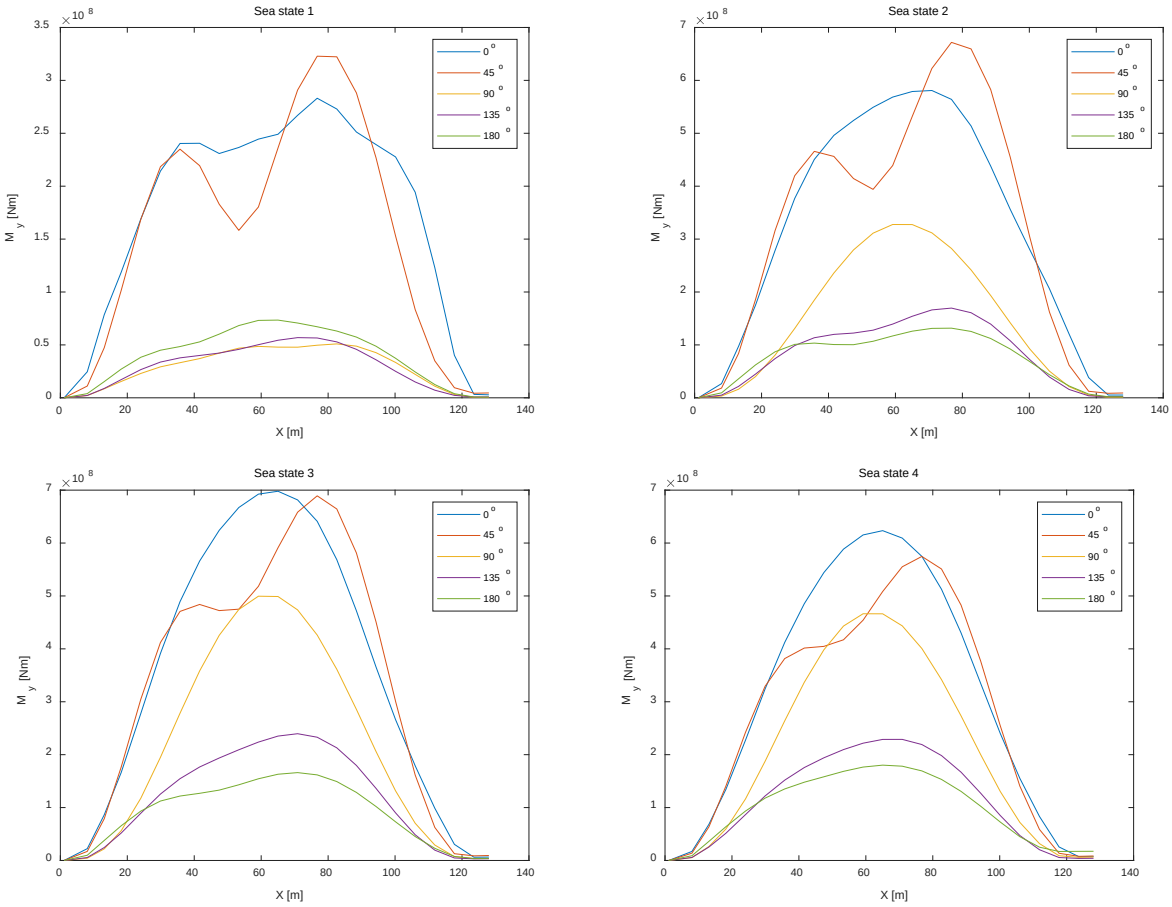

Figure 4.3 Vertical bending moment, V = 3 knot

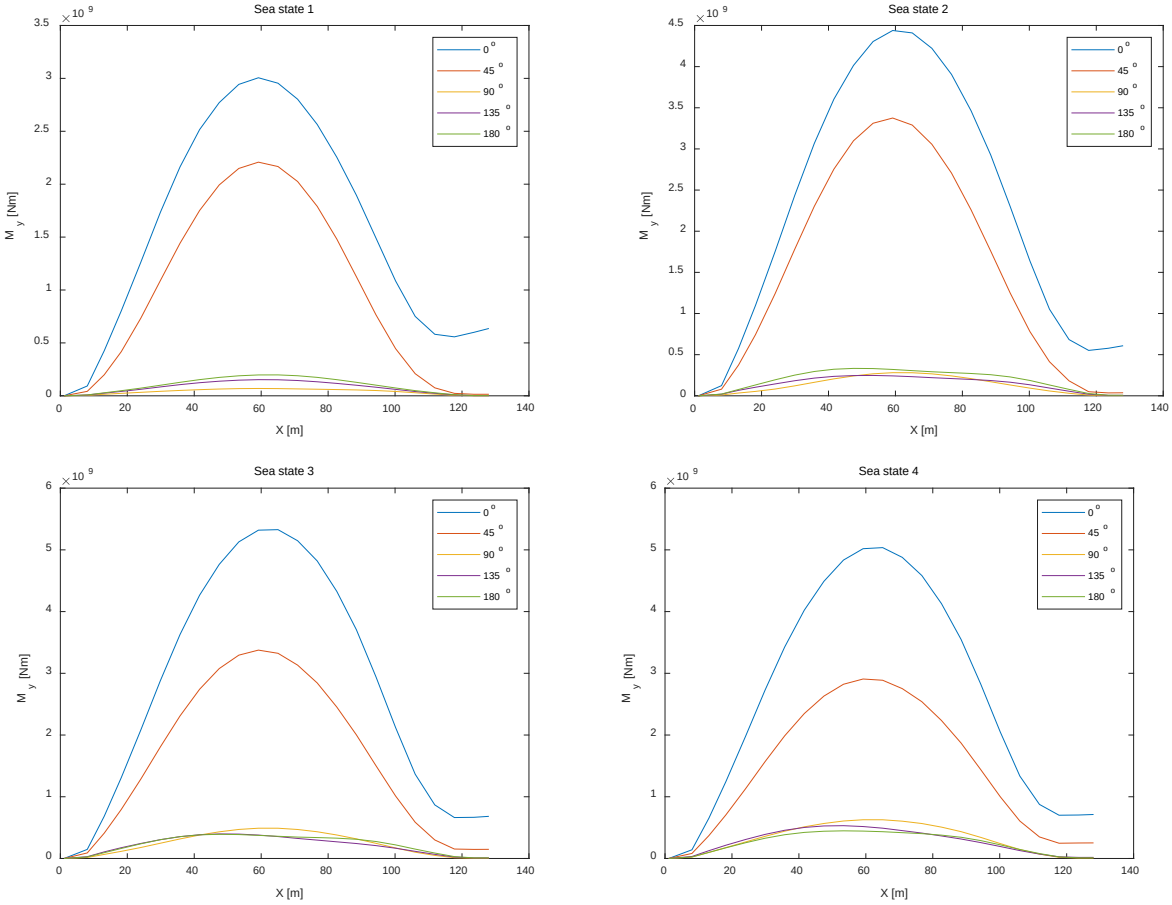

Figure 4.4 Vertical bending moment, V = 13 knot

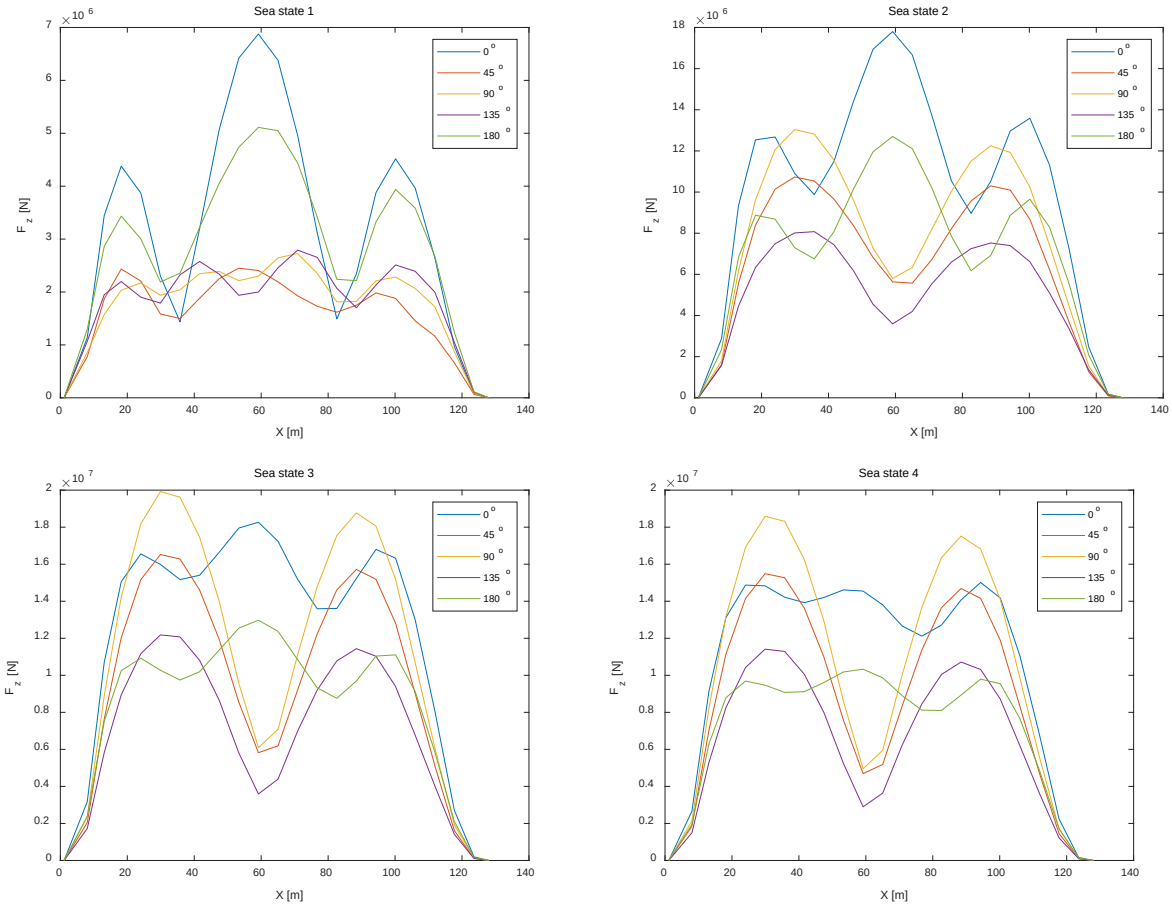

Figure 4.5 Vertical shear force, V = 0 knot

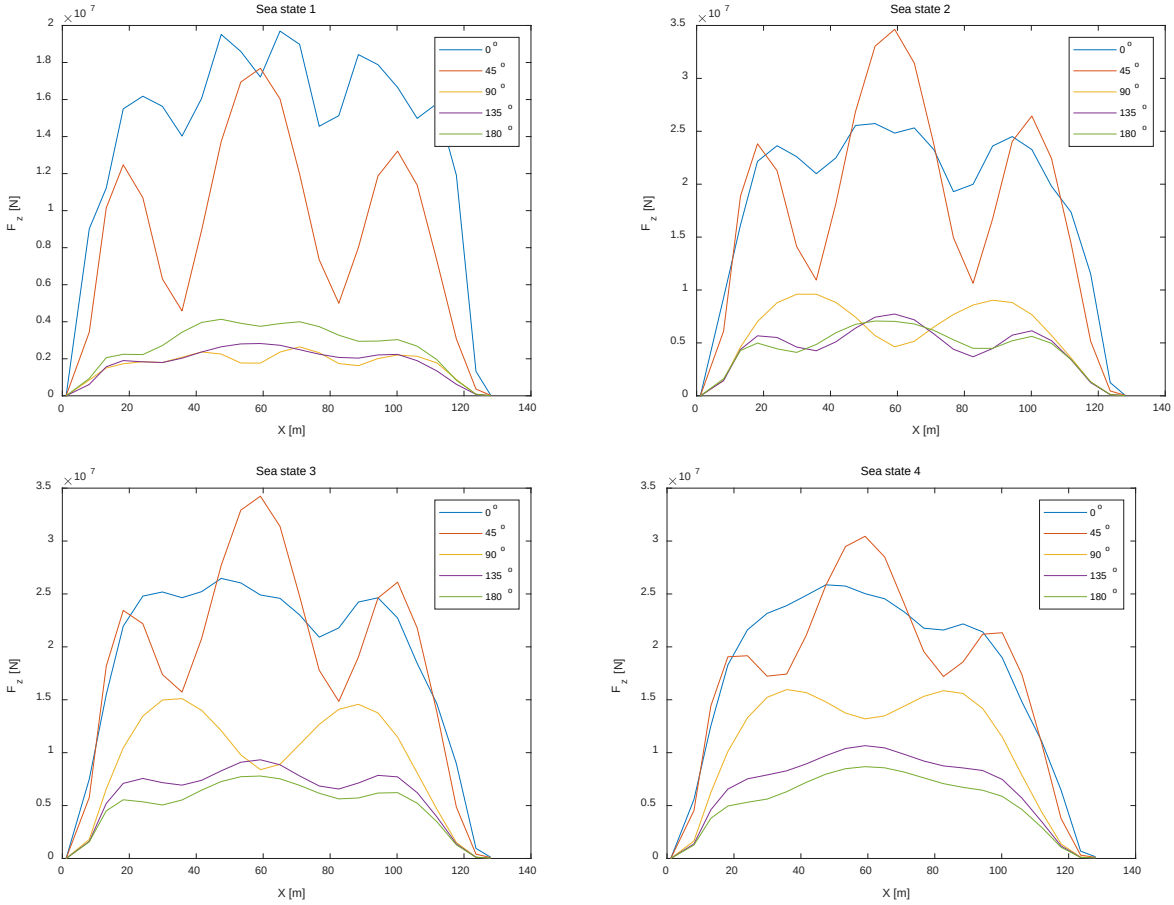

Figure 4.6 Vertical shear force, V = 3 knot

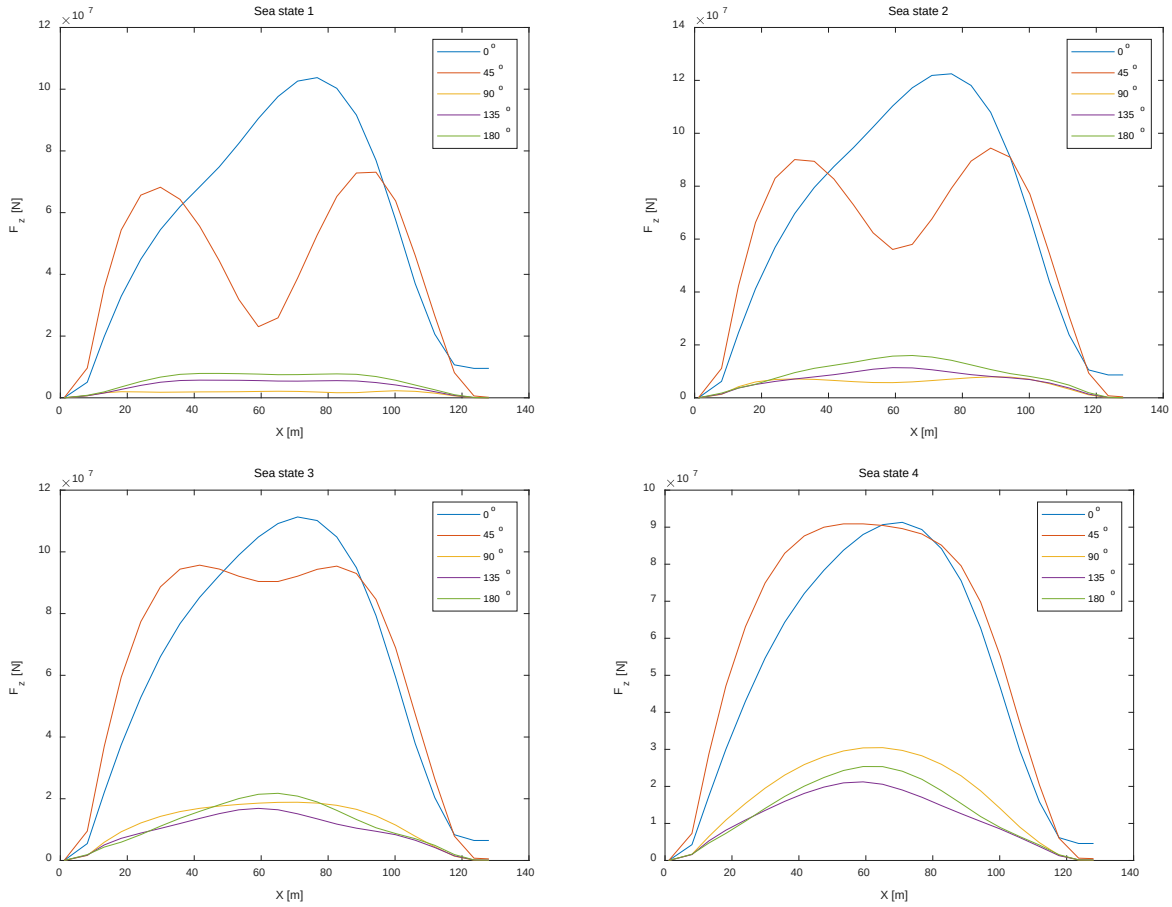

Figure 4.7 Vertical shear force, V = 13 knot

Firstly, the results show that the bending moment and shear force are most severe in sea state 3, which has the highest significant wave height and its Tz is smaller than that of sea state 4. Even though, the significant wave height of sea state 4 is same as that of sea states 3, the global forces are relatively milder than sea states 3.

Secondly, the bending moment and shear force are not apparently influenced by the wave directions at zero speed. However, they are notably higher at 0^o and 45^o. The influence of advancing speed is proportional to its magnitude. Therefore, the ship experiences tougher condition in the following sea and quartering sea from the aspect of global load.

Analysis of global loads in NAPA included only the bending moments due to license problems on school computers. Bending moment calculations only at sea states with significant wave height of $H_{1/3} = 9.5\ m$ and $H_{1/3} = 14.5\ m$ and ship velocity of 13 knots are presented in this report, because the sea state with $H_{1/3} = 2.5\ m$ and lower speed of ship caused significantly less bending moments than the two previously mentioned sea states. Results for bending moments caused by these sea states with different wave headings are presented below in Figures 4.8 and 4.9.

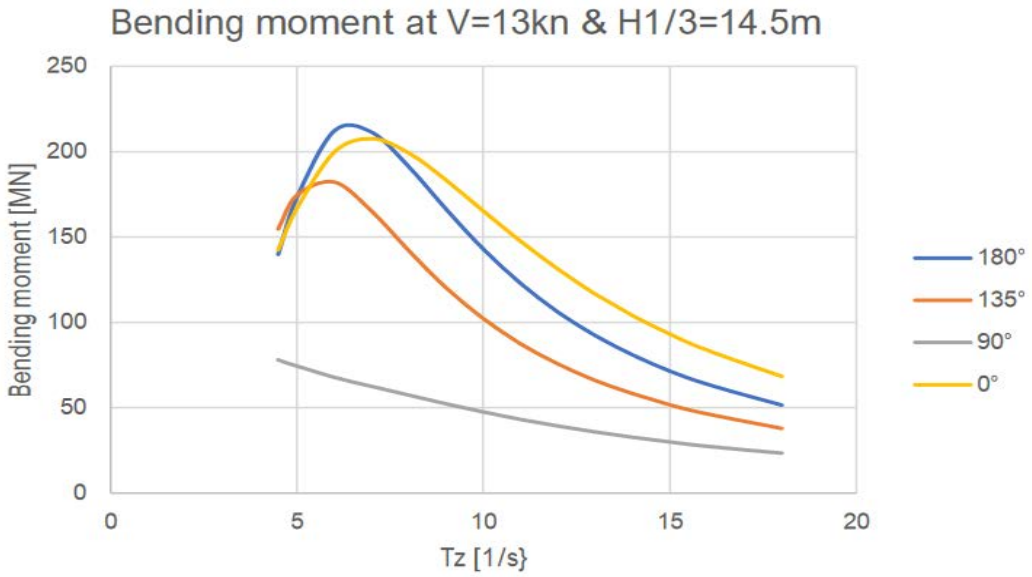

Figure 4.8 Bending moments at 13 knots with 14.5m significant wave height

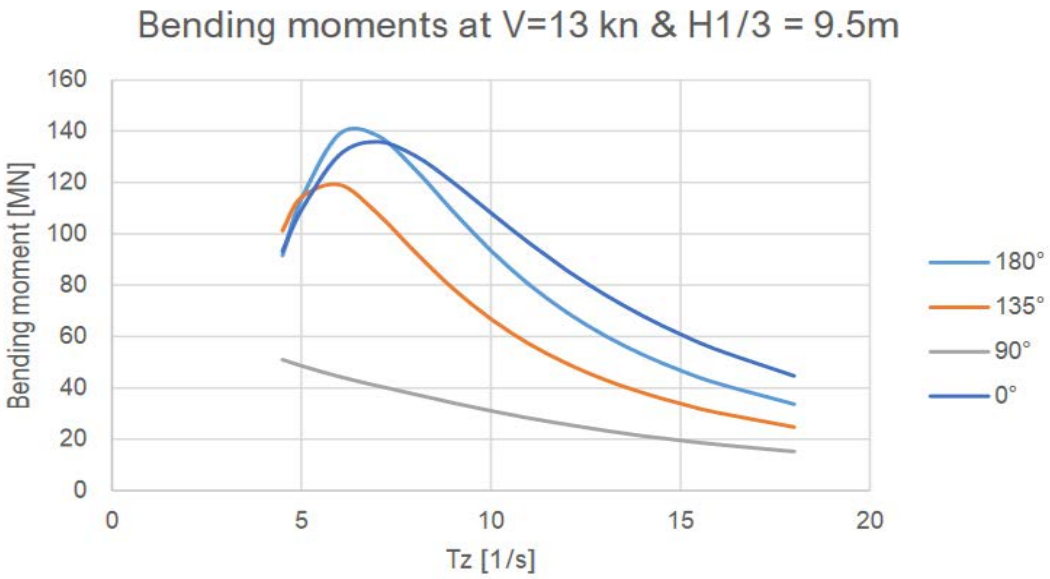

Figure 4.9 Bending moments at 13 knots with 9.5m significant wave height

4.2 Discussion

The aim of this chapter is to review selected ship dynamics literature and validate the computed RAOs and responses. It is unrealistic to expect to find studies for ships exactly like Khione, so only qualitative comparison can be done here.

Paper by Kukkanen & Matusiak (2014) evaluate various nonlinear methods to calculate hull responses in waves. Kukkanen & Matusiak computed the 3-hour maximum shear forces and

bending moments for a 173m RoPax vessel in head seas. The ship has a block coefficient of 0,55 and is assumed to be stationary. The results are displayed in figure 4.10.

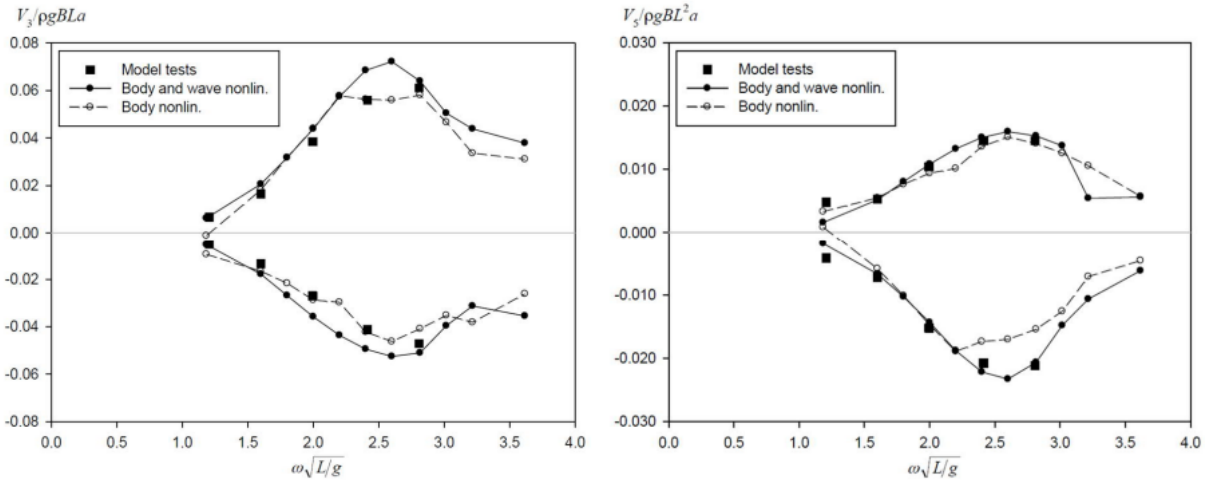

Figure 4.10. Midship shear forces and bending moments for a RoPax vessel in a dimensionless form.

The results are given for a wave with a/L-ratio of 0.013, which in Khione's case, corresponds to wave height of 3,3m. Since the data is presented as dimensionless, we can assume linear scaling and use the amplitude of 9.5m. This way, the maximum magnitude of bending moment is about **300 MNm** in hogging condition, occuring at wave frequency of 0.7 rad/s. The maximum shear force occurs at same frequency and its magnitude is about **10 MN.**

Stationary bending moments and shear forces obtained from Hydrostar are reasonably close to moments and shears of this study, indicating that no major error has been done during the calculation.

4.3 Literature review

The book chapter covered in this section is chapter 8.7 "Internal Loads" of the book: Offshore Hydrodynamics published by Delft University of Technology (Journée et al. 2015) The chapter covers static, quasi-static and dynamic loads on a ship.

4.3.1 Static Loads

A ship floats because the weight of the ship is counteracted by the buoyancy force due to its displacement. However while the ship in its entirety is in static equilibrium, individual sections of the ship may have a higher or lower weight than their individual buoyancy. This causes both a varying shear load and a varying bending load along the hull. The loads on single section are schematically shown in Figure 4.11.

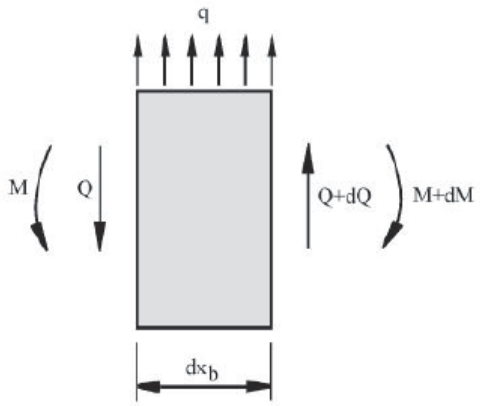

Figure 4.11 Loading of a single section along the ship's length.

From the above figure, the equations to find the static vertical shear and bending moment at the cross-section at $x_b = x_1$ can be found by integrating the loads over the x-direction:

$$q_z(x_b) = \rho \cdot A_x(x_b) \cdot g - m'(x_b) \cdot g \tag{4.1}$$

$$Q_z(x_1) = -\int_{stern}^{x_1} q_z(x_b) \cdot dx_b \tag{4.2}$$

$$M_y(x_1) = \int_{stern}^{x_1} q_z(x_b) \cdot x_b \cdot dx_b + Q_z(x_1) \cdot x_1 \tag{4.3}$$

In which q_z is the distributed shear load in z-direction, Q_z is the shear force in z-direction and M_y is the moment about the y-axis. $m'(x_b)$ is the sectional mass and $A_x(x_b)$ is the cross-sectional area. While static loads are not the topic of the course, they must be included to accurately estimate the loads of a ship in wave conditions, as a ship will always be subjected to a buoyancy and weight force.

4.3.2 Quasi-Static Loads

Quasi-static loads are dynamic loads that vary so slowly that they act like static loads onto the structure. Mooring and anchor lines as well as wind and currents tend to induce transverse loads that act at different elevations on the ship's side. As a result the ship will come to a static roll angle, which can make capsizing more likely in rough seas. Furthermore, point loads like mooring and anchor lines will induce a torsional load into the structure as well. The propeller's thrust also induces a quasi-static compressive load into the bottom of the structure in front of the thrust bearing. This actually increases the compressive load in the bottom structure when the ship is hogging while decreasing the tensile load in the bottom structure when the ship is sagging. For ship sections aft of the thrust bearing, the thrust will induce tensile stress and the effect on the bending loads will be opposite. In relation to this ship project, quasi-static loads are not so relevant because the course focusses on ship dynamics and the calculation of these quasi-

static loads is more of a topic for structural design, however they should be taken into account when designing a real ship.

4.3.3 Dynamic loads

Dynamic loads are induced by waves and also by mooring lines and anchors. They can be caused by both linear and non-linear effects; however, the chapter is limited to linear effects and only covers wave induced loads.

Lateral Dynamic Shear Force and Moments

The lateral dynamic loads can be predicted by the equations below:

$$q_y(x_b) = X'_{h_y}(x_b) + X'_{w_y}(x_b) + \rho g A_x(x_b) \cdot \phi - m'(x_b) \cdot \left[\ddot{y} + x_b \cdot \ddot{\Psi} - z'_m(x_b) \cdot \ddot{\phi} + g \cdot \dot{\phi}\right] \quad (4.4)$$

$$Q_y(x_1) = Q_{y_a} \cdot cos(\omega_e t + \varepsilon_{Q_y\zeta}) = -\int_{stern}^{x_1} q_y(x_b) \cdot dx_b \quad (4.5)$$

$$M_z(x_1) = M_{z_a} \cdot cos(\omega_e t + \varepsilon_{M_z\zeta}) = -\int_{stern}^{x_1} q_y(x_b) \cdot x_b \cdot dx_b - Q_y(x_1) \cdot x_1 \quad (4.6)$$

X'_{h_y} and X'_{w_y} are the sectional hydromechanical and wave forces in sway respectively at the location x_b. $m'(x_b) \cdot \ddot{y}$ is the inertia force from acceleration in the y direction while $m'(x_b) \cdot x_b \cdot \ddot{\Psi}$ is the inertia force at section x_b due to yaw rotation. Lastly $m'(x_b) \cdot g \cdot \dot{\phi}$ is a lateral mass-force component due to the definition of the lateral loads in the ship-bound axes system.

Vertical Dynamic Shear Force and Moments

The longitudinal and vertical load on a section of the hull in waves can respectively be calculated by the 2 equations below:

$$q_x(x_b) = X'_{h_x}(x_b) + X'_{w_x}(x_b) - m'(x_b) \cdot \left[\ddot{x} - \overline{bG}(x_b) \cdot \ddot{\theta}\right] \quad (4.7)$$

$$q_z(x_b) = X'_{h_z}(x_b) + X'_{w_z}(x_b) - m'(x_b) \cdot [\ddot{z} - x_b \cdot \ddot{\theta}] \quad (4.8)$$

The variables in these equations are as defined above but then in different directions and with $\overline{bG}$ being the distance between the centroid of the section and the x_b axis. One can then integrate these equations over the hull to find the vertical shear force and moment at the point x_1:

$$Q_z(x_1) = Q_{z_a} \cdot cos(\omega_e t + \varepsilon_{Q_z\zeta}) = -\int_{stern}^{x_1} q_z(x_b) \cdot dx_b \quad (4.9)$$

$$M_y(x_1) = M_{y_a} \cdot cos(\omega_e t + \varepsilon_{M_y\zeta}) = \int_{stern}^{x_1} q_x(x_b) \cdot \overline{bG}(x_b) \cdot dx_b + \int_{stern}^{x_1} q_z(x_b) \cdot x_b \cdot dx_b + Q_z(x_1) \cdot x_1 \quad (4.10)$$

Torsional Dynamic Loads

The torque about a longitudinal axis that is a distance z_1 above the center of gravity can be calculated using the equations below.

$$M_x(x_1, z_1) = M_{x_a} \cdot cos(\omega_e t + \varepsilon_{M_x\zeta}) = -\int_{stern}^{x_1} q_\phi(x_b, z_1) \cdot dx_b \quad (4.11)$$

$$q_\phi(x_b, z_1) = X'_{h_\phi}(x_b) + X'_{w_\phi}(x_b) + z_1 \cdot q_y(x_b) - m'(x_b) \cdot [k'^2_{xx} \cdot \ddot{\phi} - z'_m(x_b) \cdot (\ddot{y} + x_b \cdot \ddot{\Psi} + g \cdot \phi)] \quad (4.12)$$

X'_{h_ϕ} and X'_{w_ϕ} are the hydrodynamic and wave roll moments respectively, $z_1 \cdot q_y(x_b)$ is the torque induced by the off-center shear loads and the last terms are inertia forces, with k'_{xx} being the radius of gyration about the x-axis. Note that sailing into quartering seas can also induce significant torsional loads, even when the ship does not appear to be rolling much. These loads tend to be higher for lower encounter frequencies.

Fatigue Loads

Fatigue loads are cyclic loads that weaken a structure over time. The deck, bottom and side shell of the ship are susceptible to fatigue due to vertical and horizontal bending loads. The bottom and side shell are also susceptible to fatigue due to local varying pressures on the hull plating due to waves. These loads are schematically shown in Figure 4.12.

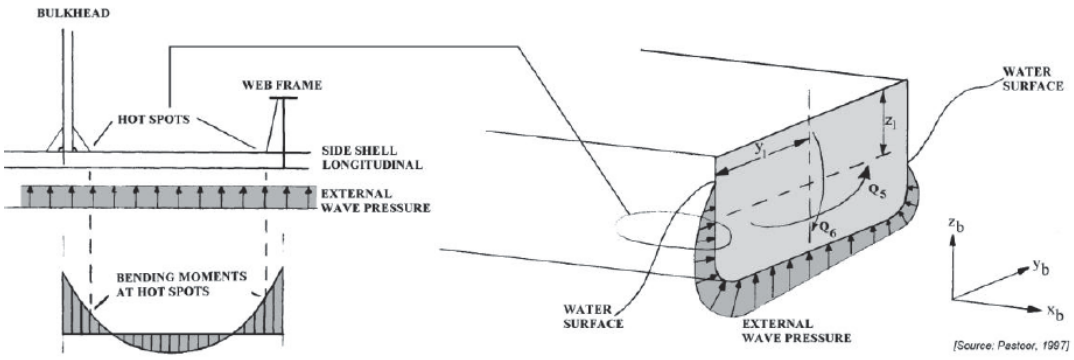

Figure 4.12 Schematic figure of the global and local loads acting on a cross-section of the hull girder.

To find the bending load on a position on the cross-section: (y_1, z_1), one must combine the horizontal and vertical bending load, which can be done by using the following equation:

$$H_{\sigma\zeta}(y_b, z_b, \omega) \cdot cos(\omega t + \varepsilon_{\sigma\zeta}) = \frac{z_1}{I_{yy}} \cdot H_{Q_5\zeta}(y_b, z_b, \omega) \cdot cos(\omega t + \varepsilon_{Q_5\zeta}) + \frac{y_1}{I_{zz}} \cdot H_{Q_6\zeta}(y_b, z_b, \omega) \cdot cos(\omega t + \varepsilon_{Q_6\zeta}) \quad (4.13)$$

Here $H_{\sigma\zeta}$ is the combined bending load, while $H_{Q_5\zeta}$ and $H_{Q_6\zeta}$ are the vertical and horizontal bending loads respectively. I_{yy} and I_{zz} are the second moment of area about the y- and z-axis

respectively. This equation can be used to be find the combined load based on different wave scatter diagrams and the period of the waves can be used to estimate the number of stress cycles. One can then input all this data in a Miner-Palgrem sum to estimate the fatigue damage over the ship’s lifetime.

5. Seakeeping Criteria, Maneuvering Tests, and Resistance

5.1 Seakeeping criteria

In this section, the seakeeping capability of Khione is assessed from the aspects of wave induced motions by using specific criteria. Basic seakeeping criteria will typically include ship motions and ship-motion related phenomena. (ITTC 2005) The seakeeping criteria is used to determine the seakeeping performance (motions and accelerations) of Khione in the specific sea states. The short-term sea states usually have a duration of three hours. The following factors can affect the seakeeping performance: 1) hull form, main dimensions, and mass distribution of Khione; 2) wave profile of sea states; 3) advancing speed; 4) wave direction; 5) the content of work and operations onboard.

International Standard ISO (195, 1997) provides severe discomfortable boundaries of vertical acceleration, frequency, and duration of exposure for motion sickness. O'Hanlon and McCauley (1974) discuss the parameter of Motion Sickness Incidence (MSI) which including the acceleration, duration, and frequency of acceleration. The seakeeping performance not only affects the feeling of crew and passengers, but it also affects the operation onboard. For example, the security of a helicopter's launch and recovery on the flight deck is intensively affected by the seakeeping performance of ship.

Vertical and lateral accelerations are considered the main affecting parameters for the seasickness. Odabasi et al. (1991) provide an estimation of maximum acceptable scale of vertical accelerations for various activities onboard, as shown in the Table 5.1.

Table 5.1 Limiting criteria for vertical acceleration (Odabasi et al., 1991)

Vertical RMS acceleration (g)	Description
0.020	Passengers on a cruise liner. Older people. Close to the lower threshold below which vomiting is unlikely
0.050	Passengers on a ferry. The international standard for 2 h exposure period. Causes symptoms of motion sickness in approximately 10% of unacclimatized adults
0.100	Intellectual work by people reasonably well adapted to ship motions (i.e. scientific personnel on ocean research vessels). Cognitive/manual work of a more demanding nature. Long term tolerable for the crew. The international standard for half an hour exposure period
0.150	Heavy manual work by people adapted to ship motions: for instance on fishing vessels and supply ships
0.200	Light manual work by people adapted to ship motions. Not tolerable for longer periods. Quickly causes fatigue
0.275	Simple light work. Most of the attention must be devoted to keeping balance. Tolerable only for short periods on high-speed craft

Sarioz and Narli (2005) present seakeeping criteria for the personnel performance, which are listed in the Table 5.2. The criteria are significant value of accelerations.

Table 5.2 Typical personnel performance criteria (Sarioz and Narli, 2005)

Application	Motion	Limit	Location
General	Vertical Acceleration	0.4 g	Bridge
	Lateral Acceleration	0.2 g	Bridge
Specific Task	MSI	20% of personnel	Task location
	MII	1/min	Task location

This report selects two locations to study the seakeeping performance of Khione, which are presented in Table 3. The bridge is selected to study the influence on the seasickness. At this location, the criteria of vertical and lateral accelerations in Table 2 are used to assess the seakeeping performance of Khione. The flight deck is selected to study the influence on the helicopter's launch and recovery. At this location, the criterion of Heavy manual work in the Table 1 is selected to assess the seakeeping performance. In addition, the criteria of roll and pitch are also selected to assess the seakeeping performance and keep the security of the helicopter's launch and recovery: limited to periods of quiescence having roll angles less than 8 degrees and pitch angles less than 3 degrees (Tadros et al., 2003)

Table 5.3 Selected locations for seakeeping performance study

Location	X [m]	Y [m]	Z [m]
Bridge	71.3	0	18.2
Flight deck	116.4	0	6

Table 5.4 shows the significant wave height and mean zero crossing period of 12 sea states. The value of mean zero crossing period are derived from Table C-2, Scatter diagram for the North Atlantic, of DNV RP C205. The significant wave height is 5.5 m, which can cover 90% sea states in the North Atlantic according to the scatter diagram. Pierson-Moskowitz spectrum is used to represent the sea states, as shown in Fig. 5.1.

Table 5.4 Sea states

Sea State	1	2	3	4	5	6	7	8	9	10	11	12
Hs [m]	2.5	5.5	5.5	5.5	5.5	5.5	5.5	5.5	5.5	5.5	5.5	5.5
Tz [s]	4.5	5.5	6.5	7.5	8.5	9.5	10.5	11.5	12.5	13.5	14.5	15.5

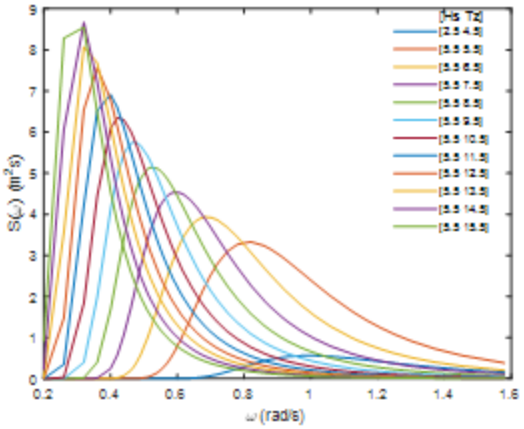

Figure 5.1 Spectra of selected sea states

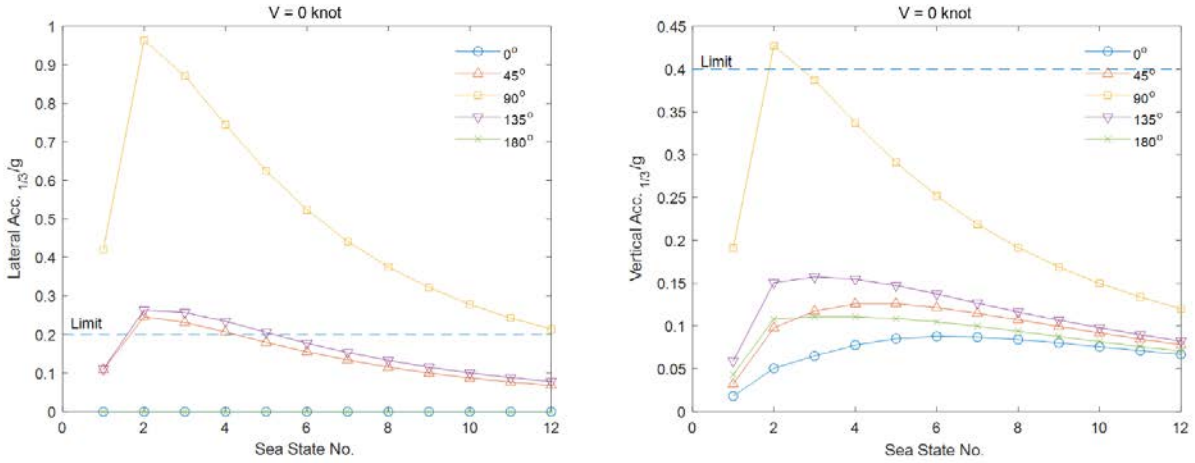

Figure 5.2 Lateral and vertical accelerations at bridge, V = 0 knot

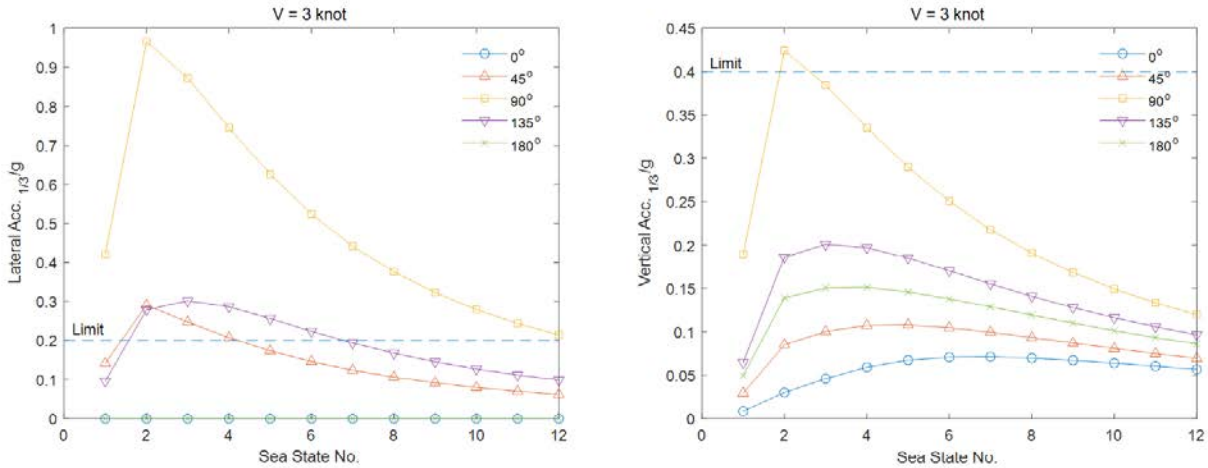

Figure 5.3 Lateral and vertical accelerations at bridge, V = 3 knot

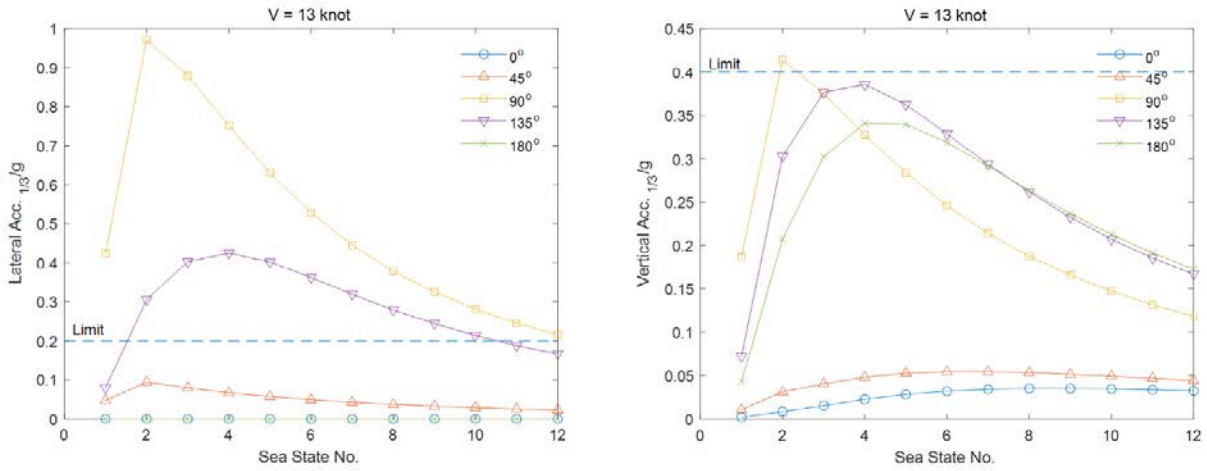

Figure 5.4 Lateral and vertical accelerations at bridge, V = 13 knot

Figure 5.2-5.4 show the lateral and vertical accelerations at bridge in various sea states. The criteria are shown as dash lines in these figures. In the beam sea, the lateral acceleration is much larger than the criterion. The large lateral acceleration is induced by the large roll motion. Thus, the lateral acceleration could be reduced by decreasing the roll response of Khione. Therefore, the suggestion is to increase the width of Khione or to install the stabilization systems. Because Khione often voyages in the waters with ice, the active fins and bilge keels are not recommended. Thus, the passive and active tanks would be a good solution. In all cases, the vertical accelerations are below or close to the criteria so Khione's seakeeping performance in the vertical acceleration is good at the bridge.

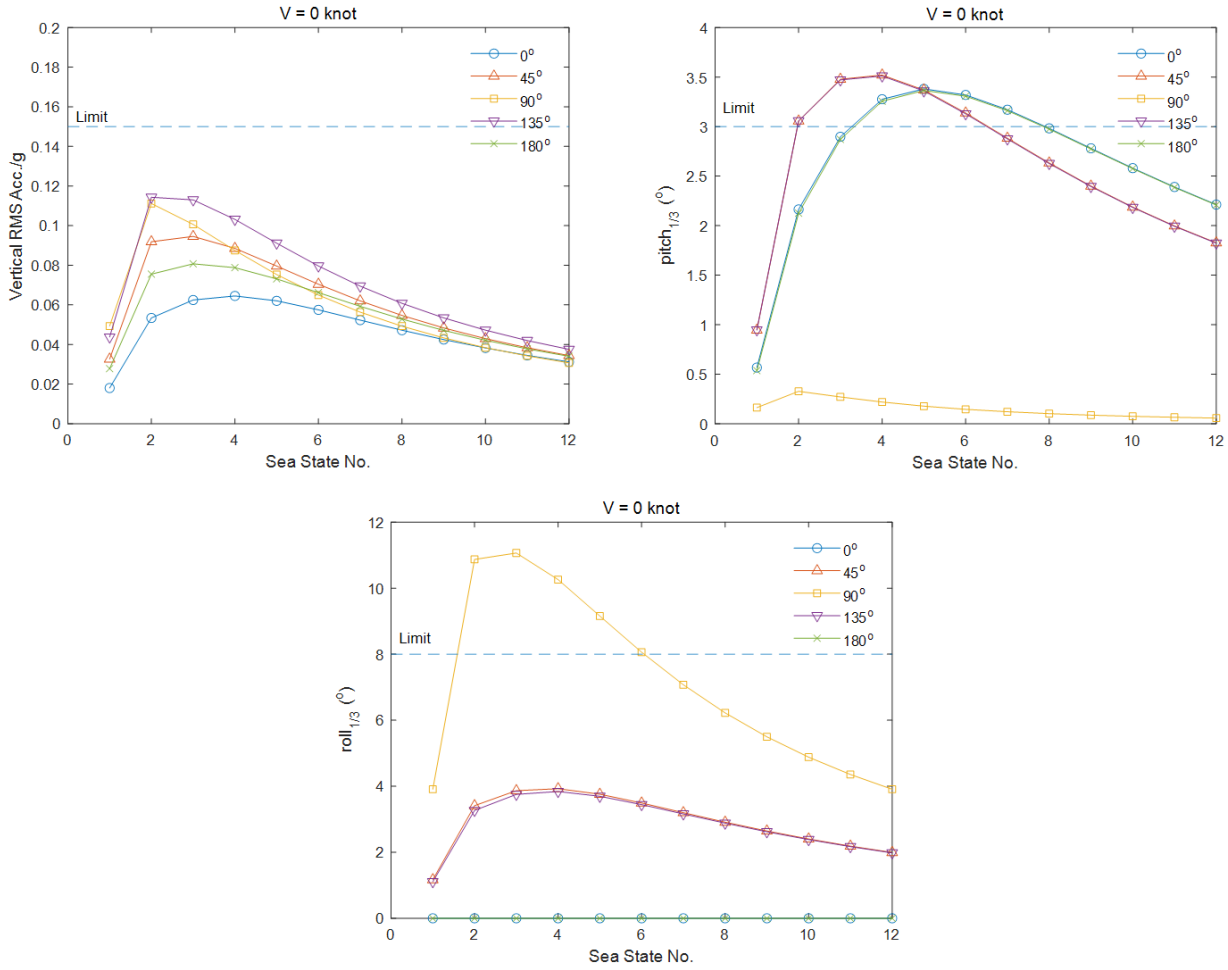

Figure 5.5 Vertical accelerations, pitch and roll response at flight deck, V = 0 knot

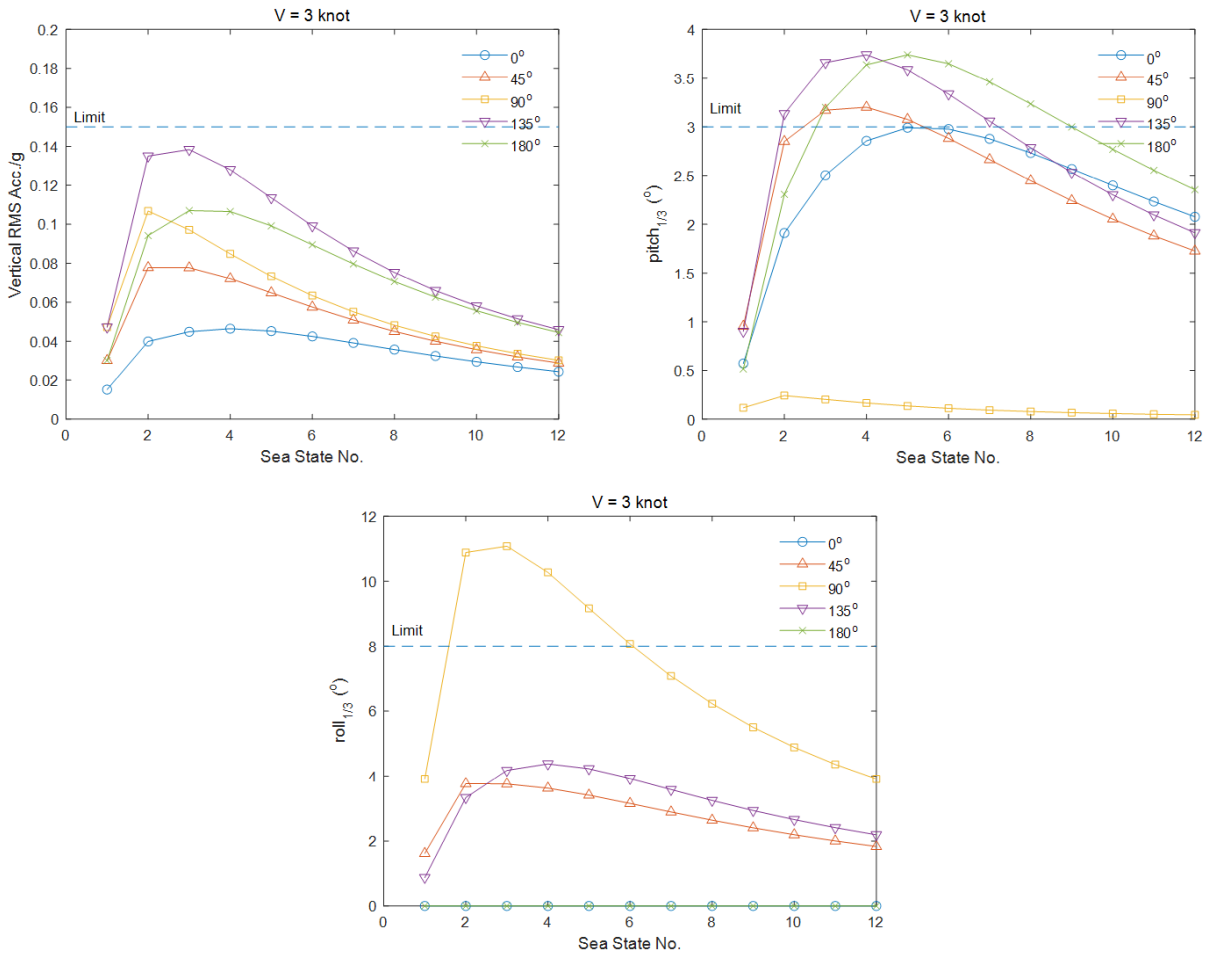

Figure 5.6 Vertical accelerations, pitch and roll response at flight deck, V = 3 knot

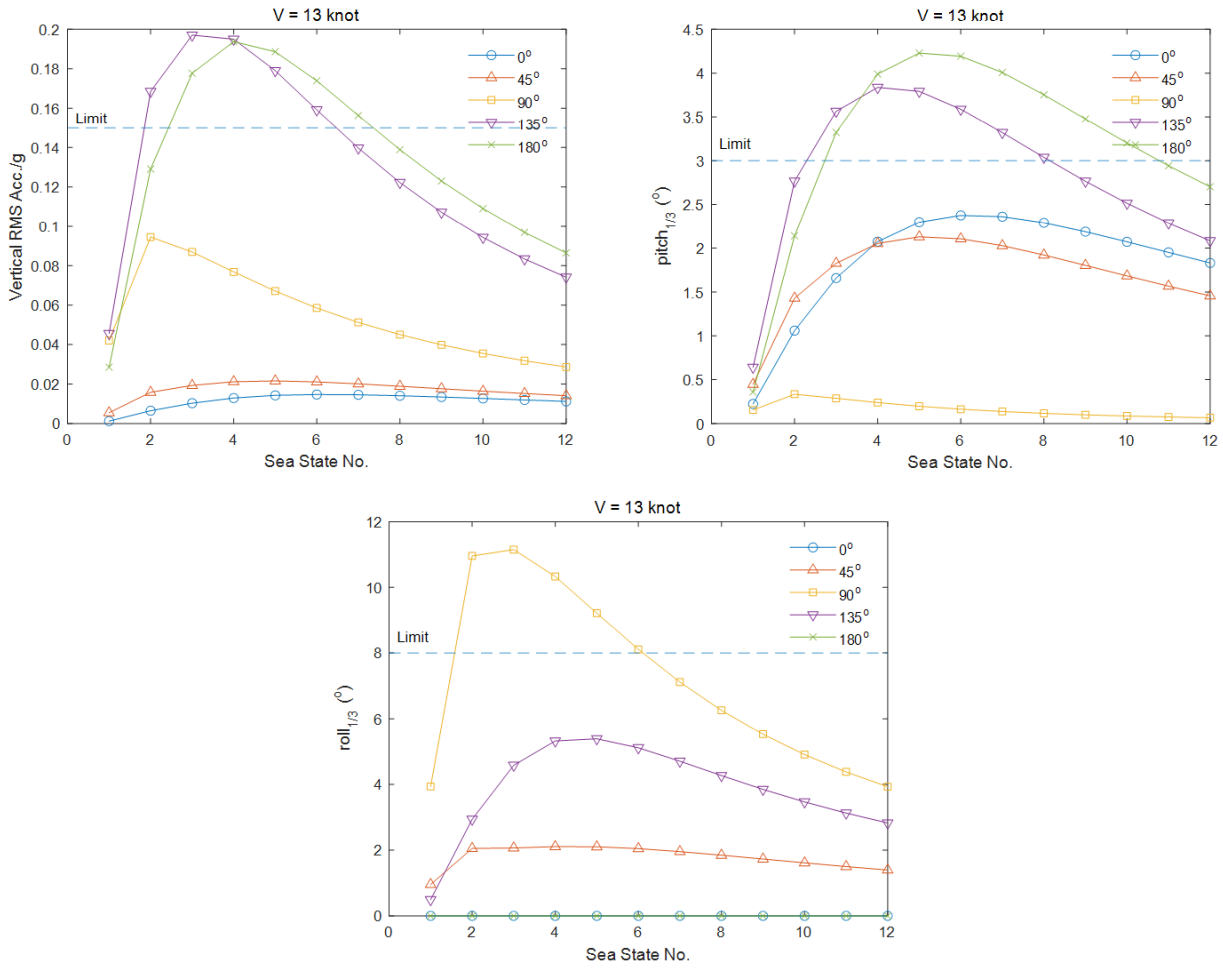

Figure 5.7 Vertical accelerations, pitch and roll response at flight deck, V = 13 knot

Figure 5.5-5.7 show the vertical accelerations, pitch, and roll response at flight deck in various sea states. The vertical accelerations are lower than the criteria except some cases in the bow and head seas when the speed is at 13 knots. The pitch motion is a main affecting factor on the vertical acceleration so the situation could be better if the flight deck moves towards to the midship. The pitch motion is a severe influence on the security of launch and recovery of helicopter. The pitch motions are higher than the criteria in most cases in the bow and head seas, especially at the speed of 13 knots. One potential solution is to change the hull profile or to change the mass distribution. The flight deck is not severely affected by the roll motion except few cases. The stabilization systems reducing the roll of Khione could make the roll motion at the flight deck satisfy the criteria.

Accuracy of the obtain results

The accuracy of the method used in this report is good enough for the engineering application. However, there is still some factors undermining the accuracy.

First, the potential flow theory ignores the viscosity of water and consequently ignore the rotation of water particle.

Second, the boundary element model only considers the mean wet surface. The hull motions do not change the wet surface. In addition, the model uses flat panels to replace the accurate geometry of the hull. Thus, the model does not represent the hull.

Third, the mass distribution and COG of Khione is not well known at this design stage. This firstly affects the calculation of wave induced motions. Secondly, this affects the calculation of hull girder loads.

5.2 Maneuvering tests

Khione is going to operate in harsh environments surrounded by many potential hazards. In Arctic and Antarctic areas maneuvering is especially important because of the special features of the areas. In the cold areas of the world Khione can encounter icebergs and thick ice ridges, which require good maneuverability to be dodged. It is well known what can happen if a ship cannot maneuver away from an iceberg. The ship is meant to perform research and resupply operations in remote areas, where space for operating the ship may be limited. Thus, the turning circle test of the ship is crucial. Based on previously presented reasoning at least emergency stop test and turning circle test simulations are essential for our ship.

The most notable feature of operational areas of Khione is cold temperatures, which have effect on operations, but also on emergency response. A man overboard -situation is always potentially lethal but in icy waters the time to rescue is very much limited. Thus, it is sensible to simulate a man overboard-situation to determine best plan of action in case of emergency.

The maneuvering simulations were performed using the Maneuvering Subsystem in NAPA. This subsystem simulates maneuvers with 4 degrees of freedom: surge, sway, yaw and roll. Heave and pitch are not taken into account. Furthermore, the simulation can take the following external forces into account: wind, current, drift forces and added resistance. Added resistance will be covered in the next chapter.

Emergency stop -simulation

Simulation was performed at design speed of 13 knots and at fully loaded and ballast condition. Results presented in Figure 5.8 and 5.9. Measures are given in cables, which is 1/10 of nautical mile.

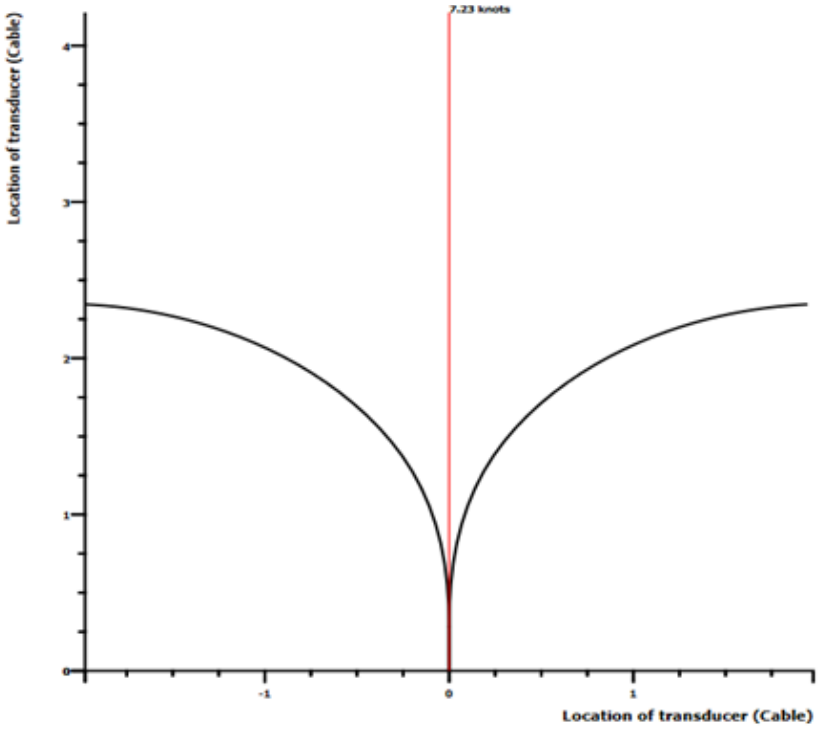

Figure 5.8 Emergency stop in fully loaded condition.

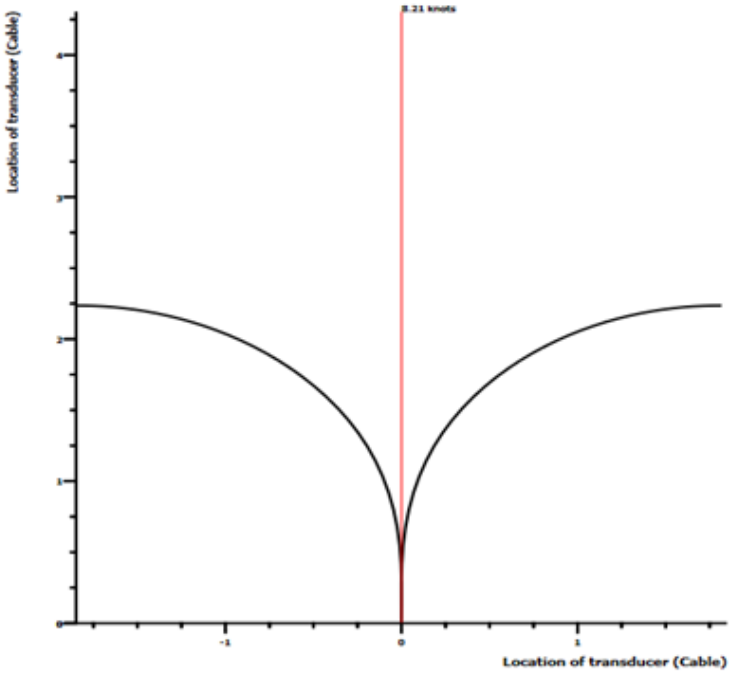

Figure 5.9 Emergency stop in ballast condition.

Turning circle -simulation

Simulation was performed at initial speed of 13 knots. Three separate cases were simulated: fully loaded in deep water, ballast load in deep water and fully loaded in shallow water. Length of the turning radius, required time and speed of the ship during the maneuver can be seen from the results presented in Figure 5.10.

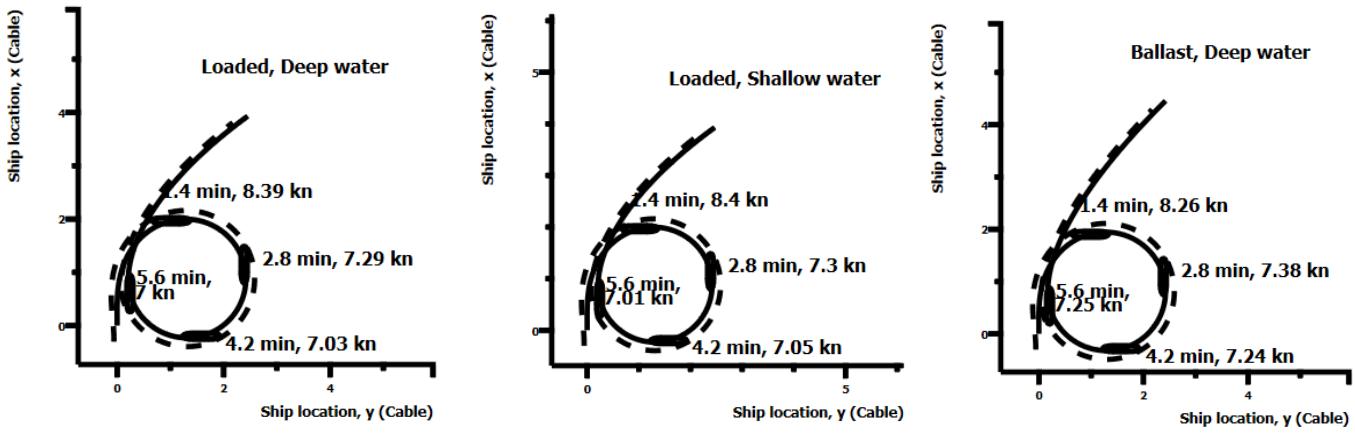

Figure 5.10 Results of turning circle -simulations

Man overboard -simulation

Simulation was performed with initial speed of 13 knots and with fully loaded condition. Man overboard maneuver simulation is conducted with intention to perform Williamson turn. Results show the extent of the maneuver and required time to perform it. All together the maneuver takes 8 minutes 53 seconds. Figure 5.11 illustrates the results.

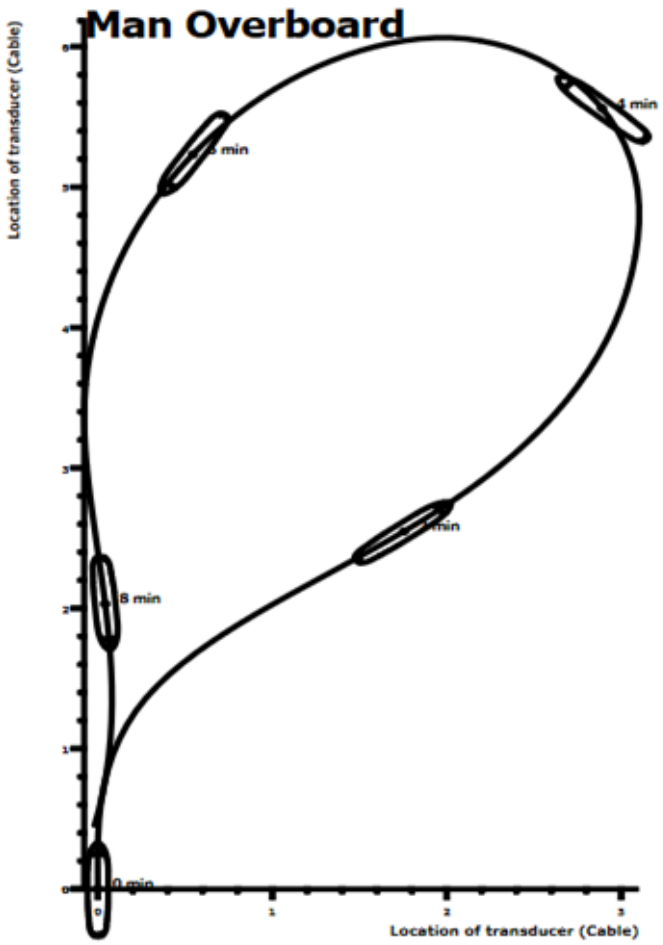

Figure 5.11 Result of MOB simulation.

5.3 Added Resistance

The calm water resistance of Khione was calculated in a previous course, the results of which are presented in Table 5.5. Figure 12 shows the total added resistance from the table plotted against the speed. It is clear that the calm water resistance increases with speed, specifically with the square of the speed.

Table 5.5 Calm water resistance of Khione at different speeds.

Fn	Vs	Rt	Pe	RHull	Rwind	RVisc	Rwave
	knots	kN	MW	kN	kN	kN	kN
0.000	0.000	0	0.000	0	0	0	0
0.015	1.000	1	0.001	1	0	1	0
0.029	2.000	5	0.005	5	0	4	0
0.044	3.000	11	0.018	11	1	9	0
0.058	4.000	20	0.040	19	1	15	0
0.073	5.000	30	0.077	28	2	23	0
0.087	6.000	42	0.131	40	2	33	0
0.102	7.000	57	0.204	54	3	44	0
0.116	8.000	73	0.301	69	4	56	0
0.131	9.000	92	0.426	87	5	70	1
0.145	10.000	114	0.584	108	6	85	2
0.160	11.000	139	0.787	132	7	102	5
0.174	12.000	170	1.049	161	9	119	12
0.189	13.000	210	1.407	200	10	139	26
0.204	14.000	256	1.843	244	12	159	44
0.218	15.000	329	2.536	315	14	182	87
0.233	16.000	407	3.354	392	16	205	134
0.247	17.000	480	4.202	463	18	230	174
0.262	18.000	618	5.722	598	20	256	276
0.276	19.000	855	8.354	833	22	283	475
0.291	20.000	1117	11.495	1093	24	311	699
0.305	21.000	1296	13.997	1269	27	341	836
0.320	22.000	1399	15.835	1370	29	372	897

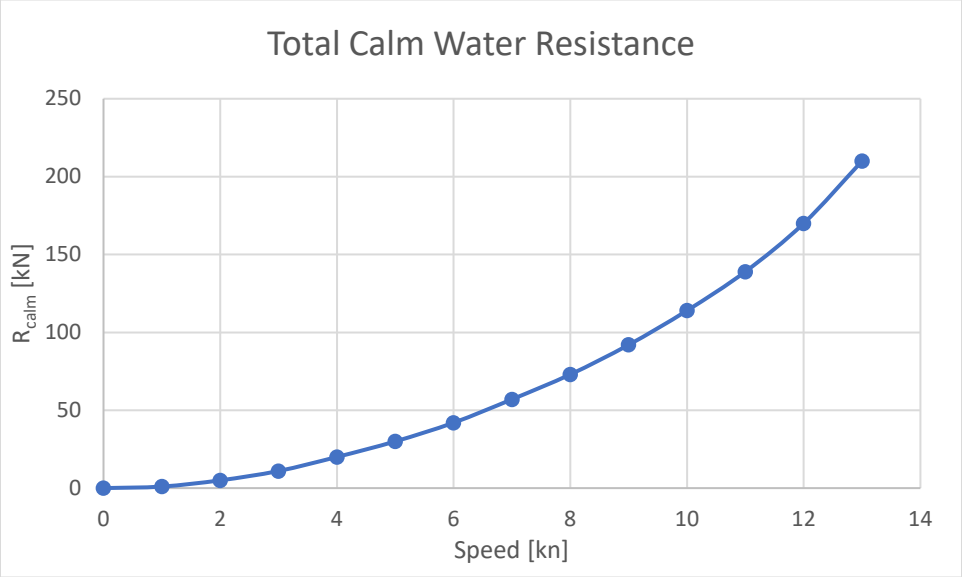

Figure 5.12 Total calm water resistance plotted against speed, based on Table 5.5.

Waves cause an extra resistance component, known as *added resistance*. Added resistance varies with the wave direction, height, frequency as well as the ship speed. The added resistance of Khione was estimated using NAPA, which uses the Gerritsma & Beukelman's method (NAPA Group, 2021). This method is based on the strip theory method and is thus based on the same assumptions and simplifications (Spyridon Cheirdaris, 2021) :

- The fluid is inviscid
- The ship is slender
- The hull is rigid
- Lift generated is negligible
- Motions are small
- Hull sections are wall-sided
- Deep water approximation applies; the water depth is much greater than the wavelength
- The waves are not affected by the presence of the hull

Furthermore, Gerritsma & Beukelman's method can only accurately calculate the added resistance in head to beam seas. Napa only calculates the head seas case. This should not be an issue, because the added resistance of a ship should be highest in head waves.

The assumption that hull sections are wall-sided is accurate, as shown in Figure 5.13. Furthermore, Khione is too heavy for the lift generated at its top speed of 13 knots to have any significant effect on the results. The ship is slender enough for strip theory, since it has an L/B of 5.7 at the waterline while strip theory is accurate for a L/B $\geq$ 3 (Journée et al., 2015). Lastly, the rigidity of the hull is not yet determined so no meaningful conclusions can be made based on that. The viscosity of the water, the motion amplitude and the effect of the hull on the waves are consequences of strip theory, not assumptions applying to the ship itself.

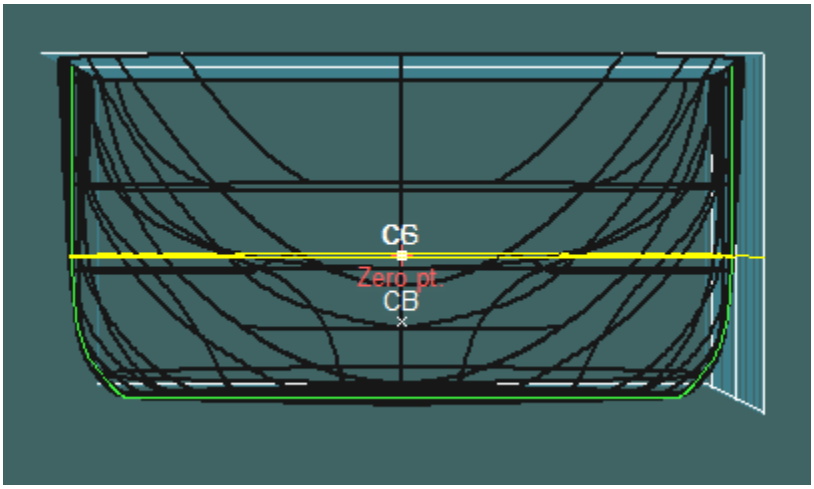

Figure 5.13 Front view of Khione, the yellow line shows the waterline. At the waterline, the hull shell is almost perpendicular to the waterline.

Figure 5.14 shows the added resistance in head seas plotted against the wave frequency at 6 different speeds. The wave height used is 16.5 m, which is the highest wave height Khione is expected to encounter. The most common periods associated with this wave height around 11.5 s, which gives a sine wavelength of about 200 m (Jiang et al., 2021). Since Khione usually sails through waters deeper than 1000 m, the deep water assumption holds.

Unlike the calm water case, the added resistance in Figure 5.14 actually decreases with higher ship speed. This seems strange, as the faster the relative speed between the incoming waves and the ship, the greater the force with which the wave is expected to push back. However, Gerritsma & Beukelman's method does not calculate the resistance using the pushing force of a wave but is based on the energy that radiates away from the ship in the form of waves caused by oscillations. It is possible that these oscillations are actually greater at lower speeds than at higher speeds, in turn taking away more energy.

Comparing the added resistance at this high wave height to the calm water resistance, shown in Figure 5.15, it becomes clear that the calm water resistance is negligible by comparison. For a small wave height of 3 m however, the calm water resistance is generally higher than the added resistance.

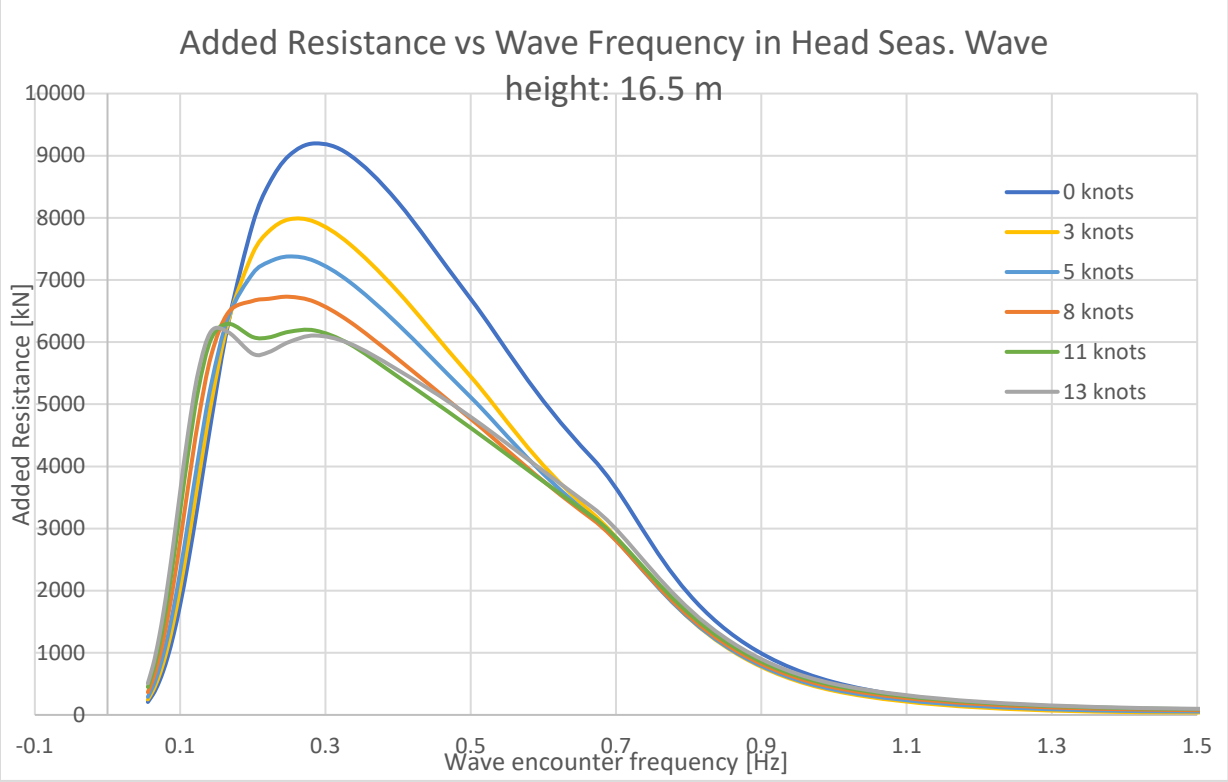

Figure 5.14 Added resistance in head seas plotted against wave frequency at 6 different speeds. The wave height is 16.5 m. Calculated using NAPA.

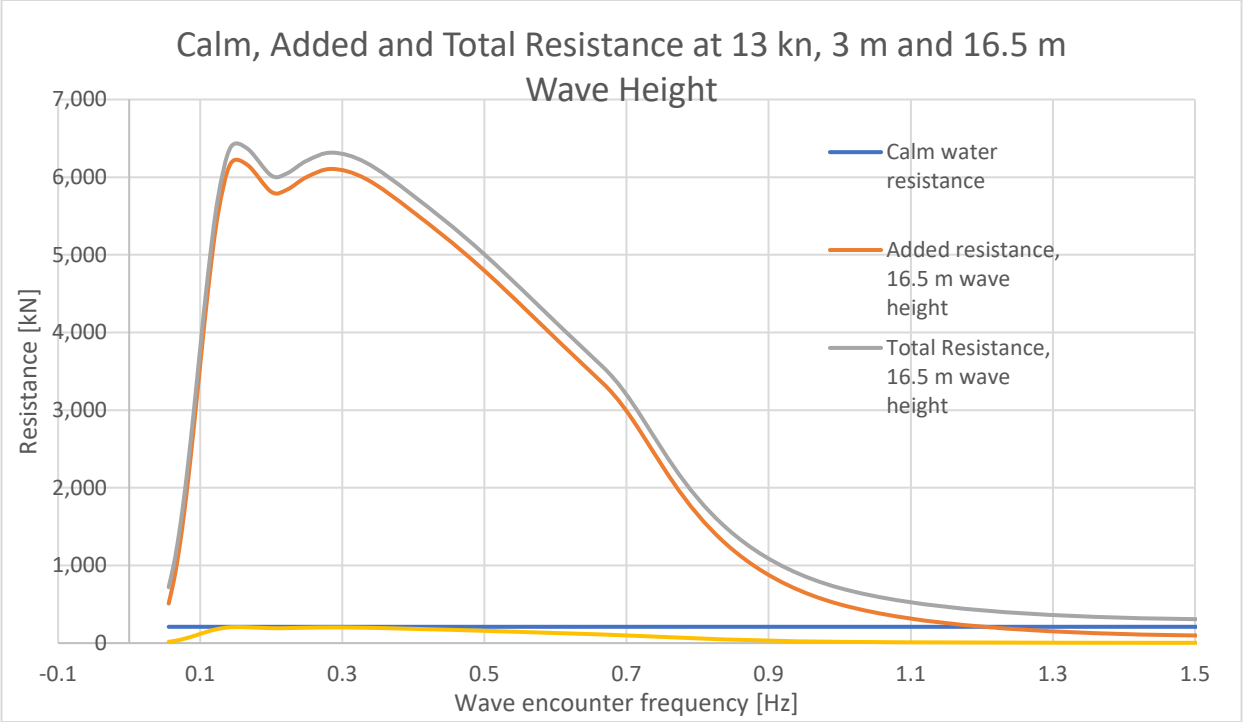

Figure 5.15 Plot showing the calm water resistance, added resistance and their sum. The wave condition is head waves at a 3 m and 16.5 m wave height. The ship speed is 13 kn. The calm water resistance does not depend on the wave frequency.

5.4 Literature review

5.4.1 Bertram, Practical ship hydrodynamics: 6.2.8 CFD for maneuvering

The hydrodynamic forces of main interest in maneuvering are: the longitudinal force (resistance) X, the transverse force Y and the yaw moment N. These quantities are a function of the longitudinal speed and acceleration, transverse speed and acceleration, yaw rate and acceleration and obviously the rudder angle. For heavy maneuvers resulting in heel, the heel will also contribute considerably into forces and moments.

After respective forces and moments are made non-dimensional, they may be approximated by equations like Eq 5.1, where subscripted Y' represent hydrodynamics coefficients.

$$Y' = Y_{\dot{v}}' \cdot \dot{v}' + Y_{\dot{r}}' \cdot \dot{r}' + Y_{v}' \cdot v' + Y_{v^3}' \cdot (v')^3 + Y_{vr^2}' \cdot v'(r')^2 + Y_{v\delta^2}' \cdot v'\delta^2 + Y_{r}' \cdot r' + Y_{r^3}' \cdot (r')^3 + \ldots \quad (5.1)$$

These coefficients can be found out with CFD simulations or with model tests. Catalogues such as that of Wolff (1981) list these hydrodynamic coefficients for various ship types, providing a good starting point for maneuvering analysis. However, there is high variations in hull form even

amongst single ship type, so more accurate methods are needed. As the computational power has been exponentially increasing during last decades, Khione might benefit from maneuvering analysis conducted via CFD. If the CFD proves still an unrealistic goal, the team should refer to catalogues like that of Wolff for hydrodynamic coefficients.

Bertram states that traditional maneuvering analysis results in linearized equations that are very numerically sensitive, hence producing large errors with small turning rates. With high turning rates, non-linear phenomena such as cross-flow resistance and vortex shedding require full RANS/LENS-simulations to obtain accurate body forces for maneuvering. Bertram notes that the field of CFD maneuvering is still an emerging one: the presence of vortices require extensive mesh size, and simplifications result in high errors. He presents 3 known approaches for CFD maneuvering analysis.

Lifting surface method

In this technique, the flow is assumed to be inviscid plate flow. The plate has zero thickness, the flow is smooth along the trailing edge and the vortices are of horseshoe type, symmetrical to water surface. The vortex strength within the body is determined for by assuming that the flow is parallel to the wall sided midship at collocation points. The vortices are assumed to be located at quarter of the chord length from the bow, while the collocation points are at three quarters of the chord length from the bow. The resulting linear system yields the transverse forces by assuming that the body forces equal the force exerted on created vortices by the undisturbed flow. Alternatively, the pressure difference between starboard and port plates can be integrated along the hull, yielding the transverse forces.

Lifting body method

A slight improvement of lifting surface method, the lifting body method incorporates the transverse thickness of the hull, resulting in higher lift. The flow smoothness at stern can be ensured via equal pressures. For dull stern geometries, the flow separation point is unclear, resulting in high errors in forces. Bertram notes that generally, the lifting body method is quite difficult to use, but can predict rudder-hull interaction with sufficient accuracy. If rudder angle is increased beyond stall angle, only full viscous simulations can predict the forces accurately.

Field methods

As of 2010, the RANS and LES simulations were mostly confined to research application. According to Bertram, the problems of such simulations mostly revolve around the scale of the shed vortices, requiring a fine mesh along the entire hull and extending quite far from the surface. He states that while such simulations can predict transverse forces quite accurately, the resistance prediction leaves much to be desired. The implementation of free-surface boundary condition is expected to improve the precision of field methods.

5.4.2 Journée, Massie, Huijsmans; Offshore hydromechanics: 8.8 Added resistance in waves

A ship moving through the seaway will generate waves not only because of the horizontal motion, but also because the vertical motion induced by the waves. The latter radiates energy from the ship and thus increases the resistance the ship experiences. The added resistance in waves is cyclical in nature and fundamentally originates from the movement of ship sections relative to water surface.

If we average the cyclical added resistance, to maintain a constant forward speed the ship's propulsion machinery must supply extra power equal to the power lost in radiation. The radiated power P due to the vertical motion per each oscillation is given by:

$$P = \frac{\pi}{\omega_e} \int_L \left(N_{33} - V * \frac{dM_{33}}{dx_b} \right) * V_{z_a}^2 * dx_b \tag{5.2}$$

where ω_e is the wave frequency, N_{33} is a force coefficient, M_{33} is a moment coefficient, V is the ship velocity, V_{z_a} is averaged vertical velocity and x_b is length-wise ship coordinate.

Further, the added resistance R_{aw} can then be solved from the equation:

$$P = R_{aw} * \left(\frac{2\pi}{-k * cos\mu} \right) \tag{5.3}$$

where k is a coefficient and μ is the viscocity.

Combining the above expressions, the transfer function for average added resistance in waves is (Gerritsma and Beukelmann):

$$\frac{R_{aw}}{\zeta_a^{\,2}} = \frac{-k \cdot cos\,\mu}{2\omega_e} \cdot \int_L \left(N_{33}' - V \cdot \frac{dM_{33}'}{dx_b} \right) \cdot \left(\frac{V_{z_a}^*}{\zeta_a} \right)^2 \cdot dx_b \tag{5.4}$$

It is unlikely that the team would need to implement such equations manually. However, understanding the theory will allow the seakeeping software user to detect unpsysical results, no matter the root cause.

References

ABB, 2019. *Azipod® VI and ICEProduct Introduction.* [Online]
Available at:
https://library.e.abb.com/public/27726b3b06fd4034b09734c4d1655731/Azipod%20VI%20and%20ICE_brochure.pdf
[Accessed 11 3 2021].

Abankawa, N., Ossont, S. & Scott, M., 2015. *Ship motion measurement using an inertial measurement unit.* Southampton, University of Southampton.

BMT, 1986. *Global Wave Statistics*. Tennington, BMT Group ltd.

Borgenhov, T. R. (2017). *Investigation of Roll Damping on an FPSO with Sponsons and Bilge Keels* (Master's thesis, NTNU).

Canada Ice Service, 2020. Annual Arctic Ice Atlas, winter 2019-2020.

Chakrabarti, S.K. (1987) “Hydrodynamics of Offshore Structures”. WIT Press.

Chen, Chao. He, Yanping. 2020. *Analysis of the Seakeeping Performance of Icebreaker Based on Maxsurf.*

Cura-Hochbaum, A. Delefortrie, G. Maron, A. Lengwinat, A. Papanikolaou, A. Sprenger, F. Zwijnsvoorde, T. 2017. *Experimental Studies on Seakeeping and Maneuverability of Ships in Adverse Weather Conditions.* Journal of Ship Research, Vol. 61, No. 3, September 2017, pp. 131–152. Available at: https://www.researchgate.net/publication/318590270_Experimental_Studies_on_Seakeeping_and_Maneuverability_of_Ships_in_Adverse_Weather_Conditions [Accessed 10 March 2021].

DNV, 2010. *DNV-RP-C205, ENVIRONMENTAL CONDITIONS AND ENVIRONMENTAL LOADS.*

Faltinsen & Svensen, (1990). *Incorporation of Seakeeping Theories in CAD.* Wageningen: Maritime Research Institute Netherlands.

Ghassemi, H. Majdfar, S. Valiollah, G. 2015. *Calculations of the Heave and Pitch RAO’s for Three Different Ship’s Hull Forms.*

Headland, R., 2020. *TRANSITS OF THE NORTHWEST PASSAGE TO END OF THE 2019 NAVIGATION SEASON,* Cambridge: University of Cambridge.

Holthuijsen, L., 2007. *Wave in Oceanic and Coastal Waters.* New York: Cambridge University Press.

IMO, 2015. *International code for ships operating in polar waters (Polar Code). MEPC 68/21/Add.1 Annex 10,* london: International Maritime Organization.

ISO, 1985. Evaluation of Human Exposure to Whole-body Vibration—Part 3: Evaluation of Whole-body z-axis Vertical Vibration in the Frequency Range 0.1 to 0.63 Hz.

ISO, 1997. Mechanical Vibration and Shock Evaluation of Human Exposure to Whole Body Vibration—Part 1: General Requirements.

ITTC, 2005. Final Report and Recommendations to the 24th ITTC. The Seakeeping Committee. Proceedings of the 24th ITTC - Volume I.

ITTC, 2011, "Numerical Estimation of Roll Damping", ITTC Recommended Procedures, 7.5-02-07-04.5, pp. 1-33.

Jiang, Z., van Reen, S., Suortti, J., Voutilainen, J. 2021. *Ship Dynamics, Assignment 2*. Espoo, Aalto University

Journée, J.M.J., Massie, W.W. and Huijsmans, R.H.M. 2015. *Offshore Hydrodynamics, Third Edition.* Delft, Delft University of Technology.

Keller J. B., (1998). *Gravity waves on ice-covered water.* Journal of Geophysical Research, vol. 103, no. C4, pages 7663-7669.

Moton, C. 1991. *OPEN-WATER RESISTANCE AND SEAKEEPING CHARACTERISTICS OF SHIPS WITH ICEBREAKING BOW*. US Naval Academy, Annapolis, Maryland. Available at: https://apps.dtic.mil/dtic/tr/fulltext/u2/a245643.pdf [Accessed 12 March 2021].

NAPA Group, (2021). *SSHM Manoeuvring and Added Resistance.* Helsinki, NAPA Group.

Ochi, Michel K. 2005. *Ocean Waves : the Stochastic Approach* . Cambridge, U.K,Cambridge University Press.

Odabasi A.Y., Fitzsimmons P.A., Ankudinov V.K., Wiley S.A., 1991. Seakeeping Considerations in Ship Design and Their Incorporation in HDDS. BMT International, Report No. HDDS.P2.SPEC.

O'Hanlon, J.F., McCauley, M.E., 1974. Motion sickness as a function of the frequency and acceleration of vertical sinusoidal motion. Aerospace Medicine 45 (4), 366–369.

Riska, K. 2010. *DESIGN OF ICE BREAKING SHIPS*. Helsinki, Finland and University of Science and Technology, Trondheim, Norway.

Sariöz, K., & Narli, E. (2005). Effect of criteria on seakeeping performance assessment. Ocean Engineering, 32(10), 1161-1173.

Semedo, A., Dobrynin, M., Lemos, G., Behrens, A., Staneva, J., De Vries, H., & Murawski, J. (2018). CMIP5-derived single-forcing, single-model, and single-scenario wind-wave climate ensemble: Configuration and performance evaluation. Journal of Marine Science and Engineering, 6(3), 90.

Schothorst, J. G., 'EFFECT OF SHIP MOTION ON SONAR DETECTION PERFORMANCE'. Den Haag, The Netherlands, RVO/TNO

Spyridon Cheirdaris, (2021). *Lecture 7: Seakeeping methods*. Espoo, Aalto University.

Tadros, A.R., Langlois, R. G. and LaRosa, M. (2003). Ship Flight Deck Motion Parameters for Ensuring Safety of Helicopter Operation.

Veritas, B. (2016). Hydrostar for experts, user manual. Research Department of Bureau Veritas.

Wärtsilä, 2019. *Wärtsilä 31*. [Online]
Available at: https://www.wartsila.com/docs/default-source/product-files/engines/ms-engine/brochure-o-e-w31.pdf?utm_source=engines&utm_medium=dieselengines&utm_term=w31&utm_content=brochure&utm_campaign=msleadscoring
[Accessed 11 3 2020].